Next Generation of Electrospun Textiles for Chemical and Biological Protection and Air Filtration

by

Liang Chen

B.S. in Chemical Physics, University of Science and Technology of China, 2001
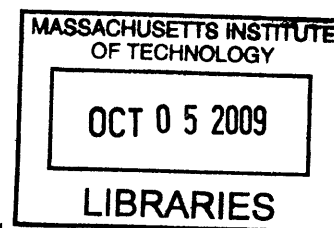
M.S. in Chemistry, Brown University, 2004

M.S.C.E.P. in Chemical Engineering, Massachusetts Institute of Technology, 2006

Submitted to the Department of Chemical Engineering in partial fulfillment of the requirements for the degree of

Doctor of Philosophy in Chemical Engineering

at the
Massachusetts Institute of Technology
September, 2009
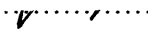
Signature of Author............................
Department of Chemical Engineering
July 23, 2009

Certified by.............................
$\mathcal{U}$ $\mathcal{C}$ $\mathcal{U}$ Gregory C. Rutledge
Lammot du Pont Professor of Chemical Engineering
Thesis Supervisor

Certified by..
T. Alan Hatton
Ralph Landau Professor of Chemical Engineering Practice
Thesis Supervisor

Accepted by...
William M. Deen
Professor of Chemical Engineering
Chairman, Committee for Graduate Students

1. REPORT DATE **SEP 2009**	2. REPORT TYPE	3. DATES COVERED **00-00-2009 to 00-00-2009**
4. TITLE AND SUBTITLE **Next Generation of Electrospun Textiles for Chemical and Biological Protection and Air Filtration**		5a. CONTRACT NUMBER
		5b. GRANT NUMBER
		5c. PROGRAM ELEMENT NUMBER
6. AUTHOR(S)		5d. PROJECT NUMBER
		5e. TASK NUMBER
		5f. WORK UNIT NUMBER
7. PERFORMING ORGANIZATION NAME(S) AND ADDRESS(ES) **Massachusetts Institute of Technology,77 Massachusetts Avenue,Cambridge,MA,02139-4307**		8. PERFORMING ORGANIZATION REPORT NUMBER
9. SPONSORING/MONITORING AGENCY NAME(S) AND ADDRESS(ES)		10. SPONSOR/MONITOR'S ACRONYM(S)
		11. SPONSOR/MONITOR'S REPORT NUMBER(S)
12. DISTRIBUTION/AVAILABILITY STATEMENT **Approved for public release; distribution unlimited**		
13. SUPPLEMENTARY NOTES		

14. ABSTRACT

Protective clothing systems in current use are primarily based upon either full barrier protection through blocking contaminant permeation, or on air-permeable adsorptive protective overgarments in which all the toxins are adsorbed on contact. The adsorptive protective multilayer fabric systems are bulky and possess low moisture vapor permeability. These challenges motivate the development of a new generation of protective clothing system that is lightweight, breathable, and capable of selectively decomposing toxic agents on the fabric surfaces. Electrospun fabrics are remarkably breathable and lightweight; their high specific surface area can be used to functionalize the material by the attachment of functional compounds. In this dissertation, we aimed at developing electrospun fiber-based chemical and/or biological detoxifying protective fabrics containing a-nucleophilic oxime moieties that are capable of hydrolytically decomposing toxic organophosphate (OP) chemical nerve agents and pesticides, and/or biocides acting against bacterial contaminants. Oxime-functionalized electrospun fiber mats were obtained via electrospinning of a polymer blend containing reactive polyacrylamidoxime (PAAO) and parent polyacrylonitrile (PAN). The function of PAAO/PAN fiber mats was evaluated by the hydrolysis of p-nitrophenyl acetate (PNPA), mimicking toxic OP nerve agents and pesticides. The presence of PAAO in the reactive fiber mats significantly accelerated the hydrolysis of PNPA compared to its spontaneous hydrolysis. The effect of the fiber size on reaction rate indicated that intra-fiber diffusional resistances may limit the accessibility of the reactive oxime sites inside the fibers with the oxime-assisted hydrolysis occurring primarily on the fiber surfaces. In addition, the capability of PAAO powder to decompose combat chemical warfare agents, such as soman (GD) and VX was demonstrated. Prefabricated PAN submicron fiber mats were chemically modified via an efficient, onestep oximation reaction with excess hydroxylamine, resulting in conversion of the surfaces of the fibers to reactive amidoxime groups. Nucleophilic amidoximes enable the fiber mat to decompose OP nerve agent simulant, diisopropyl fluorophosphate (DFP), as monitored by 31P MAS NMR spectroscopy. The hydrolytic degradation of DFP occurs only in the presence of water, which serves as a medium promoting the nucleophilic action of the amidoximes in the fibers. Bactericidal fiber mats were produced from electrospinning of blends containing a biocide chlorhexidine (CHX). A small amount of high molecular weight poly(ethylene oxide) was incorporated into the blends to facilitate the electrospinning and a dimensionless Deborah number (De) was introduced to determine the spinnability of the blends. The resultant fiber mats demonstrated bactericidal properties, killed representative bacteria of E. coli and S. epidermidis not

15. SUBJECT TERMS

16. SECURITY CLASSIFICATION OF:			17. LIMITATION OF ABSTRACT	18. NUMBER OF PAGES	19a. NAME OF RESPONSIBLE PERSON
a. REPORT	b. ABSTRACT	c. THIS PAGE	**Same as Report (SAR)**	**163**	
unclassified	**unclassified**	**unclassified**			

To my parents, Guangyao and Yanping

To my wife, Jun

To my unborn baby

Next Generation of Electrospun Textiles for Chemical and Biological Protection and Air Filtration

by

Liang Chen

Submitted to the Department of Chemical Engineering on July 23, 2009,
in partial fulfillment of the requirements for the degree of
Doctor of Philosophy in Chemical Engineering

Abstract

Protective clothing systems in current use are primarily based upon either full barrier protection through blocking contaminant permeation, or on air-permeable adsorptive protective overgarments in which all the toxins are adsorbed on contact. The adsorptive protective multilayer fabric systems are bulky and possess low moisture vapor permeability. These challenges motivate the development of a new generation of protective clothing system that is lightweight, breathable, and capable of selectively decomposing toxic agents on the fabric surfaces. Electrospun fabrics are remarkably breathable and lightweight; their high specific surface area can be used to functionalize the material by the attachment of functional compounds. In this dissertation, we aimed at developing electrospun fiber-based chemical and/or biological detoxifying protective fabrics containing α-nucleophilic oxime moieties that are capable of hydrolytically decomposing toxic organophosphate (OP) chemical nerve agents and pesticides, and/or biocides acting against bacterial contaminants.

Oxime-functionalized electrospun fiber mats were obtained via electrospinning of a polymer blend containing reactive polyacrylamidoxime (PAAO) and parent polyacrylonitrile (PAN). The function of PAAO/PAN fiber mats was evaluated by the hydrolysis of p-nitrophenyl acetate (PNPA), mimicking toxic OP nerve agents and pesticides. The presence of PAAO in the reactive fiber mats significantly accelerated the hydrolysis of PNPA compared to its spontaneous hydrolysis. The effect of the fiber size on reaction rate indicated that intra-fiber diffusional resistances may limit the accessibility of the reactive oxime sites inside the fibers with the oxime-assisted hydrolysis occurring primarily on the fiber surfaces. In addition, the capability of PAAO powder to decompose combat chemical warfare agents, such as soman (GD) and VX, was demonstrated.

Prefabricated PAN submicron fiber mats were chemically modified via an efficient, one-step oximation reaction with excess hydroxylamine, resulting in conversion of the surfaces of the fibers to reactive amidoxime groups. Nucleophilic amidoximes enable the fiber mat to decompose OP nerve agent simulant, diisopropyl fluorophosphate (DFP), as monitored by ^{31}P MAS NMR spectroscopy. The hydrolytic degradation of DFP occurs

only in the presence of water, which serves as a medium promoting the nucleophilic action of the amidoximes in the fibers.

Bactericidal fiber mats were produced from electrospinning of blends containing a biocide chlorhexidine (CHX). A small amount of high molecular weight poly(ethylene oxide) was incorporated into the blends to facilitate the electrospinning and a dimensionless Deborah number (De) was introduced to determine the spinnability of the blends. The resultant fiber mats demonstrated bactericidal properties, killed representative bacteria of $E.$ $coli$ and $S.$ $epidermidis$ not only through a gradual release of unbound CHX from the fibers but also via contact with CHX bound to the fibers. In addition, antibacterial fiber mats were obtained by a post-spin treatment of cellulose acetate fibers. The latter material allowed for the covalent CHX immobilization on the fibers via titanate linkers.

The layer-by-layer (LbL) electrostatic assembly technique was applied in combination with electrospinning technique to fabricate novel, breathable electrospun fiber-based protective fabrics and filters for both chemical and biological protection. Reactive polyanion, polyhydroxamic acid, which can decompose OP nerve agents, and antimicrobial polycation, poly (N-vinylguanidine), were synthesized and LbL-assembled onto electrospun fibers to achieve multifunctional coatings. The capability of these functionalized fabrics to detoxify representative chemical and biological toxic agents and their mimics was demonstrated. The breathability of the functionalized electrospun fiber-based systems was addressed.

Thesis Supervisor: Gregory C. Rutledge
Title: Lammot du Pont Professor of Chemical Engineering

Thesis Supervisor: T. Alan Hatton
Title: Ralph Landau Professor of Chemical Engineering Practice

4

Acknowledgements

Table of Contents

List of Figures

11

13

List of Tables

Chapter 1

Introduction

1.1. Motivation

Military, fire fighting and medical personnel require a high level of protection when they face potential chemical or biological threats such as intentional or accidental release of chemical or biological agents. Chemical and biological protective clothing made of many different fabric materials has been widely used to provide effective protection for various specific applications.[1] These protective systems are based upon full barrier protection through blocking contaminants or air-permeable adsorptive protective overgarments by absorbing all the toxins on contact. For example, hazardous materials (HAZMAT) response suits are made from impermeable laminated fabrics, providing protection by completely blocking the penetration of vapor and liquid into the fabrics. In order to effectively block toxins, one such suit, Chemfab's Challenge Ultra Pro fabric system, consists of five alternating layers of fluoropolymers, nonwoven aramid fiber layers and a conductive layer. This multilayered system is bulky and heavy in weight and requires additional breathing apparatus to make it comfortable to wear over a long operational period. In addition, in order to improve comfort level at higher workloads over longer periods, a semi-permeable adsorptive carbon liner is incorporated into protective clothing (*e.g.,* joint service lightweight integrated suit technology (JSLIST)), which can absorb organic vapors and liquids that pass into the clothing and simultaneously allow air and water vapor exchange. Although such JSLIST may offer sufficient protection, there are several disadvantages associated with currently used protective fabrics:

(a)   Effective protection comes at the cost of wearing a bulky multilayered fabric system with impaired wear performance (*e.g.,* poor moisture vapor permeability).

(b)   Toxic chemical and biological agents are not immobilized or neutralized on protective suits. Extensive contamination may arise when they leave the surface of protective clothing as aerosols or vapors.

(c)   The adsorptive carbon layer may be saturated by toxins and the excess

17

toxic chemicals may penetrate into the clothing.

Therefore, there is a need to develop next generation of protective clothing systems. The new protection fabrics should be lightweight and convenient to wear, which allow for permeation of water vapor while remaining resistant to the permeation of organic molecules (Figure 1.1). Furthermore, the new generation of protective fabrics is envisioned not only to absorb or block toxic chemical and biological agents, but also to detoxify them to reduce the risk of secondary contamination (Figure 1.1).
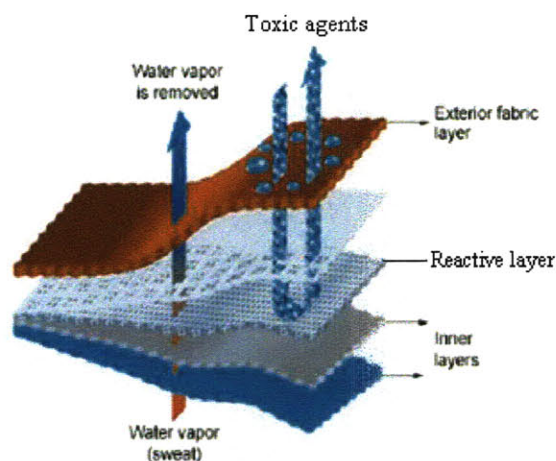
Figure 1.1. Multilayered protective suits

Electrospinning technology provides a new means to produce porous fiber fabrics. The electrospun fiber mats possess remarkable properties such as small fiber diameter, high specific surface area, high porosity and low fabric weight. Schreuder-Gibson and coworkers demonstrated that lightweight electrospun fabrics exhibit proper breathability, which impedes the water vapor diffusion to a lesser degree than barrier materials, while displaying better air flow resistance and enhanced aerosol particle retention compared to current commercially used membranes.[2-4] In addition, Obendorf et al. showed that the laminated fabrics with electrospun polypropylene fiber layer significantly limit the penetration of liquid pesticides while still

maintaining good water vapor permeability.[5]   The combination of breathability and high barrier performance of electrospun fabric makes it a promising candidate for the new generation of protection clothing.   Moreover, high specific surface area of the electrospun fiber mats allows for attachment of functional compounds to obtain chemical and biological detoxifying protective clothing.   In this regard, we aim at developing electrospun fiber-based self-detoxifying protective fabrics for chemical and biological protection.

1.2. Background

1.2.1. Organophosphates

The toxic chemical agents we target are organophosphates (OP). The utilization of organophosphates in agricultural pesticides/insecticides and chemical warfare agents (CWA) poses great risks to human health and the environment. Almost 1,300,000,000 agricultural workers worldwide are exposed to potential pesticide poisoning, including 3.3 million people in the United States. It was reported that the number of intoxications with OP pesticides and insecticides is estimated to be 3,000,000 per year and the number of deaths and casualties over 300,000 per year worldwide.[6] Since the event of September 11, there is increased concern over potential chemical and biological threats to the US military and civilians from terrorists. According to the report of the US General Accounting Office, the United States budgets about $1 billion per year on military defense against chemical and biological threats and additional $1.4 billion for civilian preparedness.[7] OP-based nerve agents constitutes a major CWA group. These OP agents pose a challenge in developing countermeasures providing effective protection of military personnel, emergency responders and agricultural workers when they face potential threats.
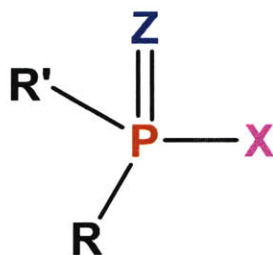
Figure 1.2. General chemical structure of organophosphates

Organophosphate (OP) compounds are usually esters, amides, or thiol derivatives of phosphoric, phosphonic, or phosphinic acids, which have the general structural formula as shown in Figure 1.2. In this Figure; R and R' are alkyl or alkoxy groups, Z is a doubly bonded oxygen or sulfur atom, and X is an easily displaceable group such as F, CN or p-$OC_6H_4NO_2$.
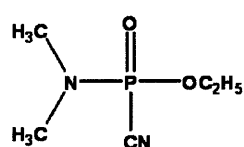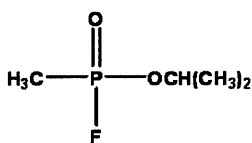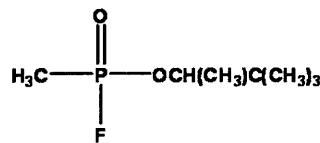
Tabun (GA)   Sarin (GB)   Soman (GD)

G-type nerve agents
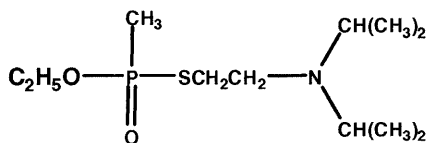
VX

V-type nerve agent

Figure 1.3. Chemical structures of nerve agents

OPs represent 70% of 100 million pounds of insecticides applied in various fields. Chemical nerve agents, one of the major groups of CWA, are primarily organophosphate compounds. Figure 1.3 shows chemical structures of several common nerve agents. Tabun (GA), sarin (GB), soman (GD) are among G-type nerve agents and VX belongs to V-type nerve agent. These nerve agents are too dangerous to be directly used in our study. Only less toxic OP simulants such as DFP and paraoxon will be used with cautions in this study (Figure 1.4).

21
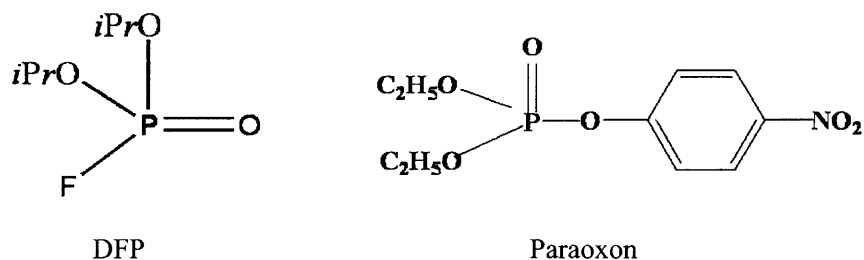
Figure 1.4. Common OP simulants

1.2.2. Organophosphate toxicity

OP pesticides and nerve agents are known to be very toxic. Approximate lethal dosage of nerve agents, for a 70 kg adult breathing in 15 L/min, for inhalation exposure and skin exposure are shown in Table 1.1.[8,9] The V-type nerve agents are over ten-fold more toxic than the G-type nerve agents. A few breaths of a vapor or aerosol of such an agent will kill a person in less than a minute. Liquid nerve agent splashed on the skin may kill people after 15 minutes.[9] The agent acute toxicity is primarily due to the inhibition of acetylcholinesterase (AChE), an enzyme critical to the normal function of nerve systems. The basic function of the AChE enzyme is to convert acetylcholine (ACh), a neurotransmitter, into the inactive metabolites, choline and acetate. The inhibition of AChE by nerve agents results in continuous stimulation of the muscles, glands and central nervous systems due to the aggregation of acetylcholine (ACh) at nerve synapses. Figure 1.5 demonstrates the mechanism of the OP poisoning. In terms of normal function, to hydrolyze ACh, the hydroxyl group of the serine at the active sites of the enzyme AChE is acetated, releasing the choline moiety. If the inhibition occurs, OPs bind to AChE, resulting in the phosphorylation at the hydroxyl group of the serine active sites of AChE. Compared to the rate of deacetylation, whose half-life is about 0.15 ms, the half-life of dephosphorylation is much longer (*e.g.*, 60 hours for diethyl phosphoryl-AChE), which prevents the regeneration of the AChE active sites from further functioning.[10] Therefore, OPs' toxicity is primarily determined by the extent of irreversibility of the

phosphorylation process. The electrophilicity of phosphorus atom in OPs is critical to the lethality of OPs. The presence of the electron withdrawing groups, such as halogens, nitro and cyano, will enhance the toxic effect.
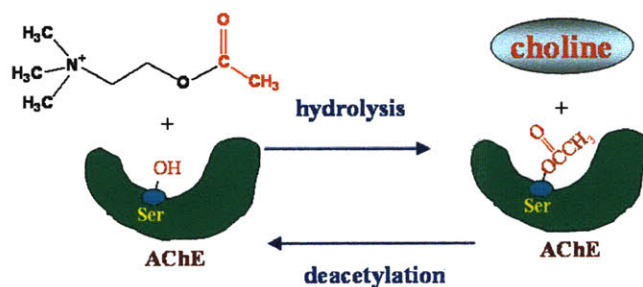
(a) Hydrolysis of acetylcholine by AChE

Sarin: R=CH(CH₃)₂ Soman: R=CH(CH₃)CH₂(CH₃)₃
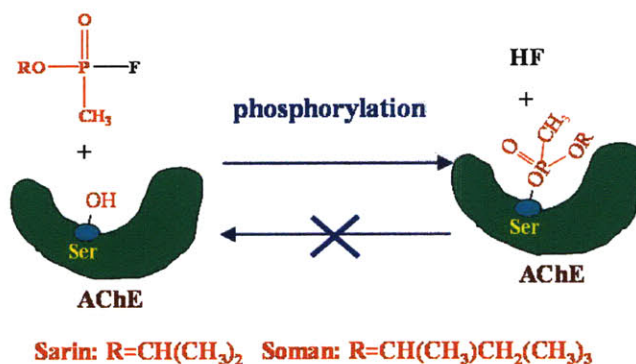
(b) Inhibition of AChE by nerve agents

Figure 1.5. Mechanism of OP poisoning

Agent	LCt$_{50}$ (inhalation mg min/m^3)	LC$_{50}$ (skin mg/individual)
GA (Tabun)	200	4000
GB (Sarin)	100	1700
GD (Soman)	50	100
VX	10	6

LCt$_{50}$: the product of concentration and the length of exposure
50: 50% of exposed population will die

Table 1.1. Lethal dosage of nerve agents

1.2.3. Organophosphate decontamination

The acute toxicity of organophosphates used as chemical nerve agents and agricultural pesticides has led to extensive efforts to develop various methods to decontaminate them.[10-14] Figure 1.6 summarizes major techniques currently used to decompose organophosphate compounds.
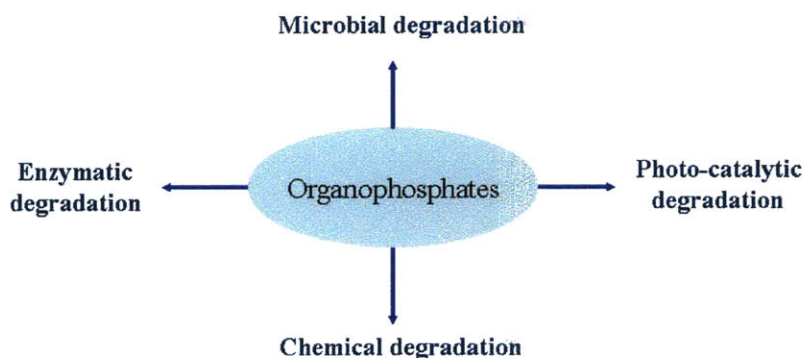
Figure 1.6. Degradation routes of organophosphates

Enzymatic degradation is a selective approach, which utilizes enzymes such as organophosphorous hydrolase, in the OP decomposition. It has been shown that the enzyme-based, "clean" decontamination can result in efficient hydrolysis of a range of OPs containing P-F, P-O, P-S and P-CN bonds.[15-17] However, the low stability of these OP-degrading enzymes significantly limits their practical application in the decontamination of OPs. For example, the observed half-life of native

organophosphorous hydrolase is only 2.7 days when stored at 20 °C. Furthermore, the lack of availability of the OP-degrading enzymes in sufficient quantities and their inherently high costs hinder their practical utilization in the OP detoxification.
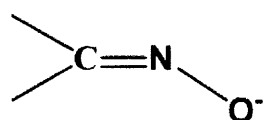
Oximate
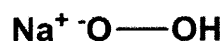
Sodium hydroperoxide
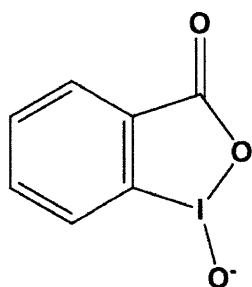
Iodosobenzoate
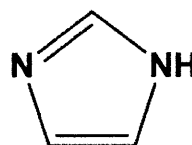
Imidazole

Figure 1.7. Chemical structures of α-nucleophiles

Another simple and effective method to decontaminate OPs is their chemical degradation by acid- or base-catalyzed hydrolysis or nucleophile-aided hydrolysis.[11-12,18-19] The hydrolytic degradation of OPs can be dramatically enhanced in a basic or acidic environment. In the base-catalyzed hydrolysis, alkali nucleophilically attack and break the P-X bond to detoxify OPs. In this regard, α-nucleophiles such as peroxide, hypochlorite, iodosobenzoate, imidazole, and oxime have been extensively investigated alone or in concert with surfactants to decontaminate OP-based toxic agents.[11-14,20-22] The chemical structures of several α-nucleophilic functional groups are shown in Figure 1.7. These α-nucleophiles are at least two orders of magnitude more reactive than ordinary nucleophiles.[23] The

α-effect results from electron repulsion between the lone electron pairs on the nucleophilic atom and on the adjacent atom. During the nucleophilic attack, a lone pair on the nucleophilic atom is shared partially with the electrophilic target atom. This substantially reduces the electron repulsion between lone pairs of the electrons and stabilizes the transition state. A schematic process of the cleavage of OPs catalyzed by oximates, commonly used antidotes for OP poisoning, is shown in Figure 1.8. The utilization of metal cations, such as copper or lanthanide in concert with nucleophiles was demonstrated to further facilitate the hydrolytic degradation of OPs.[24-26]
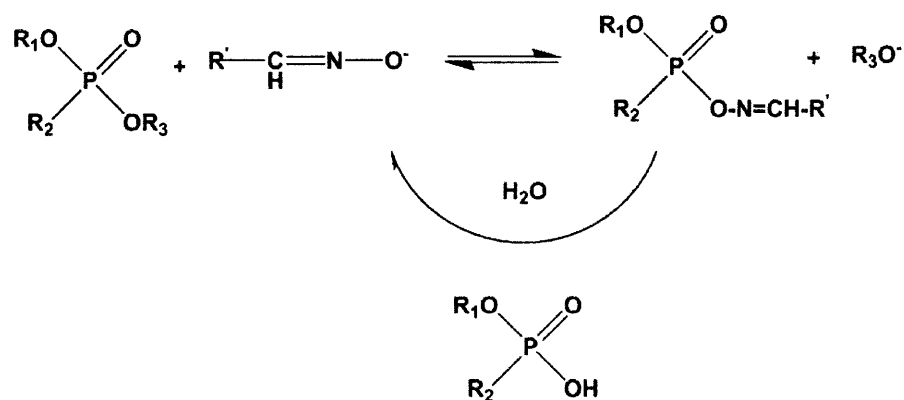
Figure 1.8. Schematic diagram of cleavages of OPs by oximate

1.2.4. Bactericides

Adhesion and proliferation of bacteria on the surface of materials can induce severe health and environmental hazards.[27] Pathogenic bacteria such as anthrax spores have been used to pose biological threats recently. Hence, there is a great demand to develop bactericidal, antiseptic, and bacteriostatic materials that can prevent attachment, proliferation and survival of microbes on the material surface. A broad range of antibacterial agents such as silver, iodine and iodide complex, quaternary ammonium compounds, biguanide compounds, hydantoin derivatives, phosphonium compounds, and tetracycline antibiotics (Figure 1.9) have been

incorporated in or attached onto the surface of various materials such as textiles and medical devices, to kill bacteria.[28-33] Herein, we were specifically interested in cationic compounds or polymers with biguanide groups due to their potent antimicrobial activity. We aim at developing fiber-based fabrics containing these biocides serving as antimicrobial filters or to create biological protective clothing.
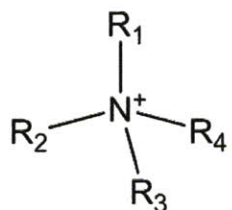
R: alkyl groups
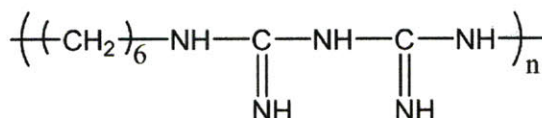
Quaternary ammonium   Poly (hexamethylene biguinide)
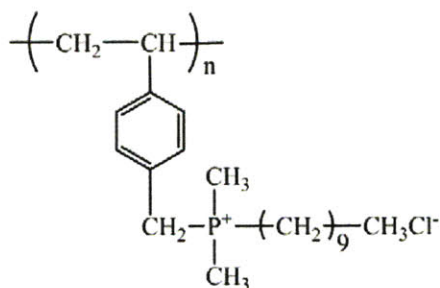
Poly[dimethyldecyl(4-vinylbenzyl) phosphonium chloride]
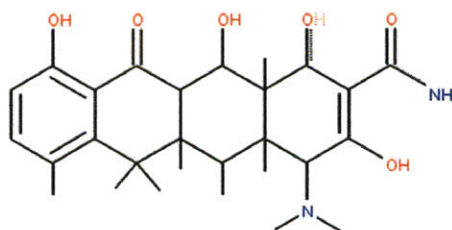
Tetracycline structure

Figure 1.9. Several representative biocides

1.2.5. Electrospinning

1.2.5.1 General description

Electrospinning is a fiber spinning technology that produces polymer fibers with a diameter range from micrometers down to several nanometers, two to three orders

of magnitude smaller than those produced by conventional fiber making methods. The electrospinning technology has been known for a long time. The discovery of electrospinning process dates back to the 1900s. In 1902, Morton patented the first electrospinning experimental setup for the production of fibers using electrostatic forces.[34] In the 1930s and 1940s, Formhals published a series of patents on the processing and apparatus to produce electrospun fibers.[35-38] However, at that time electrospinning gained little interest outside the filter industry due to its low output, low molecular orientation, poor mechanical strength of the fibers, and wide diameter distribution of the electrospun fibers. Until the 1990s, Reneker and coworkers reintroduced this technique as a facile way to produce submicron fibers.[39,40] Since then, electrospinning technology has attracted growing scientific interest and hundreds of natural and synthetic polymers have been processed into fibers by electrospinning for various applications.[41-47]
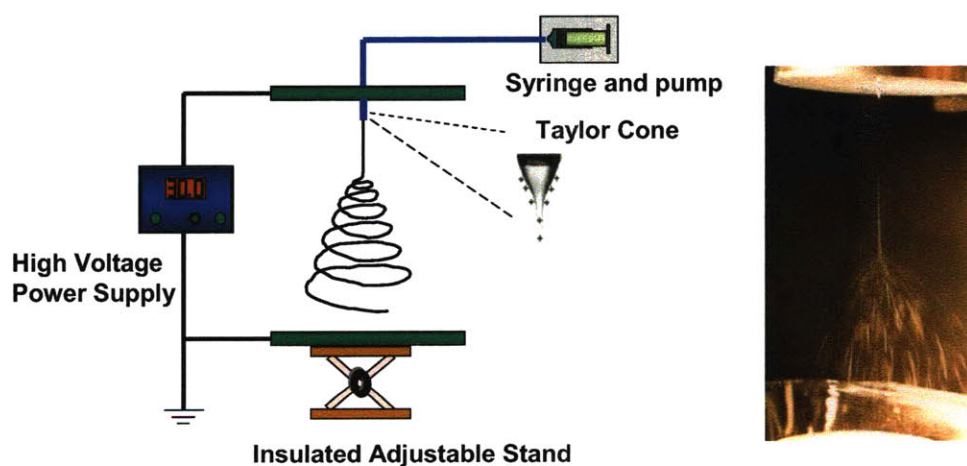
Figure 1.10. Electrospinning experimental setup

Electrospinning apparatus can be manufactured in different sizes and shapes. A schematic diagram of commonly used electrospinning experimental setup is shown in Figure 1.10. A polymer solution or melt is placed in a container and pumped through feed line to a nozzle. A high electric field is applied to polymer fluid such

that charges are induced within the fluid. Generally 10 to 40 kilovolts at around 100 microamperes of direct current (DC) are applied to the capillary during electrospinning. A typical distance between nozzle and grounded collector is 10 cm or more. Various grounded collectors have been used in the electrospinning. The most basic one (Figure 1.10) is one metallic disk or plate connected to the ground. Other designs include a conveyor belt or a coagulating solvent bath. In some cases, a rotating drum was used to collect aligned fibers.[48] The electrospinning process consists of three major regions: the cone region, the steady jet region and the instability region.[49] During the initial stage, a pedant drop of fluid is charged at the tip of the nozzle and deformed into a conical shape, the Taylor cone. When induced charges reach the critical point, a fluid jet erupts from the apex of the cone. In the steady jet region, the jet travels in a straight path ranging from 1 to 20 cm. In the instability region, the jet deviates from a straight path, undergoes a whipping instability and dries rapidly to produce porous fiber mats on the grounded collector. Please check the references [42, 47, 50-56] for more details about electrospinning process.

Although hundreds of polymer solutions and melts have been electrospun into fibers, not any polymer solutions can be processed by electrospinning. Furthermore, under different conditions, the morphology of the resultant electrospun fibers can be varied from beaded fibers to fibers with pores on their surfaces. Therefore, the parameters that affect the electrospinning process are of great interest and have been extensively studied.[47] The governing parameters can be primarily classed into two groups: polymer solution properties and processing conditions. Polymer solution properties have the most significant influence on the electrospinning process and resultant fiber morphology. They include solution viscosity, molecular weight of polymer, surface tension, solution conductivity, and dielectric effect of solvent. Although less important than solution properties, processing conditions, such as applied voltage, flow rate, temperature, humidity, design of collector, diameter of nozzle, and distance between nozzle and collector have a certain effect on the fiber

morphology. Please read the references [47, 57-68] for more details on how these parameters affect the electrospinning process and resultant fiber morphology. With the understanding of the effect of these parameters, it is possible for us to manipulate the electrospinning process, and design electrospun fiber materials and their morphologies.

1.2.5.2. Potential application in protection clothing and filters

Electrospun fibers are continuous and their assembly and processing is economically feasible as compared to carbon-based nanomaterials produced by bottom-up methods. Electrospun fiber mats possess remarkable properties such as small fiber diameter, high specific surface area, high porosity and low fabric weight. These unique properties have triggered a broad range of potential applications in composite materials, protective clothing and filtration membranes, catalysis, sensors, electronics, tissue engineering, drug delivery, magneto-responsive fibers, superhydrophobic membranes, energy storage devices and so on.[69-78]

The potential for application of electrospun fiber mats in protective clothing was first demonstrated by Schreuder-Gibson and coworkers.[2-4] They have studied the transport properties of electrospun fiber mats as barrier materials. Figure 1.11 shows that the electrospun nonwoven resistance to water vapor diffusion is much lower than the commercially available membrane laminates. On the other hand, the convective flow resistance of the electrospun fiber mats is much larger than that of the commercial clothing materials. They illustrated that the electrospun fiber mats possess high filtration efficiency for aerosol particle retention as well. In addition, Obendorf et al. showed that the addition of electrospun polypropylene or polyurethane fibers to a nonwoven fabric significantly limit the penetration of liquid pesticides while still maintaining good water vapor permeability.[5,79] The excellent breathability of electrospun materials with high rates of water vapor diffusion and low air permeability makes them promising candidates for protective fabrics applications.

30

(a)

Water Vapor Diffusion Resistance (s/m)

10^5
10^4
10^3
10^2
10^1
10^0

●········● Commercial Membrane Laminate (Sympatex)
O········O Commercial Membrane Laminate (Gore-Tex)
◇········◇ Polyacrylonitrile electrospun membrane
◻──────◻ PTFE microporous membrane
▽──────▽ Polybenzimidazole electrospun membrane

.2   .4   .6   .8

Mean Relative Humidity

(b)

Darcy Flow Resistance (m^{-1})

10^{10}
10^9
10^8
10^7
10^6

PBI Electrospun

PTFE Microporous Membrane (Wind Barrier)

PAN Electrospun

Tightly-Woven Cotton Fabric
Which Shows Humidity-Dependent Permeability

Knit Polyester Fabric

Nonwoven Batting (thermal insulation layer)

0   .2   .4   .6   .8   1.0

Relative Humidity

Figure 1.11. Transport properties of electrospun materials. (a) water vapor transport; (b) convective gas flow resistance. (reprinted from reference [2])

Besides the excellent breathability, the high specific surface areas of electrospun fiber mats provide a carrier for the attachment of functional compounds to obtain self-detoxifying protective clothing. Ramakrishna *et al.* successfully electrospun fibers with a reactive compound, (3-carboxy-4-iodosobenzyl) oxy-β-cyclodextrin, and showed that these reactive fabrics can decompose paraoxon, a chemical warfare agent (CWA) simulant.[80] In another study, electrospun composite materials containing zinc titanate or MgO nanoparticles were produced and tested as reactive sorbents able to detoxify nerve and mustard agent simulants.[81,82] Layer-by-layer electrostatic assembly technique was applied to take advantage of high surface area of electrospun materials for producing protection clothing as well. Photo-catalytic titanium dioxide

31

functional coatings were assembled onto various electrospun materials to provide protection against mustard agent stimulant or toxic industrial chemicals.[83,84] Various biocides such as silver nanoparticles, quaternary ammonium salts or their derivatives, compounds with biguanide groups, and N-halamine, have been incorporated into electrospun fiber membranes to serve as antimicrobial filters or to create a biological protective clothing.[85-88]

1.3. Research goal

The overall research goal of this thesis is to develop electrospun fiber-based reactive and/or bactericidal fabrics for chemical and biological protection and air filtration, which can be potentially incorporated as key functional layer(s) in the next generation of protective clothing and air filtration media. There are several specific objectives involved in this work:

1. Development of reactive and catalytic electrospun fabrics containing α-nucleophiles for selective capture and decomposition of organophosphate chemical nerve agents and pesticides

2. Development of electrospun fabrics containing biocides for biological protection

3. Evaluation of the performance of reactive and/or bactericidal fabrics as functional layer(s) for chemical and biological detoxifying protective fabrics

4. Evaluation of breathability of functionalized electrospun fabrics for protective fabrics filters and masks.

1.4. Research Overview

This dissertation describes the author's work in the development of electrospun fiber-based lightweight, breathable, chemical and biological detoxifying protective fabrics. Figure 1.12 shows the general strategies used in this thesis to generate functionalized electrospun fiber mats containing α-nucleophilic oxime functional compounds and/or bactericidal agents with biguanide functional groups.
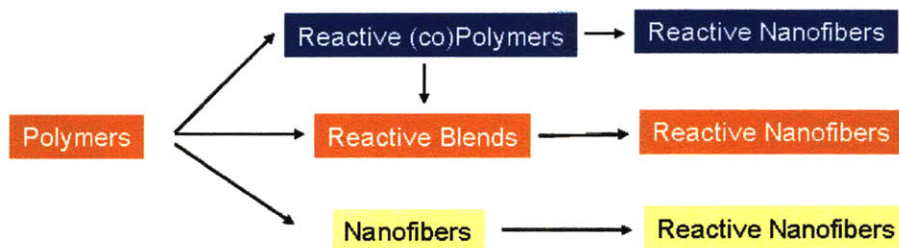
Figure 1.12. General strategies applied to generate functionalized fiber mats

In chapter 2, we present a strategy of electrospinning a polymer blend containing reactive polyacrylamidoxime and parent polyacrylonitrile to fabricate reactive/catalytic fiber mats. In chapter 3, we develop a surface chemical modification strategy to convert surfaces of prefabricated polyacrylonitrile fibers to reactive amidoxime functional groups. The excellent performance of these reactive fibers to decompose toxic organophosphate toxic agents in the presence of moisture is demonstrated. In chapter 4, we apply similar strategies used in chapter 2 and 3 to develop bactericidal fiber mats either by electrospinning polymer blends containing a biocide, chlorhexidine, or by a post-spin treatment strategy to immobilize covalently chlorhexidine onto fibers via titanate crosslinkers. In chapter 5, we adopt layer-by-layer electrostatic assembly technique to functionalize the surfaces of electrospun fibers with reactive polyanion, polyhydroxamic acid, and antimicrobial

polycation, poly(*N*-vinyl guanide), which are capable of decomposing both toxic chemical nerve agents and bacterial contaminants simultaneously. In chapter 6, we conclude this thesis and provide suggestions for future work.

1.5. References

1. Schreuder-Gibson, H. L.; Truong, Q.; Walker, J. E.; Owens J. R.; Wander, J. D.; Jones, W. E. *MRS Bulletin* 2003, *28*, 574.

2. Gibson, P.; Schreuder-Gibson, H. L.; Rivin, D. *Colloids Surf. A* 2001, 187-188, 469.

3. Gibson, P. W.; Schreuder-Gibson, H. L.; Rivin, D. *AICHE Journal* 1999, 45, 190.

4. Gibson, H. L.; Gibson, P.; Senecal, K.; Sennett, M.; Walker, J.; Yeomans, W.; Ziegler, D.; Tsai, P. P. *J. Adv. Mater.* 2002, 34, 44.

5. Lee, S.; Obendorf, S. K. *J. Appl. Polym. Sci.* 2006, 102, 3430.

6. Eyper, P. *Toxicol. Rev.* 2003, 22, 165.

7. Liddell-Hart, B. H. A History of the World War, 1914-1948, Boston: Little. Brown & Co.

8. Sadik, O. A. *et al* Electroanalysis 2003, 15, 1149.

9. Robinson, J. R. The Problem of Chemical and Biological Warfare, vol. 1, the Risk of CB Weapons. New York: Humanities Press; 1971.

10. Chambers, J. E. Organophosphates: chemistry, fate and effects, San Diego, California: Academic Press, Inc. 1992.

11. Yang, Y. *Acc. Chem. Res.* 1999, 32, 109.

12. Yang, Y. *et al.* , *Chem. Rev.* 1992, 92, 1729.

13. Wagner, G. W. *et al.*, *Ind. Eng. Chem. Res.* 2002, 41, 1925.

14. Bromberg, L.; Hatton, T. A. *Ind. Eng. Chem. Res.* 2005, 44, 7991.

15. Benning, M. M. *et al.*, *Biochemistry* 1994, 33, 15001.

16. Lai, K. *et al.*, *Arch. Biochem. Biophys.* 1995, 318, 59.

17. Rastogi, V. K. *et al.*, *Biochem. Biophys. Res. Commun.* 1997, 241, 294.

18. Magee, R. S. Chemical stockpile disposal program: The search for alternative technologies. In *Effluents from Alternative Demilitarization Technologies*; Holm, F. W., Ed.; Kluwer: Dordrecht, The Netherlands, 1998; Vol. 22.

19. Amos, D.; Leake, B. *J. Hazard. Mater.* 1994, 39, 107.

20. Mass, R. A. *et al., J. Org. Chem.* 1990, 55, 2064.

21. Mar Herrador, M. *et al., J. Med. Chem.* 1985, 28, 146.

22. Simanenko, Y. S. *et al., Langmuir* 2001, 17, 581.

23. Couderc, S.; Toullec, J. *Langmuir* 2001, 17, 3819.

24. Bracken, K.; Moss, R. A.; Ragunathan, K. G. *J. Am. Chem. Soc.* 1997, 119, 9323.

25. Takasaki, B. K.; Chin, J. *J. Am. Chem. Soc.* 1995, 117, 8582.

26. Furue, M.; Sumi, K.; Nozakura, S. *J. Poly. Scil, Poly. Lett.* 1982, 20, 291.

27. Costerton, J. W.; Stewart, P.S.; Greenberg, E. P. *Science* 1999, 284, 1318.

28. Lin, J.; Qiu, S.; Lewis, K.; Klibanov, A. M. *Biotechnol. Bioeng.* 2003, 83, 168.

29. Sun, Y.; Sun, G. *J. Appl. Polym. Sci.* 2003, 88, 1032.

30. Danese, P. N. *Chem. Biol.* 2002, 9, 873.

31. Ruggeri, V.; Francolini, I.; Donelli, G.; Piozzi, A. *J. Biomed. Mater. Res. A* 2007, 81A, 287.

32. Morris, C.E.; Welch, C. M. *Textile Res. J.* 1983, 53, 143.

33. Tashiro, T. *Macromol. Mat. Eng.* 2001, 286, 63.

34. Morton, M. Methods of dispersing fluid, 1902, US Patent 705691.

35. Formhals, A. Processing and apparatus for preparing artificial threads, 1934, US Patent 2,077,373.

36. Formhals, A. Method of producing artificial fibers, 1939, US Patent 2,158,415.

37. Formhals, A. Production of artificial fibers from fiber forming liquids, 1943, US Patent 2,323,025.

38. Formhals, A. Method and apparatus for spinning, 1944, US Patent 2,349,950.

39. Doshi, J.; Reneker, D. H. *Journal of Electrostatics* 1995, 35, 151.

40. Reneker, D. H.; Chun, I. *Nanotechnology* 1996, 7, 216.

41. Dzenis, Y. *Science* 2004, 304, 1917.

42. Rutledge, G. C.; Fridrikh, S. V. *Adv. Drug Delivery Rev.* 2007, 59, 1384.

43. Reneker, D. H.; Yarin, A. L. *Polymer* 2008, 49, 2387.

44. Greiner, A.; Wendorff, J. H. *Angew. Chem. Int. Ed.* 2007, 46, 5670.

45. Li, D.; Xia, Y. *Adv. Mater.* 2004, 16, 1151.

46. Ramakrishna, S.; Fujihara, K.; Teo, W. E.; Yong, Y.; Ma. Z. W.; Ramaseshan, R. *Materials Today* 2006, 9, 40.

47. Ramakrishna, S.; Fujihara, K.; Teo, W.-E.; Lim, T.-C.; Ma. Z. *An Introduction to Electrospinning and Nanofibers*, World Scientific Publishing Company: Singapore, 2005.

48. Theron, A.; Zussman, E.; Yarin, A. L. *Nanotechnology* 2001, 12, 384.

49. Yu, J. H. Electrospinning of polymeric nanofiber materials: process characterization and unique applications, MIT thesis, 2007.

50. Reneker, D. H.; Yarin, A. L.; Fong, H. Koombhongse, S. *J. Appl. Phys.* 2000, 87, 4531.

51. Yarin, A. L.; Koombhongse, S.; Reneker, D. H. *J. Appl. Phys.* 2001, 89, 3018.

52. Yarin, A. L.; Koombhongse, S.; Reneker, D. H. *J. Appl. Phys.* 2001, 90, 4836.

53. Shin, Y. M.; Hohman, M. M.; Brenner, M. P.; Rutledge, G. C. *Appl. Phys. Lett.* 2001, 78, 1149.

54. Hohman, M. M.; Shin, M.; Rutledge, G.; Brenner, M. P. *Phys. Fluids* 2001, 13, 2201.

55. Hohman, M. M.; Shin, M.; Rutledge, G.; Brenner, M. P. *Phys. Fluids* 2001, 13, 2221.

56. Fridrikh, S. V.; Yu, J. H.; Brenner, M. P.; Rutledge, G. C. *Phys. Rev. Lett.* 2003, 90, 144502.

57. Shenoy, S. L.; Bates, W. D.; Frisch, H. L.; Wnek, G. E. *Polymer* 2005, 46, 3372.

58. Zhong, X. H.; Kim, K. S.; Fang, D. F.; Ran, S. F.; Hsiao, B. S.; Chu, B. *Polymer* 2002, 43, 4403.

59. Megelski, S.; Stephens, J. S.; Chase, D. B.; Rabolt, J. F. *Macromolecules* 2002, 35, 8456.

60. Zeng, J.; Xu, X.; Chen, X.; Liang, Q.; Bian, X.; Yang, L.; Jing, X. *J. Control Release* 2003, 92, 227.

61. Choi, J. S. *et al.*, *Int. J. Bio. Macromol.* 2004, 34, 249.

62. Son, W. K. *et al.*, *Polymer* 2004, 45, 2956.

63. Lee, K. H. *et al.*, *Polymer* 2003, 44, 1287.

64. Deitzel, J. M. *et al.*, *Polymer* 2001, 42, 261.

65. Demir, M. M. *et al.*, *Polymer* 2002, 43, 3303.

66. Yang, Y. *et al.*, *J. Polym. Eng.* 2008, 28, 67.

67. Liu, H. Q.; Hiseh, Y. L. *J. Polym. Sci. Pol. Phys.* 2002, 40, 2119.

68. Mo, X. M. *et al.*, *Biomaterials* 2004, 25, 1883.

69. Ma, Z. W.; Kotaki, M.; Inai, R.; Ramakrishna, S. *Tissue Eng.* 2005, 11, 101.

70. Roso, M.; Sundarrajan, S.; Pliszka, D.; Ramakrishna, S.; Modesti, M. *Nanotechnology* 2008, 19, 285707/1-285707/6.

71. Yoon, K.; Hsiao, B. S.; Chu, B. *J. Mater. Chem.* 2008, 18, 5326.

72. Thavasi, V.; Singh, G.; Ramakrishna, S. *Energy Environ. Sci.* 2008, 1, 205.

73. Kim, I. D.; Rothschild, A.; Lee, B. H.; Kim, D. Y.; Jo, S. M.; Tuller, H. L. *Nano Lett.* 2006, 6, 2009.

74. Wang, M.; Hsieh, A. J.; Rutledge, G. C. *Polymer* 2005, 46, 3407.

75. Wang, X.; Kim, Y.; Drew, C.; Ku, B.; Kumar, J.; Samuelson, L. A. *Nano Lett.* 2004, 4, 331.

76. Li, D.; Wang, Y.; Xia, Y. *Nano Lett.* 2003, 3, 1167.

77. Jin, H.-J.; Chen, J. Karageorgious, V.; Altman, G. H.; Kaplan, D. L. *Biomaterials* 2004, 25, 1039.

78. Pinto, N, J.; Johnson, A. T.; MacDiarmid, A. G.; Mueller, C. H.; Theofylaktos, N.; Robinson. D. C. *et al.*, *Appl. Phys. Lett.* 2003, 83, 4244.

79. Lee, S.; Obendorf, S. K. *Fibers and Polymers* 2007, 8, 501.

80. Ramaseshan, R.; Sundarrajan, S.; Liu, Y.; Barhate, R. S.; Lala, N. L.; Ramakrishna, S. *Nanotechnology* 2006, 17, 2947.

81. Ramaseshan, R.; Ramakrishna, S. *J. Am. Ceram. Soc.* 2007, 90, 1836.

82. Sundarrajan, S.; Ramakrishna, S. *J. Mater. Sci.* 2007, 42, 8400.

83. Lee, J. A.; Krogman, K. C.; Ma, M.; Hill, R. M.; Hammond, P. T.; Rutledge, G. C. *Adv. Mater.* 2009, 21, 1252.

84. Krogman, K. C.; Lowery, J. L.; Zacharia, N. S.; Rutledge, G. C.; Hammond, P. T. *Nat. Mat.* 2009, 8, 512.

85. Lala, N. L.; Ramaseshan, R.; Bojun, L.; Sundarrajan, S.; Barhate, R. S.; Ying-jun, L.; Ramakrishna, S. *Biotechnol. Bioeng.* 2007, 97, 1357.

86. Fu, G-D.; Yao, F.; Li, Z.; Li, X. *J. Mater. Chem.* 2008, 18, 859.

87. Fan, L.; Du, Y.; Zhang, B.; Yang, J.; Zhou, J.; Kennedy, J. F. *Carbohydr. Polym.* 2006, 65, 447.

88. Tan, K.; Obendorf, S. K. *J. Membr. Sci.* 2007, 305, 287.

Chapter 2

Electrospun Polyacrylamidoxime Nanofiber Mats

2.1. Introduction

The first strategy, which we tried to develop to achieve reactive/catalytic electrospun fiber mats, is shown in Figure 2.1. We intend to synthesize reactive polymers first, followed by processing them into reactive fiber mats.

Monomers

Polymers

Reactive (co)Polymers → Reactive Nanofibers

Figure 2.1. The first strategy to achieve reactive fibers

Aiming at achieving reactive polymers with α-nucleophilic functional groups such as oxime or imidazole groups, we proceeded to synthesize several reactive polymers. Polyacrylonitrile (PAN) was used for modification by conversion of the acrylonitrile groups to functional acrylamidoxime, as shown in Figure 2.2. Along with the polymer modification to obtain reactive polymer, we employed free-radical polymerization to obtain copolymer poly(vinylimidazole-co-styrene) with functional imidazole groups (Figure 2.3). We have further synthesized poly(4-vinylpyridine-co-styrene) copolymer, which was oximated by a two-step synthetic route, first modifying the pyridine with phenacylketone functionality, followed by converting phenacylketone to phenacyloxime (Figure 2.3). Given the reactivity of these reactive polymers and ease of synthesis, our study primarily focused on one reactive polymer, polyacrylamidoxime (PAAO).
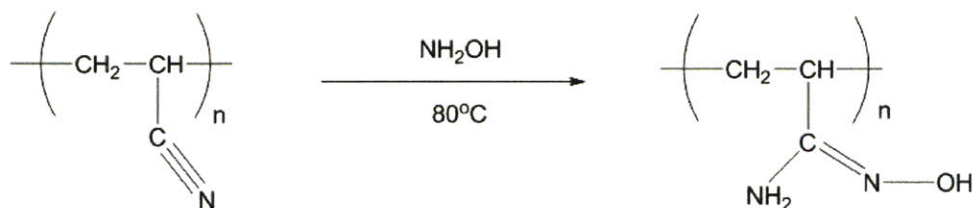
Figure 2.2. Modification of polyacrylonitrile to polyacrylamidoxime

(a)
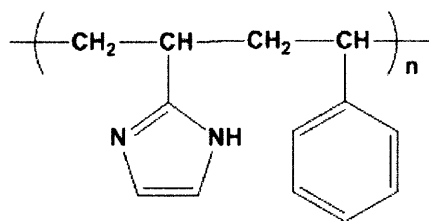
(b)
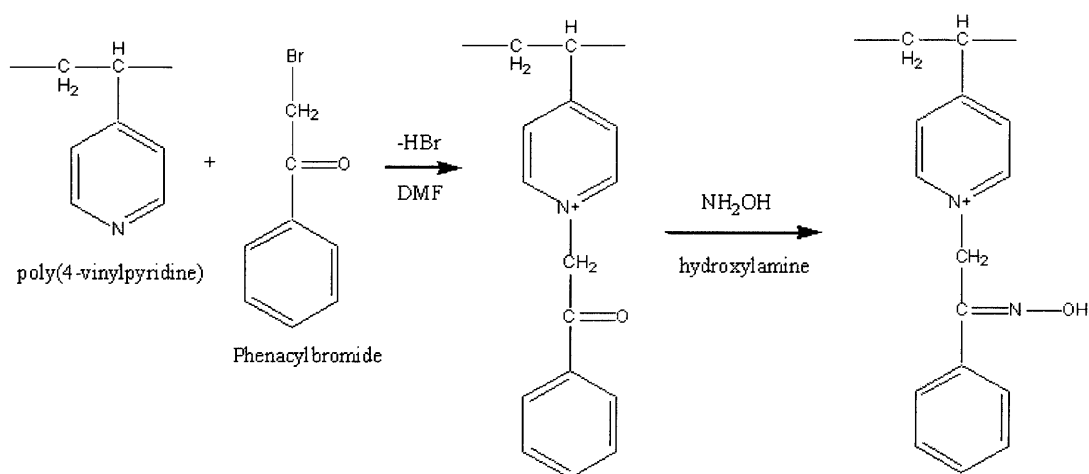
Figure 2.3. Synthesized reactive polymers. (a) poly(vinylimidazole-co-styrene); (b) poly(4-vinylpyridine-N-phenacyloxime).

In this chapter, we report on catalytic, electrospun, nonwoven nanofiber mats composed of PAAO blended with PAN, which potentially can be incorporated into chemical detoxifying protection clothing as reactive/catalytic layer(s). The oxime groups or oximate ions are among the most powerful α-nucleophiles because of the electronic repulsion between the lone electron pair on the nucleophilic oxygen atom and on the adjacent nitrogen atom, which can be reduced and consequently stabilize the transition state upon nucleophilic attack onto a substrate. Therefore, oximes are capable of nucleophilic hydrolysis of ester groups. It is known that oximate ions are 100-fold more

reactive than phenolate ions of the same pK$_a$.[1] Oximes have been widely used as reactivators of acetylcholinesterase inhibited by organophosphate pesticides or nerve agents, i.e., as antidotes.[2] Colloidal oximes in the form of micelles and particles have been studied in connection with the decomposition of organophosphates or nitrophenyl acetate,[1, 3-8] and it has been shown that the hydrolysis of phosphate esters or analogous substrates is catalyzed efficiently by oximate ions or oximes. In this work, we have selected p-nitrophenyl acetate (PNPA) as a model compound for the more toxic organophosphates or chemical nerve agents, and have studied the catalytic properties of PAAO/PAN electrospun nanofiber mats on the hydrolysis of this substrate. Hydrolytic pathways of the PNPA esterolysis have been widely used to elucidate nucleophilic decomposition of more toxic organophosphates.[9,10] In addition, the capability of PAAO to decompose combat chemical warfare agents (CWA), such as O-pinacolyl methylphosphonofluoridate (soman or GD) and S-2-(diisopropylamino)ethyl O-ethyl methylphosphonothioate (VX), was demonstrated.

2.2. Experimental method

2.2.1 Materials

Polyacrylonitrile (PAN) (M_w 150kDa) was purchased from Polysciences Inc. (Warrington, PA) and used as received. *N,N*-dimethylformamide (DMF), dimethyl sulfoxide (DMSO), hydroxylamine hydrochloride and *p*-nitrophenyl acetate (PNPA) were purchased from Sigma-Aldrich Chemical Co. (St. Louis, MO) and used as received.

2.2.2. Reactive polymer preparation
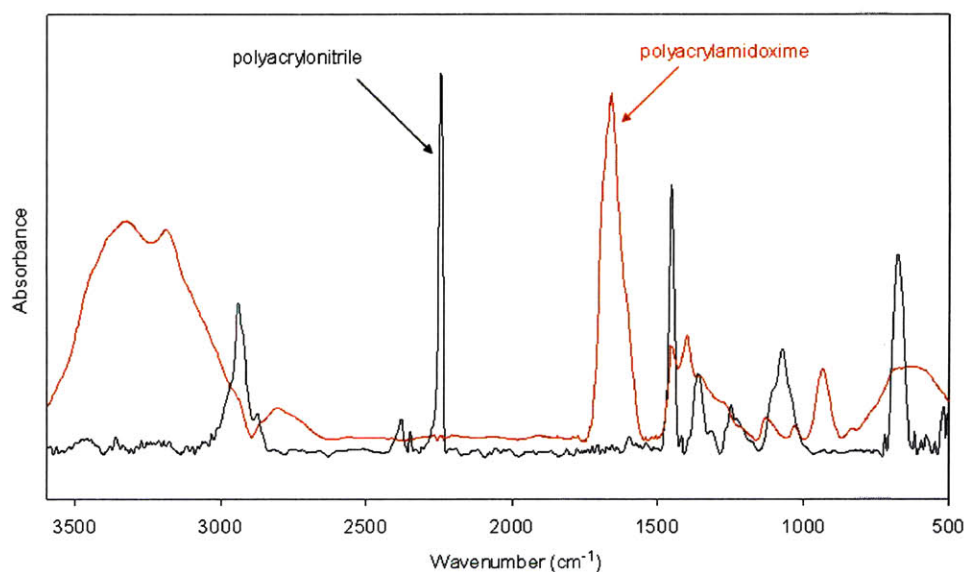
Figure 2.4. FTIR spectra of untreated PAN and PAAO that resulted from the treatment of PAN with hydroxylamine

PAN was modified to obtain reactive/catalytic PAAO by conversion of acrylonitrile groups to acrylamidoximes via reaction of PAN with excess hydroxylamine hydrochloride in methanol or DMF at 80°C under reflux for 24 hours, as shown in Figure

45

2.2. The resulting polymers were repeatedly washed with methanol, acetone and water followed by drying under vacuum until constant weight. Figure 2.4 shows FTIR spectra of the unmodified PAN and of the PAAO product. Complete conversion of acrylonitrile groups of PAN to the amidoxime groups was confirmed by observing the disappearance of the original nitrile groups of PAN at 2260 cm^{-1} (stretching vibration of nitrile group) and appearance of the acrylamidoxime groups (stretching vibration of C=N at 1670 cm^{-1}, scissors vibration of NH_2 at 1610 cm^{-1} and stretching vibration of NH_2 and OH at 3100-3600 cm^{-1}).

2.2.3. Electrospinning
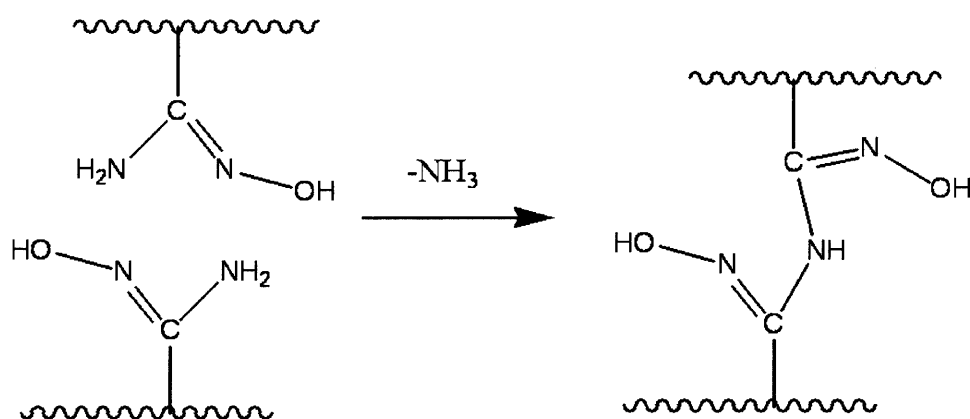
Figure 2.5. Formation of glutaroimide-dioxime bonds between polyacrylamidoxime chains.

The well-documented formation of the glutaroimide-dioxime links between PAAO segments (Figure 2.5) limits the solubility of PAAO in common organic solvents.[11] The poor solubility of PAAO in common solvents render PAAO solution/suspension lack of sufficient elasticity for successful electrospinning of pure PAAO solution/suspension into uniform fibers. Instead the spherical droplets were obtained rather than uniform fibers, as shown in Figure 2.6. Therefore, PAAO was

blended with parent PAN to increase the solution/suspension elasticity, which facilitated the electrospinning process to obtain reactive fibers containing PAAO.
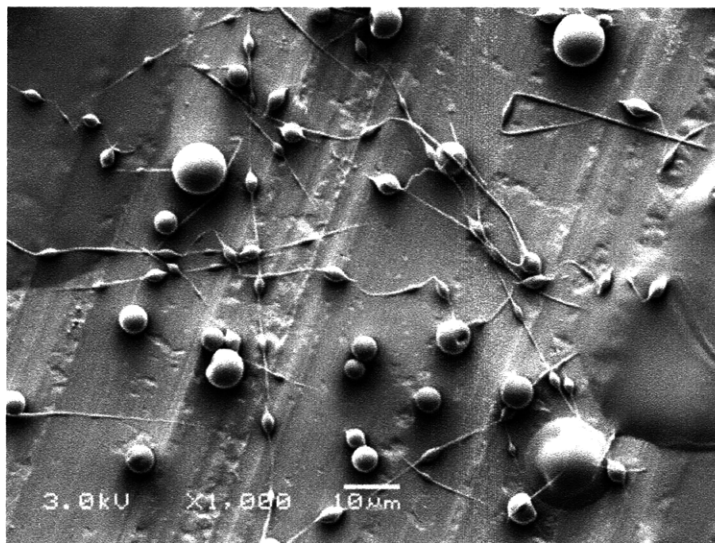
Figure 2.6. A typical SEM image of electrospun pure PAAO solution/suspension

In our experiments, the PAAO did not dissolve in DMF but was observed to form clear solutions in DMSO at polymer concentrations not exceeding 2 wt%. At larger PAAO concentrations in DMSO, some turbidity ensued. On the other hand, DMF appeared to be a good solvent for PAN and was observed to facilitate the electrospinning process. Therefore, a DMF/DMSO solvent mixture that afforded stable suspensions of partially dissolved PAAO in viscous PAN solutions was used in this work. The unmodified PAN was blended with PAAO to increase the total polymer concentration in order to provide sufficient elasticity of the solution or dispersion for successful electrospinning. A homogenized 6-8 wt% PAAO/PAN (1:1 by weight) blend was prepared by dissolution in DMF: DMSO (85:15 w/w) under vigorous stirring for several days at room temperature.
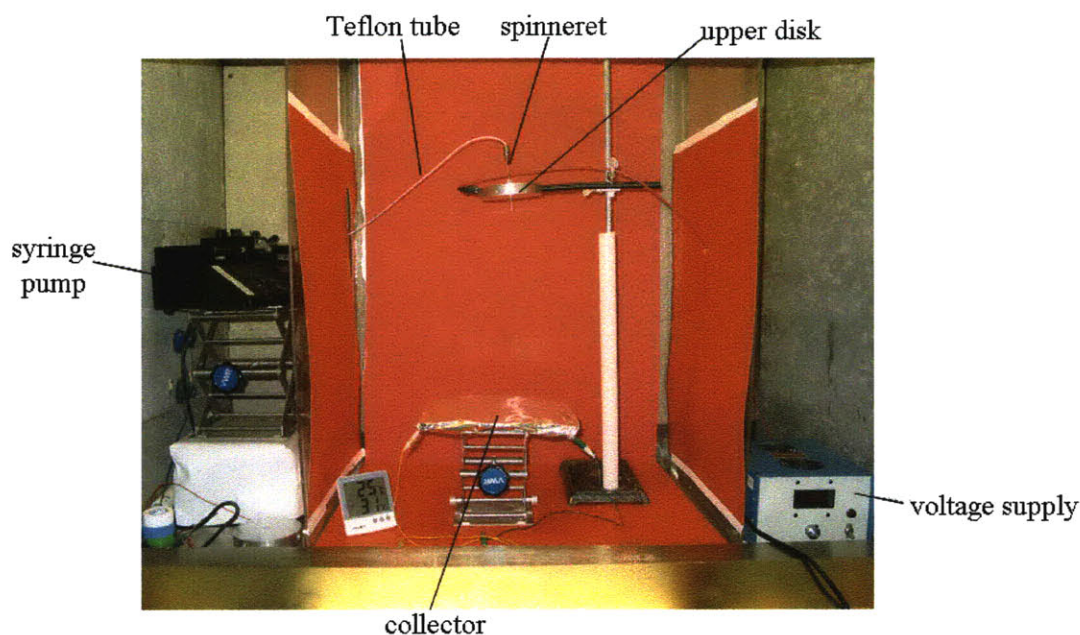
Figure 2.7. Electrospinning apparatus

A parallel plate electrospinning setup previously described by Shin *et al.*[12] was used. Figure 2.7 shows the photo image of the electrospinning apparatus used in our lab. Two aluminum disks 15 cm in diameter were arranged parallel at 20-30 cm apart. The polymer suspension was delivered to a capillary nozzle via a Teflon feedline from a syringe pump (Harvard Apparatus PHD 2000, Holliston, MA). Three sizes of nozzles were used: 1.02 mm (0.04"), 0.76 mm (0.03") and 0.51 mm (0.02") in inner diameter. Most nanofibers used in this study were electrospun from the nozzle of 1.02 mm in diameter. The other two nozzles were used for producing nanofibers of various sizes to study the effect of fiber size on the fiber performance. The spinneret protruded through the center of the upper plate to a length of 2 cm. A power supply (Gamma High Voltage Research ES-30P, Ormond Beach, FL) provided up to 30 kV to the upper disk. In some cases, a rotating drum ground electrode was used to collect the electrospun nanofibers since the nanofibers were charged and difficult to collect on a plate collector. The applied electrical potential (25-30 kV), the solution flow rate (0.005 ml/min) and the

distance between the capillary tip and the collector (20-30 cm) were adjusted to obtain a stable jet.

2.2.4. Characterization

Morphology of the electrospun fibers was visualized by scanning electron microscopy (SEM, JEOL-6060). A thin layer of gold was sputter-coated onto the nanofibers. Fiber diameters were determined using AnalySIS image processing software (Soft Imaging System Corp., Lakewood, CO).

Fourier transform infrared spectra (FTIR) were measured using a Nexus 870 spectrophotometer (Thermo Nicolet Corp., Madison, WI) in absorbance mode by accumulation of 256 scans with a resolution of 4 cm^{-1}.

BET surface areas of electrospun nanofibers were determined with an ASAP 2020 accelerated surface area and porosimetry analyzer (Micromeritics Instrument Co., Norcross, GA).

Kratos Axis Ultra Imaging X-ray Photoelectron Spectrometer (XPS) (Kratos Analytical Co., Chestnut Ridge, NY) was used to measure the surface compositions of nanofibers with a monochromatized Al K$_\alpha$ X-ray source.

2.2.5. Kinetics of PNPA hydrolysis

Hydrolysis kinetics were measured using a Hewlett Packard 8453 UV-Vis spectrophotometer equipped with a thermostated cell compartment. The time progression of the reaction of PNPA with the nanofibers was followed by measuring the appearance of the p-nitrophenolate ions at 405 nm. Because of the negligible solubility of the PNPA in water as well as limited wettability of the PAAO/PAN nanofiber surface by water, a mixture of 50 mM Tris buffer and ethanol was applied as a reaction milieu. In a typical experiment, 1 ml of freshly made PNPA/ethanol solution was added into a suspension of

a weighed amount of the electrospun nanofibers in 9 ml of stirred 50 mM Tris buffer/ethanol (1:1 by volume) solution. The pH value of the reaction medium was adjusted before the commencement of the reaction and measured after the reaction by a digital pH meter to assure the pH did not change during the course of the reaction. The temperature was maintained at 25 °C.

2.2.6. Kinetics of CWA degradation mediated by PAAO[35]

Before the kinetics measurements, a weighed PAAO powder sample was placed in a sealed vial of 100% relative humidity at room temperature to allow the polymer to absorb water until it equilibrated. The hydrated PAAO sample was packed into 5 mm zirconium high-resolution magic angle spinning (HRMAS) rotors and weighed. The weights of the polymer samples ranged between 35-85 mg, affording a large molar excess of the oxime groups compared to the CWA (soman (GD) and VX). The kinetic measurement commenced with the addition of 1 μL (~1 mg) of a CWA by a pipette onto the polymer sample. The agents appeared to rapidly soak into the polymer samples without beading up. Rotors were capped and inserted into the instrument and spun up to the MAS spinning rate. Between the NMR experiments, the samples were removed and stored at room temperature. All experiments with CWA were performed using a Bruker Avance 500 spectrometer, operating at 202.46 MHz (^{31}P). The HRMAS spectra were recorded with a 5-mm Bruker ^{31}P gradient probe at ambient temperature (23 °C) using a 1-D proton decoupled decay experiment with the magic angle spinning rate of 5000 Hz.

2.3. Results and Discussion

2.3.1. Reactive fiber characterization
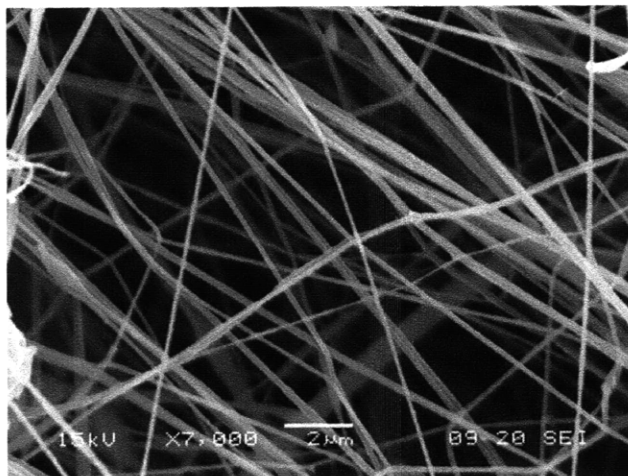
Figure 2.8. A typical SEM image of electrospun PAAO/PAN nanofibers (average fiber diameter: 170±40 nm, scale bar: 2 μm)

Figure 2.8 shows a typical SEM image of the electrospun PAAO/PAN nanofibers produced in this work. The average diameter of these nanofibers was about 170 nm with the fiber diameters ranging from 100 to 300 nm. The measured BET surface area of these nanofibers was about 14.8 m^2/g. Characteristic peaks of the nitrile groups (2260 cm^{-1}) and amidoximes (1670 cm^{-1}, 1610 cm^{-1} and 3100-3600 cm^{-1}) were observed in the FTIR spectra of PAN/PAAO nanofibers, which confirmed the presence of both PAN and PAAO in the nanofibers. Furthermore, elemental analysis showed that the initial ratio of the PAN to PAAO (1:1 by weight) set in the electrospun dispersion was maintained in the fibers.

2.3.2. PNPA hydrolysis catalyzed by PAAO/PAN fibers
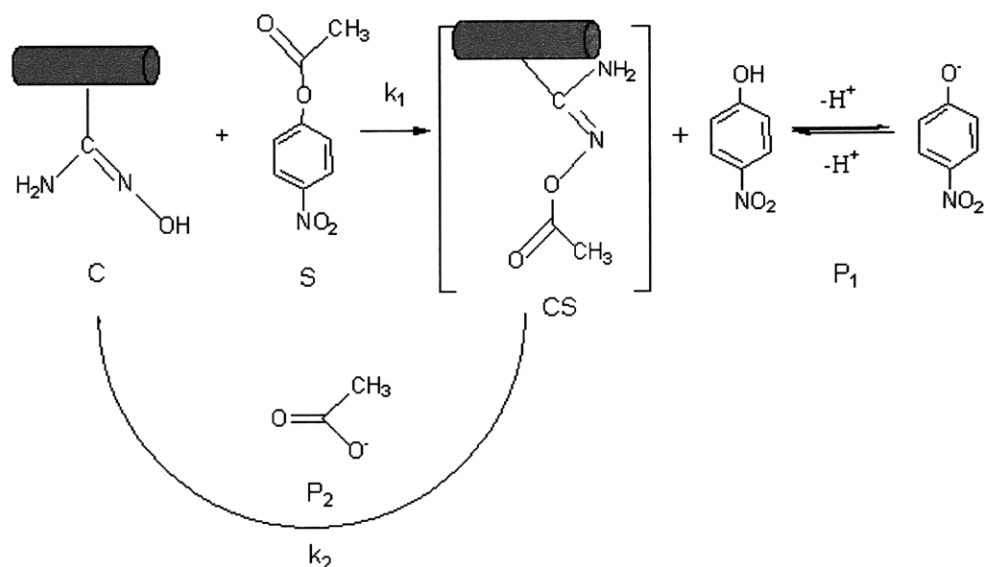
Figure 2.9. Catalytic hydrolysis of PNPA by acrylamidoxime groups on the nanofibers

The mechanism of esterolytic cleavage of PNPA by nucleophiles in homogeneous solutions has been investigated in some detail.[13-16] The novelty of this work stems from the fact that the hydrolysis occurs in a heterogeneous system with catalytic nanofibers that are insoluble in the aqueous/ethanol medium in which the substrate PNPA is dissolved. The pathway of the PNPA nucleophilic hydrolysis in aqueous media is well established.[17,18] Figure 2.9 shows a schematic diagram of the PNPA hydrolysis catalyzed by the electrospun PAAO/PAN nanofibers. The PNPA substrate (S) is attacked by the catalytic acrylamidoxime group (C), which results in a polymer with acetylated acrylamidoxime groups (CS) and a product (P$_1$) comprising a mixture of nitrophenol and nitrophenolate ions. The precise composition of the product P$_1$ depends on the pH of the reaction medium, with the p-nitrophenol possessing a pK$_a$ of 7.2.[19] Water facilitates the deacetylation of the transition compound (CS) and regeneration of the catalytic oxime groups (C), releasing the acetate product (P$_2$) into the medium.
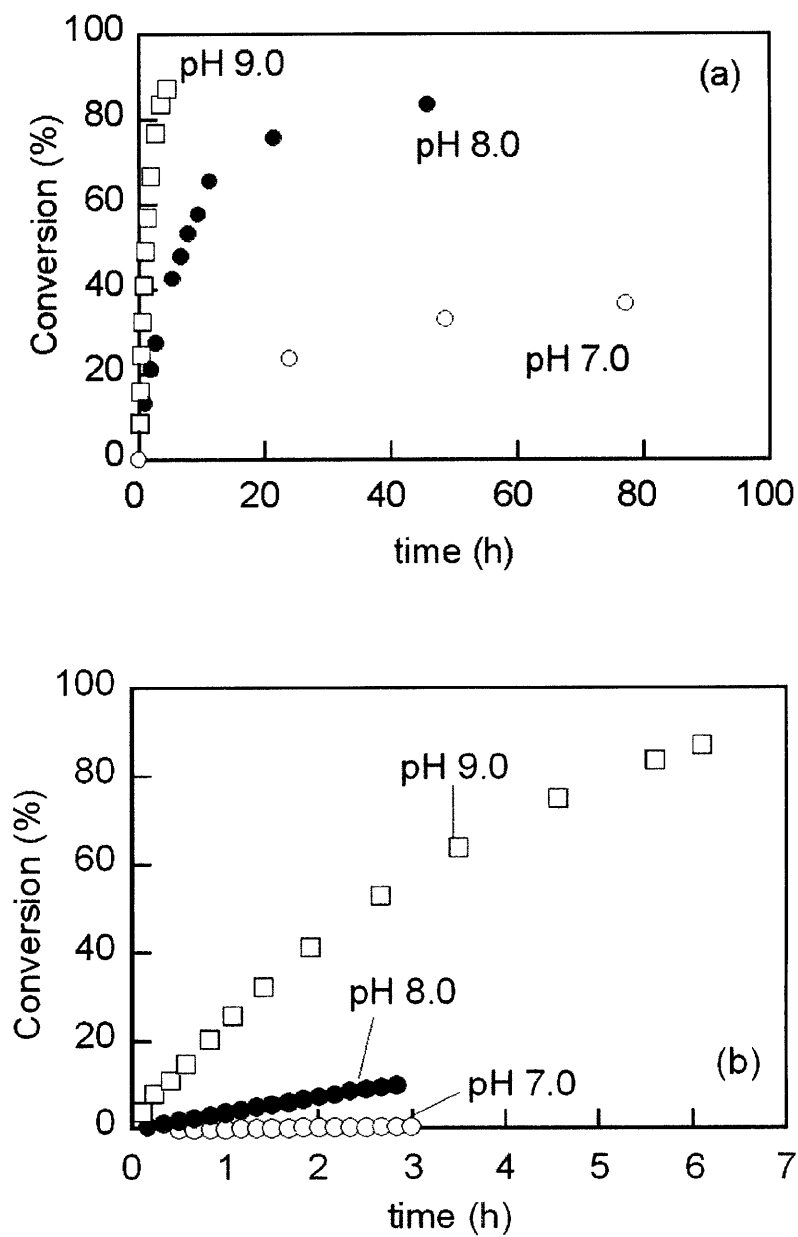
Figure 2.10. Kinetics of PNPA conversion with (a) and without (b) nanofibers presented as functions of pH. $[Ox]_a=2.91$ mM, $[PNPA]_o=5.52\times10^{-5}$ M.
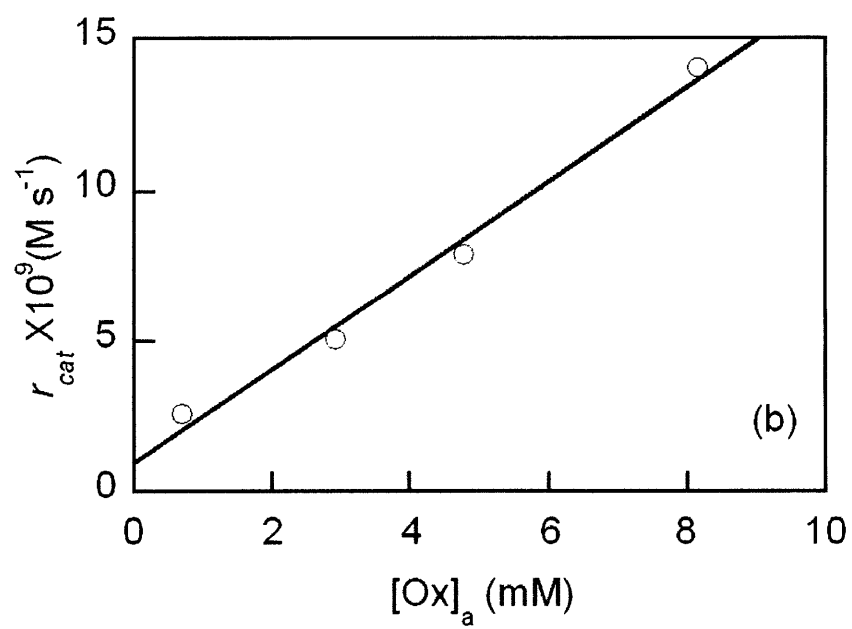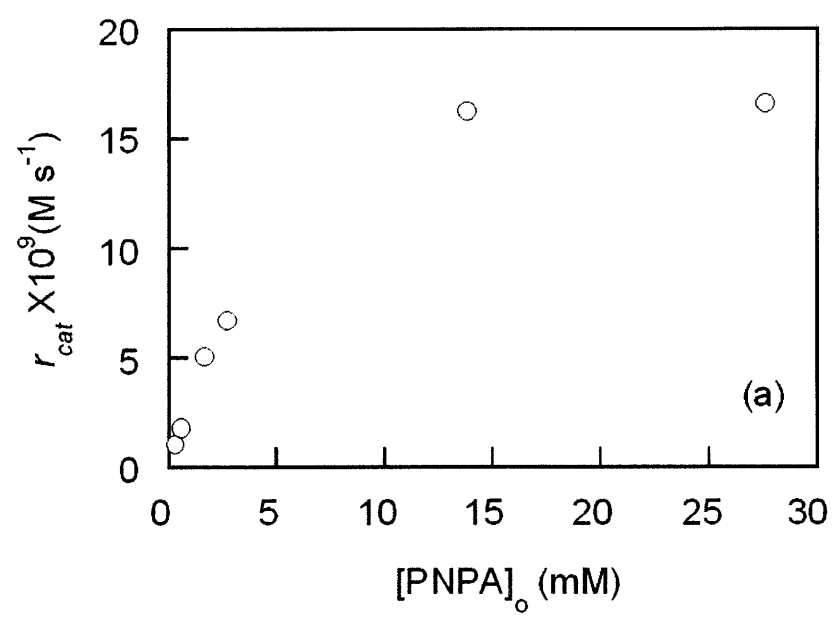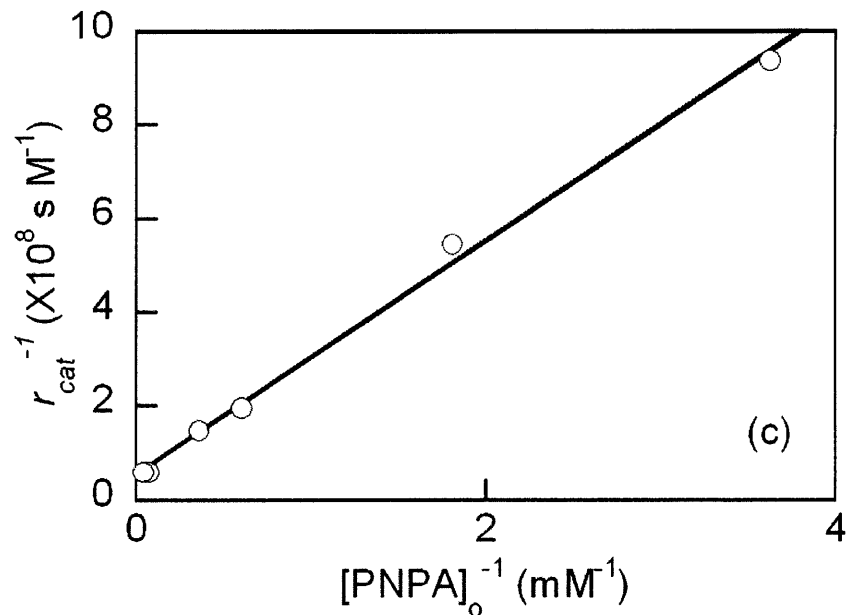
Figure 2.11. Observed catalytic reaction rate (r_{cat}) as a function of the initial substrate concentration ($[PNPA]_o$) and apparent concentration of the oxime groups in the fibers ($[Ox]_a$). pH=7.0, in (a) and (c), $[Ox]_a$=2.91 mM, in (b), $[PNPA]_o$=1.66 mM.

Figure 2.10 shows typical kinetics of the PNPA esterolytic hydrolysis in the presence of the PAAO/PAN nanofiber as well as spontaneous hydrolysis at various pHs. The catalytic reactions were carried out under conditions of excess catalytic oxime groups relative to the initial substrate concentration, i.e., $[Ox]_a$>$[PNPA]_o$, where the apparent oxime concentration, $[Ox]_a$, was defined based on the volume of the reaction solution. As shown in Figure 2.10 (a), hydrolysis in the presence of the fibers proceeded via an initial rapid formation of product P_1 followed by a slower steady process. The initial reaction rates were calculated from the initial slopes of the conversion vs. time curves:

$$r = \frac{\Delta \text{Conversion}}{\Delta t}[PNPA]_o \tag{1}$$

In the case of the fiber-aided hydrolysis, the observed reaction rate consisted of the catalytic and spontaneous terms:

$$r = r_{cat} + r_{sp} \qquad (2)$$

The rates of these hydrolysis reactions increased with increasing pH, the catalytic hydrolysis rate being 3-7-fold faster than the spontaneous hydrolysis rate at all pHs studied in the case of $[Ox]_a$ of 2.91mM. In a control experiment, the hydrolysis of PNPA in the presence of the non-catalytic PAN nanofibers under identical conditions was observed to be identical to that of the spontaneous hydrolysis of PNPA in the absence of nanofibers, which further confirmed the catalytic activity of the PAAO/PAN nanofibers.

Figure 2.11 shows two independent series of experiments in which the initial catalytic reaction rates, r_{cat}, were measured with (a) varying PNPA initial concentrations at fixed fiber apparent concentration; and (b) varying fiber content in the reaction medium at fixed initial substrate concentration. The r_{cat} is obtained by subtraction of the independently determined rate of the spontaneous hydrolysis (r_{sp}) from the experimentally measured initial reaction rate (r), according to eqn (2). As shown in Figure 2.11 (a), the initial reaction rate increased and gradually reached a plateau as the substrate concentration increased. We attribute this to full occupation of all the oxime catalytic sites by the substrate molecules when the concentration of PNPA exceeds the catalytic oxime concentration. Figure 2.11 (b) shows that the reaction rate is proportional to the fiber content in the reaction mixture if $[PNPA]_o$ is kept constant. At $[Ox]_a$=8mM, the catalytic reaction rate is 20-fold faster than that of the spontaneous hydrolysis.

According to Figure 2.9, the rate of steady-state hydrolysis can be expressed as:[18]

$$r_{cat} = \frac{d[P_1]}{dt} = \frac{k_1 k_2 [C]_o [S]}{k_1 [S] + k_2} \qquad (3)$$

56

where $[P_1]$, $[C]_o$ and $[S]$ are the product P_1 concentration, total catalyst concentration, and substrate concentration respectively (for designations, see Figure 2.9). Equation (3) allows for estimation of the rate constants of the hydrolysis (k_1) and deacetylation (k_2) reactions based on the experimental measurement of accumulation of the product, P_1. Linear fits in the initial reaction rate vs. $[Ox]_a$ plot for constant $[PNPA]_o$ and reciprocal initial rate vs. reciprocal substrate concentration for constant $[Ox]_a$ were obtained with $R^2 > 0.99$, and are shown in Figure 2.11 (b) and (c). These results, along with the measurements of the rate of spontaneous hydrolysis, enabled estimation of both k_1 and k_2, which are given in Table 2.1. Both the spontaneous hydrolysis rate constant (k_{sp}) as well as k_1 increase as the pH changes from 7.0 to 8.0, since the pH affects the basicity, $[OH^-]$, of the solution and the weight ratio of more reactive oximate ions to the neutral oxime groups in the fibers, while the deacetylation constant, k_2, shows only a weak pH-dependence. The relatively low deacetylation rate, which is comparable to that of the spontaneous hydrolysis at pH=8.0, is responsible for a low rate of recovery of the catalytic sites, and hence a reduction in the overall rates of reaction as the reaction proceeds.

pH	$k_1 \times 10^3$ $(M^{-1}s^{-1})$	$k_2 \times 10^6$ (s^{-1})	$k_{sp} \times 10^6$ (s^{-1})
7.0	1.38	4.86	0.648
8.0	7.91	5.20	9.49
9.0	–	–	64.4

– Parameters could not be accurately determined

Table 2.1. Kinetics constants of PNPA catalytic hydrolysis (k_1), product deacetylation (k_2) and spontaneous hydrolysis (k_{sp})
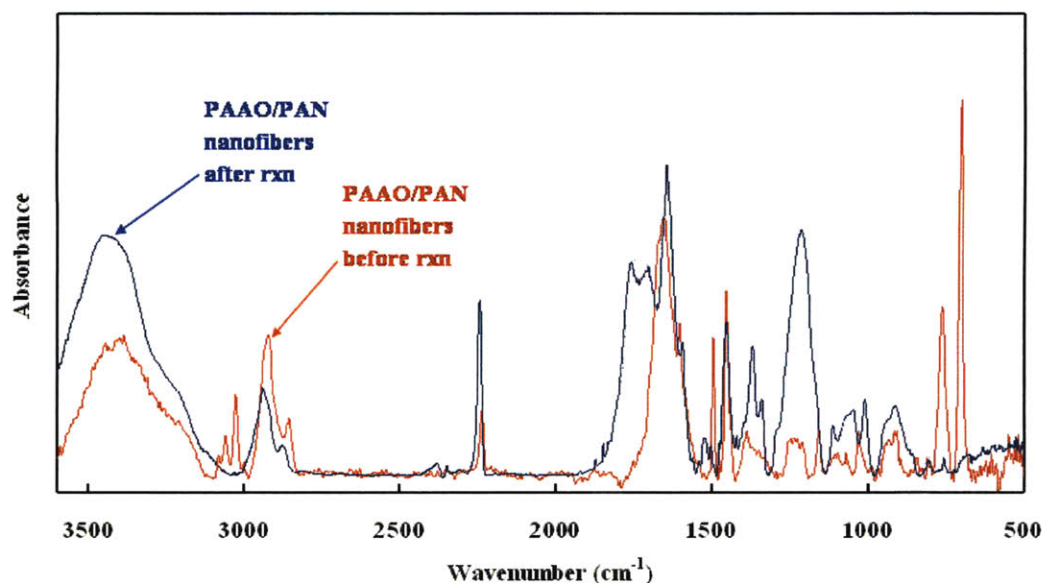
Figure 2.12. FTIR spectra of PAAO/PAN nanofibers before and after reaction with PNPA

With heterogeneous catalysis in the presence of fibers, a significant reduction in the PNPA hydrolysis rate was observed after a short, initial rapid stage, resulting in lower product conversions at pH 7.0 and 8.0 than if the rates had remained unchanged (Figure 2.10 (a)). This effect was associated with the low catalyst turnover rate, which was limited by the rate of deacetylation, k_2. It has been shown that, even in the process of homogeneous catalysis with water-soluble polymers, the rate of deacetylation of the catalytic oxime sites significantly limited the catalyst turnover rate.[17] We believe that mass transfer phenomena and the desorption of the acetate ion from the fiber could slow the deacetylation even further, effectively blocking the catalytic sites and limiting the overall hydrolysis rate at its later stage. In addition, the electrospun nanofibers with their high specific surface area could adsorb and retain undissociated nitrophenol and acetates efficiently, effectively inhibiting the catalytic activity of these sites when the nitrophenol concentration reaches a certain level after the initial stages of the hydrolysis, especially at

58

pH 7.0. The retention of nitrophenol and acetate and relatively slow catalyst turnover rate were confirmed by the FTIR spectra of the nanofibers after reaction (Figure 2.12), which were recovered, washed and dried before the measurement. After completion of the reaction, the fibers exhibited a significant degree of acetylation as evidenced by the strong band of carbonyl groups (>C=O stretch) in the area of 1700 cm^{-1} and 1760 cm^{-1}.

nozzle size (mm)	average fiber size (nm)	BET surface area (m^2/g)	$r \times 10^9$ (M/s)*
1.02	170 ± 40	14.8 ± 0.1	6.7 ± 0.7
0.76	90 ± 30	26.6 ± 0.2	10.5 ± 1.6
0.51	80 ± 30	25.9 ± 0.1	9.9 ± 0.8

* the initial reaction rates (r), defined in equation (1), were measured at pH=8.0, 25 °C, $[Ox]_a$=2.91mM and $[PNPA]_o$=2.76X10^{-4}M

Table 2.2. Fiber size effect

The narrow operational window for successful electrospinning with respect to the flow rate and the concentration of the solution/suspension did not readily permit manipulation of the size of the electrospun PAAO/PAN nanofibers over a wide range. Therefore, some control of the fiber sizes was achieved by the use of the capillary nozzles of various sizes. As shown in Table 2.2, the average nanofiber diameter was reduced from 170 to 90 nm when the smaller nozzle size, 0.76 mm in inner diameter, was employed. Further reduction in the capillary nozzle size did not lead to obvious changes in nanofiber size. Previous work has shown that there exists a terminal jet diameter that arises from an asymptotic force balance between surface tension and surface charge repulsion.[23] We speculate that this terminal jet diameter may have been reached, thus preventing further thinning of the polymer jets. The nanofiber BET surface area, which is inversely proportional to the fiber diameter, almost doubled from 14.8 to 26.6 m^2/g as the fiber size reduced by half. Experimental results indicated that the catalytic reaction rates under identical reaction conditions increased by 60 % as the surface area of the fibers increased by 80 %. It has been reported that the mass transfer, intraparticle diffusion, and catalyst structure affect the reactivity of insoluble heterogeneous polymer-supported

59

catalyst particles with the size ranging from tens to 300 nm.[20] In this work, vigorous mechanical stirring was carried out to eliminate resistances to the diffusional transport of the substrate from the bulk liquid to the catalyst surface.[20] The intra-fiber diffusion of the substrate to the active catalyst sites buried within the fibers and of the product to the external solution could significantly affect the availability of the catalyst sites in the fibers. A smaller fiber with larger surface area ensured that a greater fraction of the oxime functional groups would be located on or close to the surface of the nanofibers, and would thus be exposed to and attacked by the substrate in the solution more readily. The fibers with the smaller diameter also offer shorter diffusional paths to the active catalyst sites in the fiber cores. XPS data shown in Figure 2.13 revealed that the surface layer within 6 nm of the fiber surface consist of an atomic ratio of 16:1 of carbon to oxygen for the fibers of 170 nm in diameter, which is twice the atomic ratio of 8:1 in the bulk material composition. This result is indicative of the presence of more oxime groups in the bulk of the fibers than on their surfaces. We speculate that bonding between segments of the PAAO macromolecule tends to lead to the oxime groups being confined within the nanofibers rather than reporting to their surfaces. Although the addition of PAN facilitated the electrospinning of the PAAO, it also limited the surface concentration of the oxime groups and influenced the accessibility of the catalyst sites. We believe that the diffusional limitations of the substrate to the majority of oxime catalytic sites within the nanofiber cores significantly limited the availability of the catalyst sites in the fibers and affected the reactivity of the fiber catalysts. Our estimate of active oxime groups based on the initial oxime concentration $[Ox]_a$ ignored the diffusion inside the fibers, over-counted the accessibility of all the oxime groups in the fibers and underestimated the hydrolysis constant (k_1). This could explain the order of magnitude slower hydrolysis constant (k_1) of the PAAO/PAN nanofibers obtained in this work, compared to that in the homogeneous reaction catalyzed by a water-soluble copolymer of phenylisobutyrohydroxamic acid and 1-vinyl-2-methylimidazole in aqueous medium.[17] On the other hand, it is known that the hydrolysis of PNPA is significantly influenced by the solvent used.[13,21] The esterolysis of PNPA in ethanol is approximately 100-fold slower than that in water, which contributed to the lower k_1 as well. We surmise that significant improvements in the fiber catalyst reactivity will result

from either further reduction of the fiber diameter (minimizing the effect of the intra-fiber diffusion) or immobilization of the majority of the catalytic sites on the fibers surface, which will eliminate the limitation of the intra-fiber diffusion.
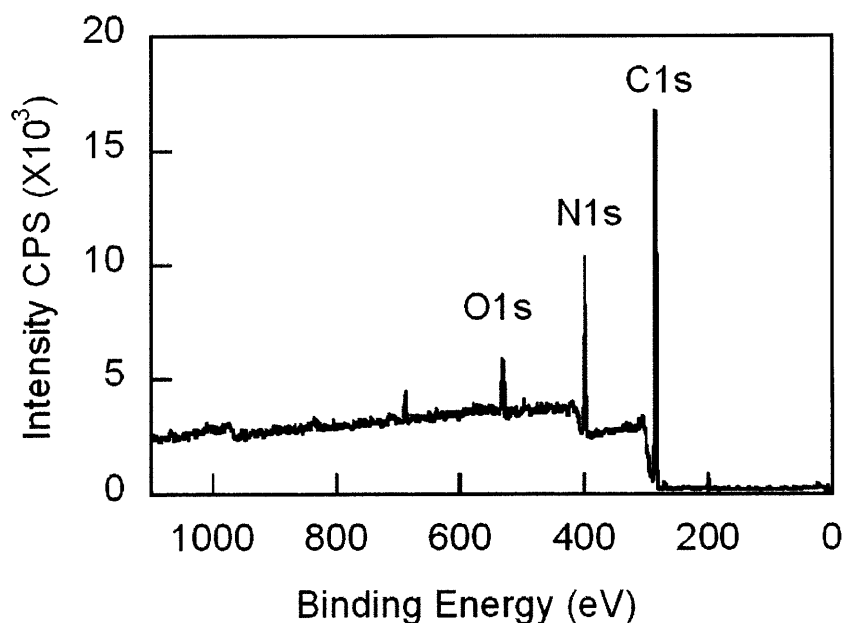
Figure 2.13. XPS spectrum of the electrospun nanofibers of the PAAO/PAN blend

2.3.3. CWA decomposition mediated by PAAO

Although PNPA can mimic organophosphate chemical warfare agents or pesticides to some extent, we are always desirable to test the reactivity of PAAO to decompose combat chemical warfare agents. By collaborating with US army Edgewood chemical biological center, our laboratory has been able to evaluate the capability of PAAO to decompose chemical warfare agents. Several representative ^{31}P HRMAS NMR spectra illustrate the kinetics of soman (GD) degradation mediated by PAAO. GD was added to PAAO powder equilibrated at 100% relative humidity and spectra measured versus time, shown in Figure 2.14. The four resonance peaks in the 26-32 ppm range are from GD, corresponding to the doublet (^{31}P split by F, J_{P-F} = 1040 Hz) for each of the two

diastereoisomers, [24] or a doublet of doublets. [24,25] The relative intensity of the two GD doublets decreased over time, while the single signal belonging to pinacolyl methylphosphonic acid (PMPA) [24,26] centered at 25.2 ppm increased. Signals of other products of GD degradation that appeared at 34.3 and 33.8 ppm were tentatively assigned to the reaction of GD with the polymer oxime group,[26] although positive identification could not be achieved due to the transient nature of these products, since they continued to react and the signals decreased in intensity. The products were bound to the polymer sample and therefore they could not be extracted for confirmation by other techniques. The chemical shifts of these products were comparable to results reported for reactions of potassium 2,3-butanedione monooximate with GD, which produced ^{31}P resonances at 38.6 and 38.2 ppm, with a doublet corresponding to the diastereomers.[26] These signals are also close to the ones that were previously assigned to pinacolyl methylphosphonic acid peroxide at 39.1 and 38.2 ppm.[27] The observed reaction rate (k_{obs}) for GD decomposed by PAAO is 1.9 $\times 10^{-4}$ s^{-1} with a half-life ($t_{1/2}$) of 1.0 hour, which is comparable to that observed for a Cu(II) complex of poly(4-vinylpyridine) quaternized with 19 mol% ethyl bromide and 36 mol% 4-chloromethyl-4'-methyl-2,2'-bipyridine.[28]

Analogously, the ^{31}P HRMAS NMR spectra of VX deposited onto hydrated PAAO (Figure 2.15) samples indicated facile degradation of VX (signal at 61 ppm) via formation of ethyl methylphosphonic acid (bound or free EMPA, signal at 26 ppm) by the cleavage of the electrophilic P-S bond (Figure 2.16). In solids, 60-63 ppm has been observed for protonated VX.[29-31] On concrete, the chemical shift of VX is about 63 ppm.[30,32] The chemical shift for VX observed in this case is consistent with protonation or salvation of VX by water. The observed reaction rate (k_{obs}) for VX mediated by PAAO is 4.5 $\times 10^{-5}$ s^{-1} with a half-life ($t_{1/2}$) of 4.3 hour, which is approximately 140-fold faster when compared with the half-lives of the VX in aqueous or aqueous/methanol solutions at pH 8-10 and at ambient temperature.[33,34]
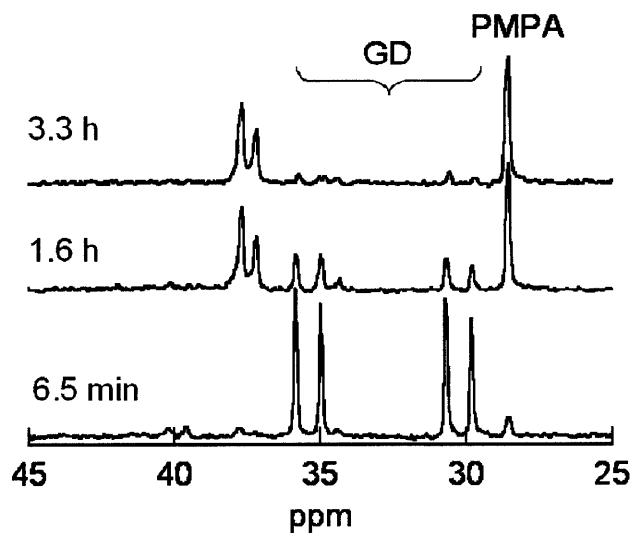
Figure 2.14. Representative 202.64 MHz ^{31}P HRMAS NMR spectra of soman (GD) deposited onto hydrated PAAO as a function of time. Total PAAO weight, 73 mg, water content, 54±9 wt%, initial GD amount, 1 µL. PMPA stands for pinacolyl methylphosphonic acid.
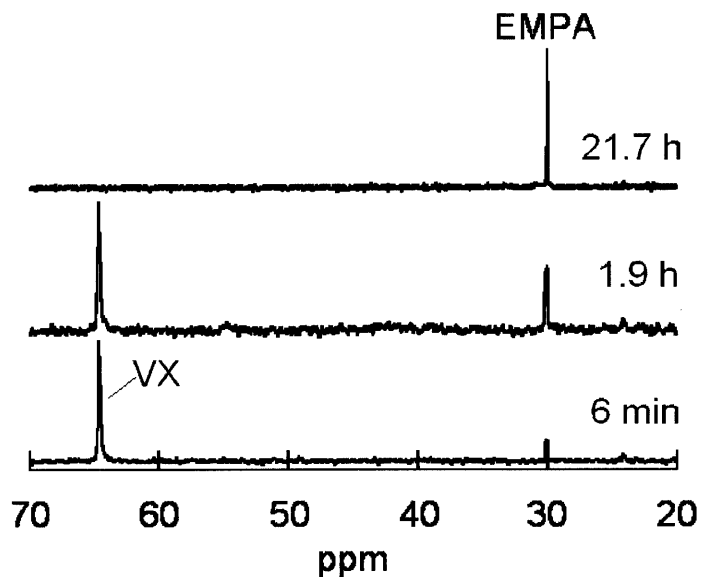
Figure 2.15. Representative 202.64 MHz ^{31}P HRMAS NMR spectra of VX deposited onto hydrated PAAO as a function of time. Total PAAO weight, 88 mg, water content, 54±9 wt%, initial VX amount, 1 µL. EMPA stands for ethyl methylphosphonic acid.
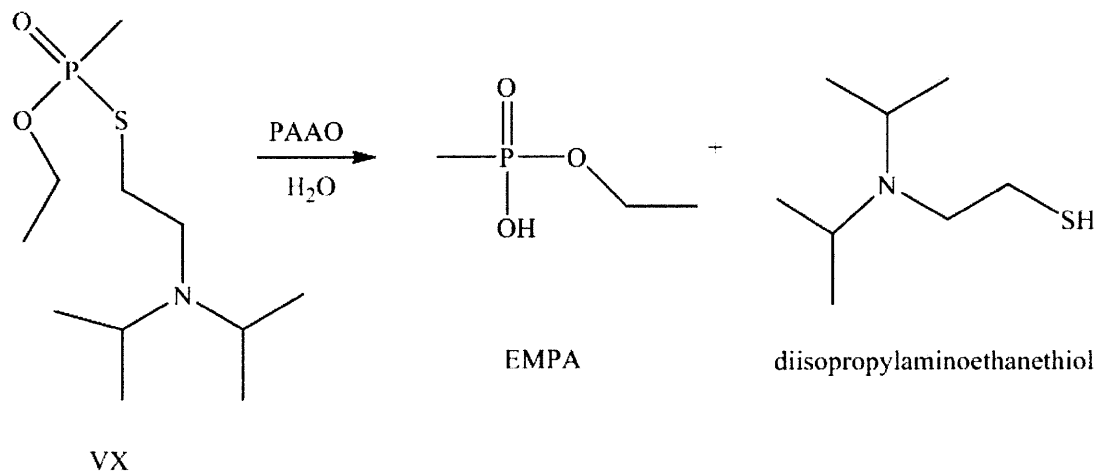
Figure 2.16. The degradation pathway of VX in the presence of wet PAAO.

2.4. Concluding Remarks

Functionalized oxime nanofibers were produced via electrospinning of a dispersion of PAAO blended with PAN. The functioning of this fiber-based heterogeneous catalyst was tested in the hydrolysis of PNPA, a model compound for the more toxic organophosphates and nerve agents. The release of nitrophenolate, as monitored by UV measurements, revealed that the presence of the PAAO/PAN nanofibers remarkably accelerated the hydrolysis of PNPA in aqueous/ethanol solutions at pHs ranging from 7.0 to 9.0. The dependence of the reaction rate on the fiber size indicated that intra-fiber diffusional limitations might affect the accessibility of oxime catalytic sites inside the fibers significantly, and that the catalytic hydrolysis probably occurs primarily on the surface of the oxime nanofibers. In addition, the capability of polyacrylamidoxime to decompose combat organophosphate chemical warfare agents was demonstrated. This work demonstrates the concept of incorporation of the α-nucleophilies into the electrospun nanofibers capable of catalytically decomposing toxic chemicals. Previously, attachment of functionalized nanoparticles to fibers and textiles has been described that imparted bioactive, fragrant, insect repellent, etc. properties to the fiber surfaces.[22] In contrast to the present work, the chemistry of the particle grafting onto the fibers did not permit maintaining the reactivity of the oxime and other nucleophilic functionalities incorporated into the fibers.[22] However, in light of possible diffusional limitations observed herein, we plan on adopting a somewhat analogous concept of having the majority of the reactive groups on the fiber surface. Allocating all of the active catalytic sites on the fiber surface rather than distribution of the catalyst in the whole volume of the fibers should improve the catalyst reactivity. We envision utilization of such self-detoxifying, lightweight nanofibers as key functional layers in a new generation of protective fabrics and filters.

2.5. References

1. Couderc, S.; Toullec, J. *Langmuir* 2001, 17, 3819.

2. Kassa, J. *J. Toxicol., Clin. Toxicol.* 2002, 40, 803.

3. Epstein, J.; Kaminski, J. J.; Bodor, N.; Enever, R.; Sowa, J.; Higuchi, T. *J. Org. Chem.* 1978, 43, 2816.

4. Bunton, C. A.; Ihara, Y. *J. Org. Chem.* 1977, 42, 2865.

5. Simanenko, Y. S.; Karpichev, E. A.; Prokop'eva, T. M.; Panchenko, B. V.; Bunton, C. A. *Langmuir* 2001, 17, 581.

6. Kunitake, T.; Okahata, Y. *Macromolecules* 1976, 9, 15.

7. Kunitake, T.; Okahata, Y.; Sakamoto, T. *J. Am. Chem. Soc.* 1976, 98, 7799.

8. Bromberg, L.; Hatton, T. A. *Ind. Eng. Chem. Res.* 2005, 44, 7991.

9. Tsang, J. S.; Neverov, A. A.; Brown, R. S. *J. Am. Chem. Soc.* 2003, 125, 7602.

10. Miller, P. D.; Spivey, H. O.; Copeland, S. L.; Sanders, R.; Woodruff, A.; Gearhart, D.; Ford, W. T. *Langmuir* 2000, 16, 108.

11. Schouteden, F. L. M. *Makromol. Chem.* 1957, 24, 25.

12. Shin, Y. M.; Hohman, M. M.; Brenner, M. P.; Rutledge, G. C. *Polymer* 2001, 42, 9955.

13. Buncel, E.; Cannes, C.; Chatrousse, A. –P.; Terrier, F. *J. Am. Chem. Soc.* 2002, 124, 8766.

14. Fornasier, R.; Tonellato, U. *J. C. S. Faraday I* 1980, 76, 1301.

15. Mancin, F.; Tecilla, P.; Tonellato, U. *Langmuir* 2000, 16, 227.

16. Fanti, M.; Mancin, F.; Tecilla, P.; Tonellato, U. *Langmuir* 2000, 16, 10115.

17. Kunitake, T.; Okahata, Y. *Bioorg. Chem.* 1975, 4, 136.

18. Bender, M. L.; Marshall, T. H. *J. Am. Chem. Soc.* 1968, 90, 201.

19. Carey, F. A. In *Organic Chemistry,* 4th ed.; McGraw Hill: Boston, 2000, p 944.

20. Tomoi, M.; Ford, W. T. *J. Am. Chem. Soc.* 1980, 102, 7141.

21. Ghosh, K. K.; Satnami, M. L.; Sinha, D.; Vaidya, J. J. *Mol. Liq.* 2005, 116, 55.

22. Soane, D. S.; Offord, D. A.; Linford, M. R.; Millward, D. B.; Ware, W.; Erskine, L.; Green, E.; Lau, R. *US Patent 6,607,994,* 2003.

23. Fridrikh, S. V.; Yu, J. H.; Brenner, M. P.; Rutledge, G. C. *Phys. Rev. Lett.* 2003, 90, 144502.

24. Segall, Y.; Waysbort, D.; Barak, D.; Ariel, N.; Doctor, B. P.; Grunwald, J.; Ashani, Y. *Biochemistry* 1993, 32, 13441.

25. Van den Berg, G. R.; Beck, H. C.; Benschop, H. P. *Bull. Environ. Contam. Toxicol.* 1984, 33, 505.

26. Boulet, C. A.; Hansen, A. S. Suffield Memorandum No. 1323, Defense Research Establishment Suffield, Ralston, Alberta, Canada, April 1990.

27. Wagner, G. W.; Sorrick, D. C.; Procell, L. R. Brickhouse, M. D.; Mcvey, I. F.; Schwartz, L. I. *Langmuir* 2007, 23, 1178.

28. Hammond, P. S.; Forster, J. S. *J. Appl. Polym. Sci.* 1991, 43, 1925.

29. Columbus, I.; Waysbort, D.; Shmueli, L.; Nir, I.; Kaplan, D. *Environ. Sci. Technol.* 2006, 40, 3952.

30. Wagner, G. W.; O'Connor, R. J.; Procell, L. R. *Langmuir* 2001, 17, 4336.

31. Wagner, G. W.; Bartram, P. W.; Koper, O.; Klabunde, K. J. *J. Phys. Chem. B* 1999, 103, 3225.

32. Wagner, G. W.; O'Connor, R. J.; Edwards, J. L.; Brevett, C. A. S. *Langmuir* 2004, 20, 7146.

33. Yang, Y. C.; Baker, J. A.; Ward, J. R. *Chem. Revs.* 1992, 92, 1729.

34. Cassagne, T.; Cristau, H.-J.; Delmas, G.; Desgranges, M.; Lion, C.; Magnaud, G.;.Torreilles, E.; Virieux, D. *Heteroatom. Chemistry* 2001, 12, 485.

35. The tests of combat CWA decomposition using NMR spectroscopy were performed by Mr. William Creasy, Mr. David McGarvey and Mr. Roderick Fry of US Army Edgewood Chemical and Biological Center, Aberdeen Proving Ground, Maryland.

Chapter 3

Chemical Protection Fabrics via Surface Oximation
of Electrospun Polyacrylonitrile Fiber Mats

3.1. Introduction

Increased awareness, concerning about the hazards of organophosphate (OP) pesticides, nerve agents and pollutants, poses a challenge to develop countermeasures. There is an urgent need to develop systems to capable of efficiently handling and neutralizing environmental pesticides and toxins. Recently, Singh *et al.* reported self-decontaminating coatings with an enzyme, organophosphorous hydrolase (OPH), which can break down organophosphorous pesticides rapidly.[1] Given the potential issues associated with the stability of the enzymes, our group has focused on chemical methods of OP degradation via hydrolysis using α-nucleophilic agents.[2,3] The high surface area inherent to electrospun fiber meshes is available for functionalization by chemical attachment of reactive compounds or functional groups onto the protective fabrics. By this approach, we can combine the advantageous properties of electrospun fibers with functionalization of their surface with α-nucleophilic moieties such as oxime groups to create a novel decontamination medium. In chapter 1, fibers functionalized by amidoxime groups have been described. Reactive polyacrylamidoxime (PAAO) was blended with unreactive polyacrylonitrile (PAN) and electrospun to produce reactive fiber mats. Catalyzed hydrolysis of 4-nitrophenyl acetate by these reactive fibers was demonstrated in aqueous ethanol solutions. However, blending with PAN dilutes the surface density of the functional amidoxime groups and mitigates the amidoxime group functionality in the fibers. Previously, the modification of PAN textiles to PAAO was reported and their ability to strongly bind a broad range of heavy metal ions in the purification of water sources has been described.[4,5] Nevertheless, the degradation of OP nerve agents or analogues by PAAO-functionalized electrospun fibers has not been established. In this chapter, a post-spin treatment strategy (Figure 3.1) was developed to chemically modify prefabricated PAN submicron fibers to generate environment-friendly, cost-effective, non-toxic PAAO-functionalized fiber mats. This strategy maximizes the surface density of the reactive amidoxime groups and eliminates the need to

control accurately the properties of polymer blends, which is crucial in the electrospinning of the polymer blend suspensions. Herein, the performance of the reactive fiber mats in OP decomposition was tested using diisopropyl fluorophosphate (DFP) mists; DFP is a widely used simulant of chemical warfare nerve agents.[6]

electrospin   post-spin modification

Polymers (PAN)   ⟶   PAN nanofibers   ⟶   Reactive PAN-Ox nanofibers
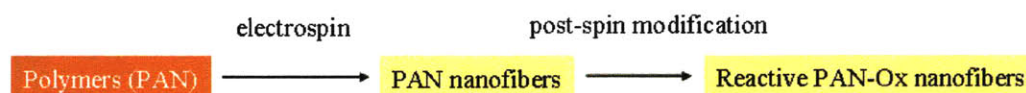
Figure 3.1. A post-spin strategy to produce reactive fiber mats

3.2. Experimental method

3.2.1. Materials

Polyacrylonitrile (PAN) (M_w 150 kDa) was purchased from Scientific Polymer Products, Inc. (Ontario, NY) and used as received. Diisopropyl fluorophosphate (99%, DFP), hydroxylamine hydrochloride (99%) and N,N-dimethylformamide (DMF) were obtained from Sigma-Aldrich Chemical Co. (St. Louis, MO) and used without further treatment.

3.2.2. Electrospinning

Clear, 10 wt% solutions of PAN in DMF were prepared by dissolving the polymer at 50-70 °C followed by stirring at room temperature. The PAN/DMF solutions were electrospun using a parallel plate setup as described in chapter 1. Briefly, two parallel aluminum disc plates (15 cm in diameter) were set apart at a distance of approximately 30 cm. A polymer solution was pumped from a syringe through a Teflon feedline to a capillary nozzle by a syringe pump (Harvard Apparatus PHD 2000, Holliston, MA). A high voltage power supply (Gamma High Voltage research ES-30P, Ormond Beach, FL) was used to charge the upper plate and, by contact, the polymer solution as it flows through the nozzle, and to create a uniform electric field between the charged upper place and the grounded collector. The applied voltage (28-30 kV), the flow rate (0.015 ml/min) and the distance between the upper plate and the collector were manipulated to stabilize the polymer jet to form fiber meshes on the grounded collector.

3.2.3. Post-spin modification to achieve PAAO-functionalized fibers
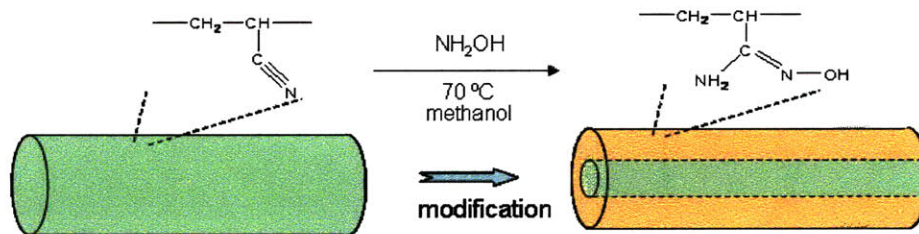
Figure 3.2. Surface oximation of PAN fibers to PAAO by hydroxylamine.

PAN fiber mats were modified to obtain PAAO-functionalized fibers by reacting with excess hydroxylamine in methanol at 70 °C (Figure 3.2). These PAAO-functionalized fibers obtained via oximation of prefabricated PAN fibers are denoted PAN-Ox fibers. Due to the small diameter and high surface area of the electrospun nanofibers, the fiber morphology could be altered in a reactive environment. It was observed that boiling of methanol at 70 °C in a flask equipped with a condenser during the oximation reaction resulted in destruction of the distinct fiber structure of the electrospun meshes. However, suppressing the boiling and cavitation of methanol at 70 °C in a sealed reactor (glass VWR media bottle) enabled fiber modification without altering the fiber structure. In a typical experiment, hydroxylamine hydrochloride (262 mg, 3.77 mmol) was added into a reactor containing anhydrous methanol (50 mL) and an equimolar amount of sodium hydroxide (151 mg, 3.77 mmol) was added to neutralize the released hydrochloric acid. The mixture was gently shaken to dissolve the solid content. Then, 100 mg of prefabricated PAN fiber mat (1.1mg/cm^2; mole ratio of hydroxylamine to nitrile group, 2) were placed into the reactor. The reactor was sealed and kept at 70 °C for 24 hours; then the reactor was equilibrated at ambient temperature and opened. No bubbling was observed throughout the course of the oximation process. The modified fiber meshes were gently removed, repeatedly washed with methanol, air-dried, washed with excess deionized water (pH=7) and dried under vacuum until constant weight was obtained. Substantial shrinkage of the fiber mats wet with methanol was

72

observed in contact with water. Hence, the drying off of methanol and of water was performed sequentially, and the process resulted in a minimal change of the fiber mat area.

3.2.4. Fiber Characterization

Fiber morphology was visualized using scanning electron microscopy (SEM, JEOL-6060). A thin layer of gold (*ca.* 10 nm) was sputter-coated onto the fiber samples prior to the measurements.

Measurements of surface chemical composition of the fiber mats were carried out with a Krato Axis Ultra Imaging X-ray photoelectron spectrometer (Kratos Analytical Co.) equipped with a monochromatized Al K_α X-ray source. The takeoff angle relative to the sample substrate was set at 90°.

FTIR spectra were measured for ground samples embedded in KBr using a Nicolet 8700 spectrometer (Thermo Scientific Corp.) in the absorbance mode by accumulation of 256 scans with a resolution of 4 cm^{-1}. The FTIR spectrometer was equipped with a Nicolet FTIR/TGA interface and a transfer line to monitor the vapors that evolved during the TGA heating scan with the sequence interval corresponding to the duration of the TGA ramp. Thermogravimetric analysis (TGA) was conducted using a Q5000IR thermogravimetric analyzer (TA Instruments, Inc., New Castle, DE). Samples were subjected to heating scans (20°C/min) in a temperature ramp mode.

3.2.5. Kinetics

Kinetics of degradation of DFP mists were assessed by ^{31}P NMR spectrometry using a Bruker Avance 400 spectrometer operating at 161.98 MHz (for ^{31}P). The high-resolution magic angle spinning (HRMAS) spectra were recorded with a 4-mm

73

Bruker ^{31}P gradient probe.

A fiber mat sample was uniformly sprayed with deionized water (pH=7) to allow the fibers to take up water homogeneously. The weight of the sample was monitored using a balance until the desired amount of water in the fiber sample was achieved. The water content was defined as follows:

$$C_w = \frac{M_f - M_{f0}}{M_{f0}}$$

where M_f and M_{f0} are the weights of the mat in wet and dry states, respectively.

The sample with a defined C_w was quickly packed into a 4-mm zirconium HRMAS rotor. In order to mist DFP, 3 μl of DFP was drawn into a 10-μl syringe, and 7 μl of air was further drawn into the syringe. Then the DFP mist was sprayed onto the fiber sample in the rotor by a rapid expulsion of the air and liquid from the syringe. The rotor was capped and weighed. To maximize the contact area of DFP with the reactive fibers, the rotor was kept at 60 °C in an oil bath for 5-7 minutes to allow DFP to evaporate and penetrate throughout the porous structure of the fiber mat. The rotor was then kept on ice at 0 °C for 5 min to condense the DFP on the fiber surfaces. The rotor was inserted into the instrument, spun at the MAS spinning rate of 5 kHz, and the NMR measurements commenced. The spectra were recorded at ambient temperature (21 °C) by accumulation of 64 scans with an overall acquisition time of 3 minutes. The reaction time was taken to be the midpoint of the acquisition period. The spectra were acquired periodically to monitor the reaction process. Triphenyl phosphate (TPP) in deuterated chloroform-d was used as an external reference (0 ppm).

3.3. Results and discussion

3.3.1. Formation of reactive fiber mats

Figure 3.3. A photo image of as-spun PAN fiber mat (left) and surface-modified PAN fiber mat (right).

The technique of the fiber oximation in a sealed flask to prevent boiling and cavitation of solvent resulted in flexible PAN-Ox fiber mats. Figure 3.3 shows the photo image of as-spun PAN fiber membrane (left) and the functionalized PAN-Ox fiber membrane (right). The PAN-Ox fiber mats shrank approximately 10% in length and width compared to the unmodified fiber mats. Typical SEM images of as-spun PAN and PAN-Ox fiber mats are shown in Figure 3.4. The average diameter of the PAN fibers electrospun from 10 wt% DMF solution is about 350 nm (Figure 3.4a), with the fiber diameters ranging from 250 to 500 nm. As can be seen in the SEM image of the PAN-Ox fibers (Figure 3.4b), the fiber morphology was not damaged by the post-spin oximation treatment. The size of the functionalized fibers was similar to that of the parent PAN fibers, while the porosity of the fiber mats after modification decreased substantially, as evidenced by the observed shrinkage in thickness by about 40%.

(a)
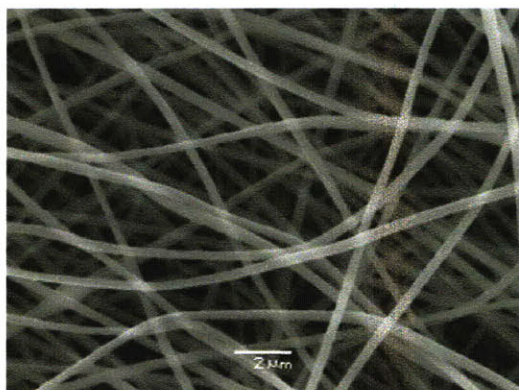
(b)
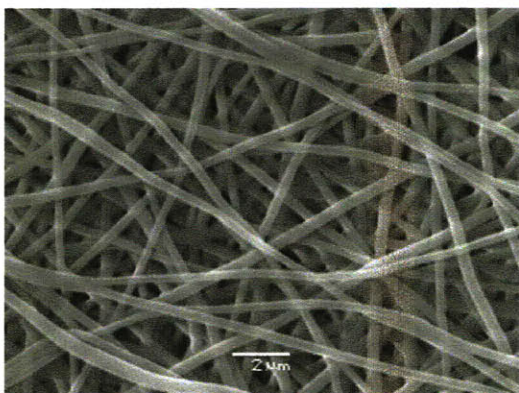
Figure 3.4. SEM images of (a) as-spun PAN fibers and (b) PAN-Ox fibers. Scale bar: 2 µm.

Figure 3.5 depicts FTIR spectra of the parent PAN and resultant PAN-Ox fibers. The characteristic peak of the nitrile groups at 2240 cm^{-1} (stretching vibration) significantly decreased, as most of the nitrile groups of PAN were converted into amidoxime groups during the modification reaction. Compared to the complete conversion of PAN to PAAO in homogeneous solution reported in chapter 1, the heterogeneous oximation rate of these fibers was limited by the diffusion of hydroxylamine into the solid fiber which hindered the complete conversion within 24 hours.
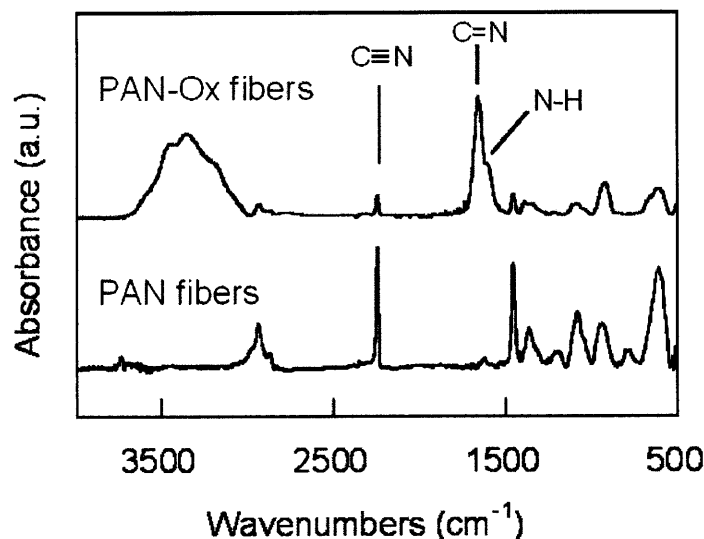
Figure 3.5. FTIR spectra of prefabricated PAN and resultant PAN-Ox fibers.

In the spectrum of the PAN-Ox fibers, a strong peak at 1660 cm^{-1} (stretching vibration of C=N) with a shoulder peak at 1610 cm^{-1} (scissor vibration of NH$_2$) and a broad peak in the range of 3100-3600 cm^{-1} (stretching vibration of NH$_2$ and OH) indicates the presence of functional amidoxime groups.[7] The functionalized fiber mats demonstrate acceptable chemical resistance in that the fibers are insoluble in water and most organic solvents such as DMF, which is believed to be due to the formation of glutaroimide-dioxime links between PAAO segments as described in chapter 1, while the reactive oxime sites remain intact. Further elemental analysis of the PAN-Ox fiber mats (Found: C, 44.55; H, 7.85; N, 29.27; O, 18.33; Calculated, based on 90% conversion of the nitrile groups and 6 wt% absorbed water: C, 44.54; H, 6.97; N, 29.68; O, 18.81) indicated that about 90 percent of the nitrile groups were converted into the amidoxime groups, approximately 50 percent of which formed glutaroimide-dioxime links. XPS spectra (Figure 3.6) show the surface chemistry of the prefabricated PAN fibers and PAN-Ox fibers within 6-10 nm of the surface layer of fibers. The presence of the characteristic peak of oxygen at 529 eV in the spectrum of the PAN-Ox fibers confirms the conversion of PAN to PAAO on the fiber

surfaces. XPS spectra also indicate that the surface density of amidoxime groups in the PAN-Ox fibers via the post-spin modification method described here is two to three times that of reactive fibers obtained via the PAN/PAAO blending method reported previously.
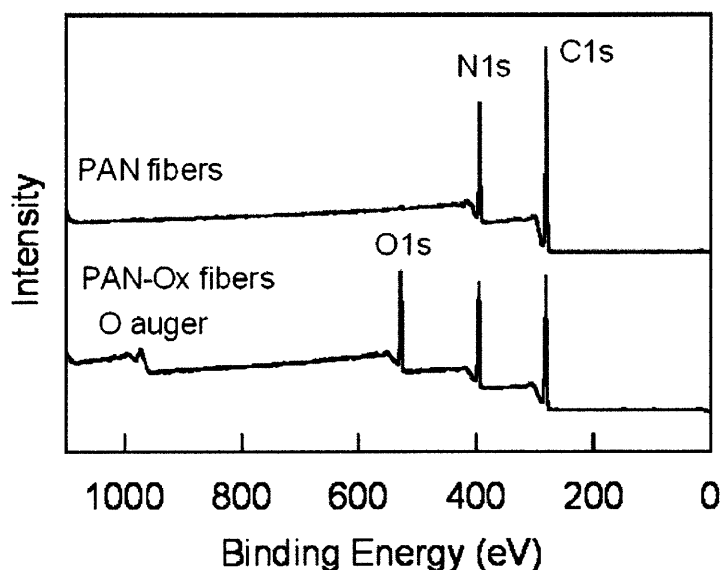
Figure 3.6. XPS spectra of PAN fibers and reactive PAN-Ox fibers

Thermal stability of the PAN-Ox and their parent PAN fiber mats was studied using TGA coupled with FTIR (Figure 3.8). Vapors evolved during the heating scans of the PAN-Ox fiber mats were monitored by FTIR as shown in Figure 3.9. Both PAN and PAN-Ox fibers were equilibrated at ambient temperature and humidity (approximately 25°C and 29%, respectively) prior to analysis. The parent PAN fibers contain about 2-3% water. This is more water than that in the unprocessed, as-received PAN (< 1%), possibly because of the moisture absorption enhancement by the high surface area of the nanofibers. PAN fibers decompose abruptly in the range of 300-350 °C, similar to that observed with the as-received PAN. In contrast, the PAN-Ox fiber mats are more hygroscopic, initially absorbing about 7% water. The PAN-Ox fibers begin to decompose around 190 °C, in line with the lower thermal

stability reported for PAAO compared with PAN.[8]   At temperatures starting around 50°C, vapors evolving from the PAN-Ox fibers contain water, peaks of which are indicated by cross symbols (+) in the spectra (Figure 3.9).   In the range of 140-180 °C, the characteristic bands of ammonium at 930 and 965 (double band, symmetric bending), 1630 (symmetric bending of H-N-H) and 3334 cm^{-1} (N-H stretching)[9] as marked by stars (*) are clearly observed (Figure 3.9), which indicates the hydrolysis of PAAO into hydroxamic acid according to Figure 3.7.[10]   Notably, the hydroxamic acid, along with the PAAO itself, is α-nucleophilic and its capability to degrade the OPs has been established previously.[11,12]   Although hydroxamic acid may be further hydrolyzed to acrylic acid, it was shown that the extent of this conversion is insignificant at ambient conditions.[13]   Further increase in temperature above 190 °C results in PAAO decomposition, with release of volatile products with signals detectable in the 2200-2400 cm^{-1} range (Figure 3.9).
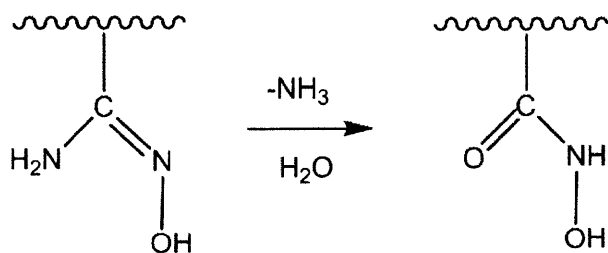
Figure 3.7. Hydrolysis of polyacrylamidoxime to polyhydroxamic acid in the presence of water.
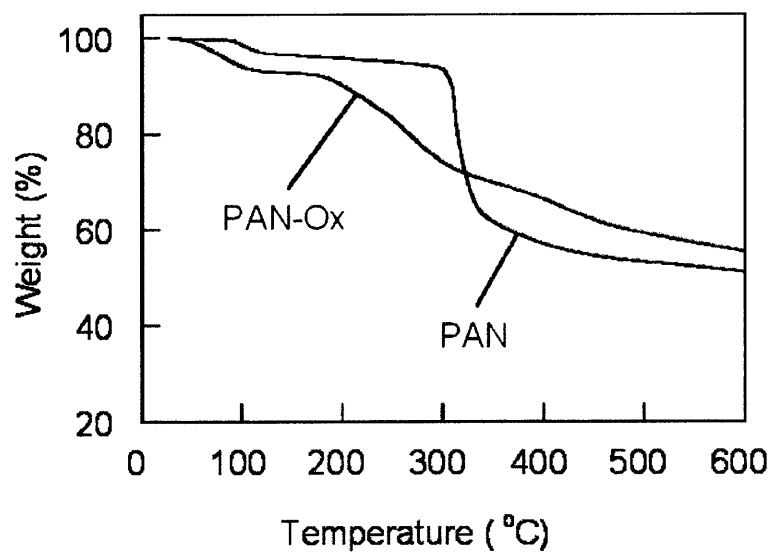
Figure 3.8. TGA curves of PAN fibers and PAN-Ox fibers
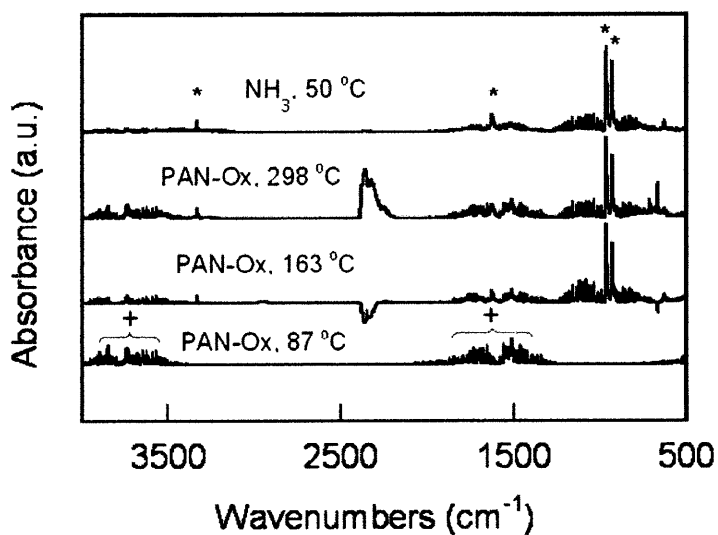
Figure 3.9. FTIR spectra of the vapor products released during TGA heating scans of the PAN-Ox fiber mats (lower 3 spectra) and of 30% ammonia aqueous solution (top spectrum). Characteristic ammonia peaks are marked by star (*) and water peaks are marked by cross symbols (+). The TGA temperature at which each scan was recorded is shown above the spectrum.

3.3.2. DFP decomposition mediated by reactive PAN-Ox fibers
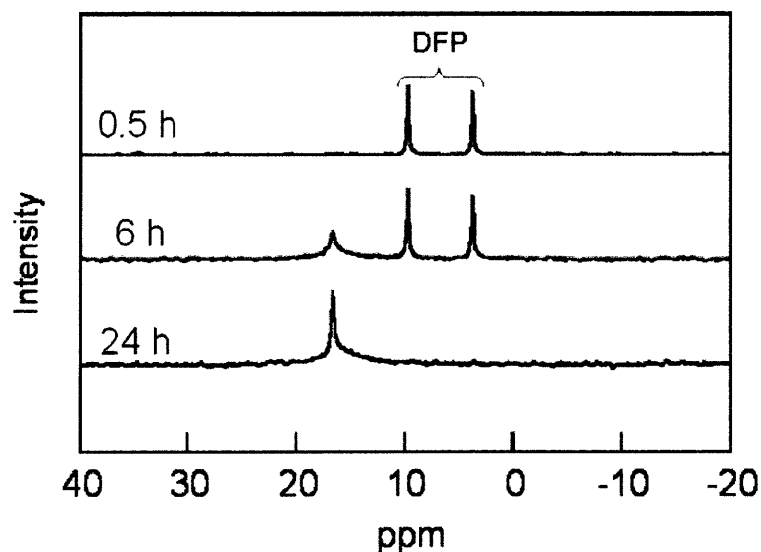
Figure 3.10. Typical 161.98 MHz ^{31}P HRMAS NMR spectra of DFP mists (3 mg) deposited onto the PAN-Ox fibers. The mass of dry PAN-Ox fiber mats, M_{fo}=30mg; the water content in the fiber mats, C_w=1.3 wt/wt. Chemical shifts are relative to external TPP in deuterated chloroform-d (0 ppm).

The performance of the PAN-Ox fiber mats as reactive fabrics was tested with a CWA simulant, DFP. Three representative ^{31}P HRMAS NMR spectra of DFP degradation by the PAN-Ox fiber mats as a function of time are shown in Figure 3.10. In these experiments, the reactions were carried out under the condition of excess reactive amidoxime groups relative to the substrate DFP. Doublets at 3.7 and 9.7 ppm coupled by the P-F bond ($J_{P-F} \approx$ 970Hz) are assigned to the reactant DFP.[14,15] A broad singlet signal centered at 16.6 ppm is attributed to the product, diisopropyl phosphate (DIP), possibly bound to the amidoxime group. The DIP originates from the cleavage of the P-F bond in DFP, hydrolyzed by the fibers. The relative intensity of the DFP doublet signal decreases while that of the product signal increases with the

progress of the reaction. All of the DFP is completely degraded by the PAN-Ox fibers within 24 hours. In the control experiment, the doublet signals of the DFP substrate remain almost intact; a very minor product signal (less than 3% relative to the initial DFP signal) is observed for the unmodified PAN fiber mats in 24 hours under identical reaction conditions due to spontaneous hydrolysis. This illustrates the capability of the PAN-Ox fiber mats to decompose toxic nerve agents in the presence of water in comparison with the unmodified PAN fibers.

The relative intensities or areas of the signals in the NMR spectra characterize the DFP conversion. Based on a series of ^{31}P NMR spectra at different time periods, we estimated the kinetics parameters of the DFP degradation in our experiments. The time-dependent relative conversion, F_t, is defined as the ratio of the sums of the area integrations,

$$F_t = \sum I_r /(\sum I_r + \sum I_p)$$

where $\sum I_r$ and $\sum I_p$ are the sums of the integrations of the signals at 3.7 and 9.7 ppm corresponding to the reactant, DFP, and at 16.6 ppm for the product, DIP, respectively.

All of the DFP hydrolyses in the presence of the PAN-Ox fiber mats in our experiments were observed to be pseudo-first order reactions, as indicated by the linear fit of the curve of $\ln(F_t)$ vs. time, with $R^2 > 0.98$ in all experiments (Figure 3.11). The slope of the linear fit yields the observed reaction rate constant, k_{obs}, based on the equation:

$$\ln(F_t) = -k_{obs}t$$

The corresponding half-life is $t_{1/2} = \ln(2)/k_{obs}$.
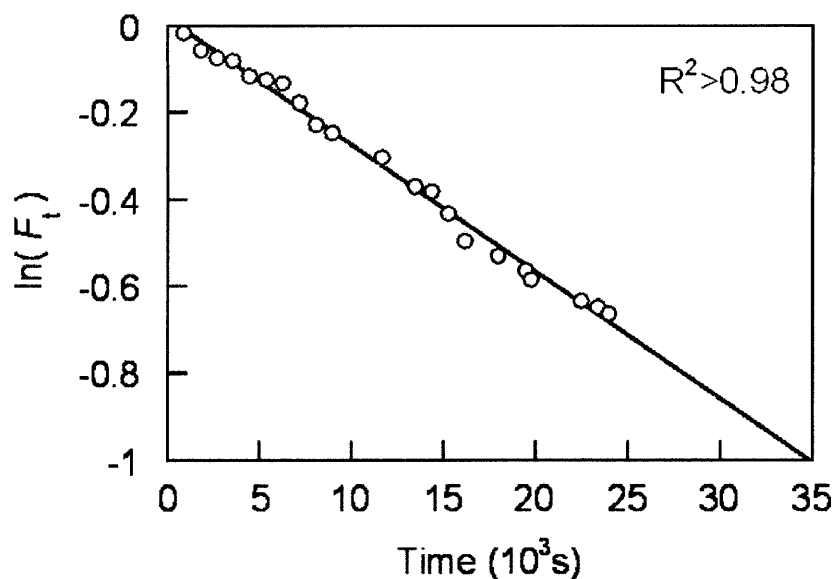
Figure 3.11. Representative kinetics of DFP degradation by the PAN-Ox fiber mats at 21 °C. The mass of dry PAN-Ox fiber mats, M_{f0}=30mg; the water content in the fiber mats, C_w=1.3 wt/wt; the amount of DFP, M_{DFP}=3 mg. The solid line represents a linear fit to the experimental data (R^2>0.98). The slope of the line is $-k_{obs}$.

Figure 3.12 shows the results of a series of experiments in which the observed reaction rates were measured with varying mass of the dry PAN-Ox fiber mats (M_{f0}, average fiber diameter, 350nm) at fixed amount of DFP (M_{DFP}=3 mg) and water content in the fiber mats (C_w=1.3 wt/wt). We observed k_{obs} to be linearly proportional to the mass of the reactive fiber mats (R^2>0.97). In the case of M_{f0}=30 mg, k_{obs} is as high as 3.0×10^{-5} s^{-1}, with a corresponding half-life of 385 min. This is 80-fold faster than the observed reaction rate with the unmodified PAN fiber mats under identical reaction conditions. The reactivity of PAN-Ox fibers towards DFP is comparable to the reaction of DFP on the self-decontaminating sorbent, γ-alumina, and faster than that on XE-555, a reagent commonly used for decontaminating personal equipment.[14] The slope of the linear fit of the curve corresponds to the apparent second-order rate constant, k_2. Considering the heterogeneous nature of the system, k_2 is defined as

$$k_2 = k_{obs} / M_{f0}$$

based on the mass of the reactive fibers, instead of the concentration of the amidoxime groups, as commonly applied in homogeneous solutions. Our experiments afford an estimate of the apparent k_2 of 1.0×10^{-6} s^{-1}mg^{-1} at a constant water content of C_w=1.3 wt/wt. Note that we did not observe any significant peak broadening with time for DFP in our experiments. The extent of the absorption of the DFP into the fibers could be limited.[14] Our estimation based on the whole mass of the reactive fibers underestimates the actual reaction constant k_2.
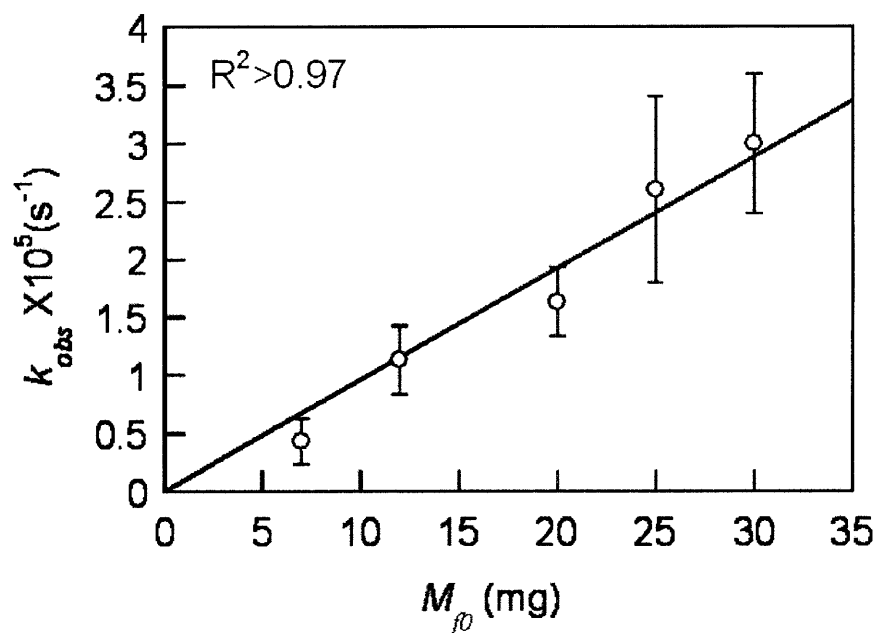
Figure 3.12. Observed reaction rates (k_{obs}) as a function of the mass of dry PAN-Ox fibers. All of the reactions were conducted at fixed water content, C_w=1.3 wt/wt and amount of DFP, M_{DFP}=3mg. Solid line is the linear fit of curve of k_{obs} vs. M_{f0}.
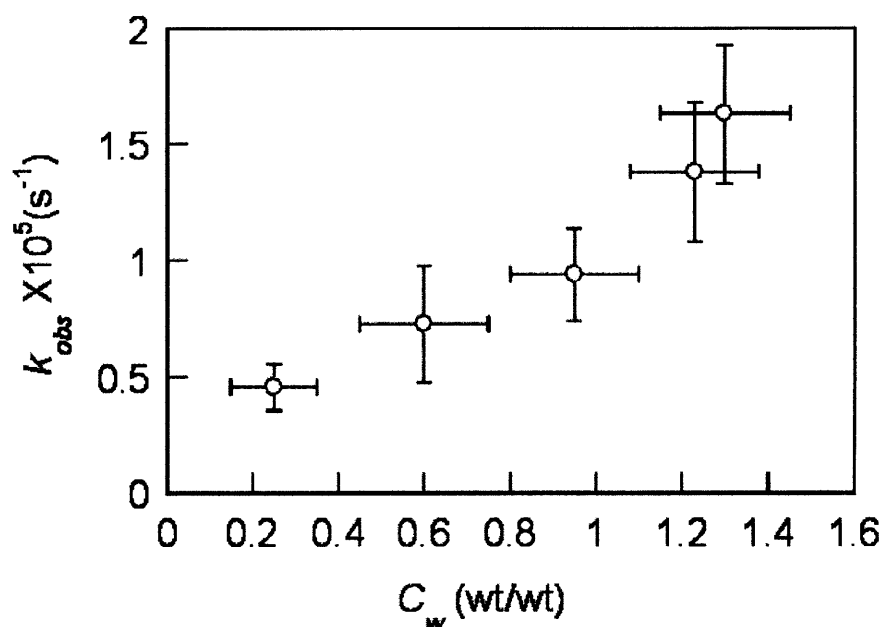
Figure 3.13. Dependence of the observed reaction rates (k_{obs}) on the water content in the fibers (C_w) at constant mass of the dry PAN-Ox fibers, M_{f0}=20mg, and amount of DFP, M_{DFP}=3mg.

The ability of the PAN-Ox fiber mats to decompose OPs is significantly affected by the presence of water. No DFP decomposition was observed in 24 hours with the dry PAN-Ox fibers. Figure 3.13 demonstrates the effect of water content in the fiber mats on the observed reaction rate, based on a series of experiments in which the observed reaction rate was measured with varying the water content, C_w, while fixing the amount of the dry PAN-Ox fiber mats (M_{f0}=20 mg, average fiber diameter, 350nm). As the amount of water in the fiber mats increases, the observed reaction rate, k_{obs}, increases. The observed reaction rate at C_w=1.30 wt/wt is three-fold faster than that at C_w=0.25 wt/wt. Given that the PAN-Ox fibers were washed and equilibrated at neutral pH of 7, and that the pK_a of polyacrylamidoxime is over 11,[13] the amidoxime groups in the PAN-Ox fibers exist predominantly in their undissociated form in our experiments. During the reaction, the nucleophilic amidoxime attacks DFP and cleaves the P-F bond (Figure 3.14). It has been

suggested that proton transfer to the nitrogen atom of the amino group increases the nucleophilicity of the attacking oxygen atom to facilitate the reaction.[16-18] This mechanism involves proton transfer to stabilize the transition state, which requires the presence of free water as a medium in the fibers. This explains the absence of DFP degradation by the dry PAN-Ox fibers. Furthermore, the effect of water to stabilize the transition state in hydrolysis has been illustrated.[19,20] Water may play a similar role in directly assisting stabilization of the transition state in this case. Recently, Schreuder-Gibson *et al.* also demonstrated that hydrolytic degradation of DFP by a film of M12, a co-polymer of poly(vinyl alcohol) and poly(vinylamine), only occurs when the film has been conditioned above a critical relative humidity of 88%.[21] It implies that bound water in the fibers lacks mobility and has little effect on promoting the action of amidoximes. Only free or bulk water in the fibers can enhance the hydrolytic degradation of DFP by the reactive PAN-Ox fibers.
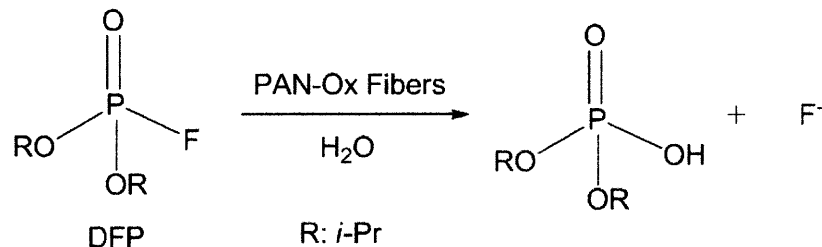
Figure 3.14. . DFP degradation by PAN-Ox fibers in the presence of water.

3.4. Conclusions

An efficient, one-step method for functionalization of PAN fibers by hydroxylamine hydrochloride was developed, resulting in conversion of the surface of the fibers into PAAO. The so-called PAN-Ox fibers thus produced are capable of hydrolytically degrading the CWA simulant, DFP, in the presence of water. At a water content (C_w) of 1.3 wt/wt, the DFP hydrolysis, monitored by ^{31}P MAS NMR, was faster by one or two orders of magnitude in the presence of PAN-Ox fiber mats than with the unmodified PAN fibers. The observed pseudo-first order reaction rate constant was found to increase with the amount of water in the fiber mats. The water serves as a medium to facilitate nucleophilic attack of amidoximes on DFP to accelerate DFP decomposition. The simplicity of preparation and efficiency of the functionalized, electrospun fiber mats in degrading toxic organophosphates make them good candidates for incorporation into a new generation of self-detoxifying, lightweight fabrics and textiles. .

3.5. References

1. Singh, A.; Lee, Y.; Dressick, W. J. *Adv. Mat.* 2004, 16, 2112.

2. Bromberg, L.; Hatton, T. A. *Ind. Eng. Chem. Res.* 2005, 44, 7991.

3. Bromberg, L.; Zhang, H.; Hatton, T. A. *Chem. Mater.* 2008, 20, 2001.

4. Karaivanova, S.; Badev, A. *Die Angew. Makromol. Chem.* 1986, 140, 1.

5. McComb, M. E.; Gesser, H. D. *J. Appl. Polym. Sci.* 1997, 65, 1175.

6. Yang, Y. –C.; Baker, J. A.; Ward, J. R. *Chem. Rev.* 1992, 92, 1729.

7. Bell, C. L.; Nambury, C. N. V.; Bauer, L. *J. Org. Chem.* 1964, 29, 2873.

8. Moroi, G.; Bilba, D.; Bilba, N. *Polym. Degrad. Stab.* 2001, 72, 525.

9. Suzer, S.; Andrews, L. *J. Chem. Phys.* 1987, 87, 5131.

10. Schouteden, F. *Makromol. Chem.* 1958, 27, 246.

11. Endres, G. F.; Epstein, J. *J. Org. Chem.* 1959, 24, 1497.

12. Stolberg, M. A.; Mosher, W. A. *J. Am. Chem. Soc.* 1957, 79, 2618.

13. Bromberg, L.; Schreuder-Gibson, H.; Creasy, W. R.; McGarvey, D. J.; Fry, R. A.; Hatton, T. A. *Ind. Eng. Chem. Res.* 2009, 48, 1650.

14. Wagner, G. W.; Bartram, P. W. *J. Mol. Catal. A: Chem.* 1999, 144, 419.

15. Segall, Y.; Waysbort, D.; Barak, D.; Ariel, N.; Doctor, B. P.; Grunwald, J.; Ashani, Y. *Biochemistry* 1993, 32, 13450.

16. Simanenko, Y. S.; Prokop'eva, T. M.; Belousova, I. A.; Popov, A. F.; Karpichev, E. A. *Theor. Exp. Chem.* 2001, 37, 288.

17. Aubort, J. D.; Hudson, R. F. *J. Chem. Soc., Chem. Commun.* 1969, 22, 1342.

18. Aubort, J. D.; Hudson, R. F. *J. Chem. Soc., Chem. Commun.* 1970, 15, 938.

19. Haeffner, F.; Hu, C.-H.; Brinck, T.; Norjin, T. *THEOCHEM* 1999, 459, 85.

20. Antonczak, S.; Ruiz-Lopez, M. F.; Rivail, J. L. *J. Am. Chem. Soc.* 1994, 116, 3912.

21. Walker, J.; Schreuder-Gibson, H.; Gibson, P.; Andzelm, J. W. Americal Chemical Society National Meeting in Philadelphia, August 17-21, 2008.

Chapter 4

Electrospun Cellulose Acetate Fibers Containing Chlorhexidine as a Bactericide

4.1. Introduction

Biological warfare agents or contaminants typically do not penetrate the cloth or skin. The primary issue associated with biological contaminants is that they can attach onto clothing or gloves in high concentration and may cause extensive contamination when they leave the surfaces. Therefore, current efforts in biological protection are aimed at the development of self-detoxifying fabrics that can kill any microorganisms attached on the protection fabrics in order to prevent further contamination. Electrospun porous materials are desirable in this regard, since they can provide high specific surface area for the attachment of biocides to enhance the function of biological protection fabric systems. Silver nanoparticles have been incorporated into electrospun fibers and shown to exhibit good antimicrobial activity.[1,2] Recently, quaternized chitosan with quaternary ammonium groups was electrospun into fibers by blending with other polymers such as poly(vinyl alcohol) and demonstrated high antibacterial activity.[3,4]
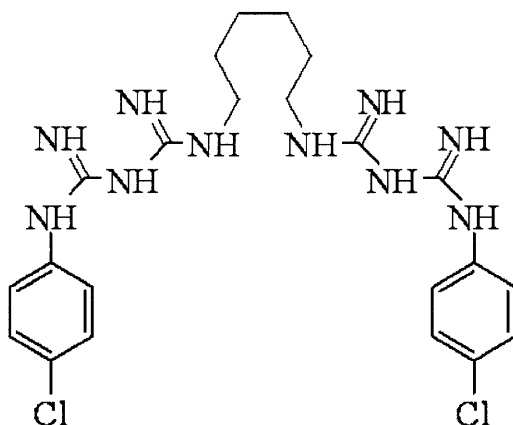
Figure 4.1. Chlorhexidine (CHX)
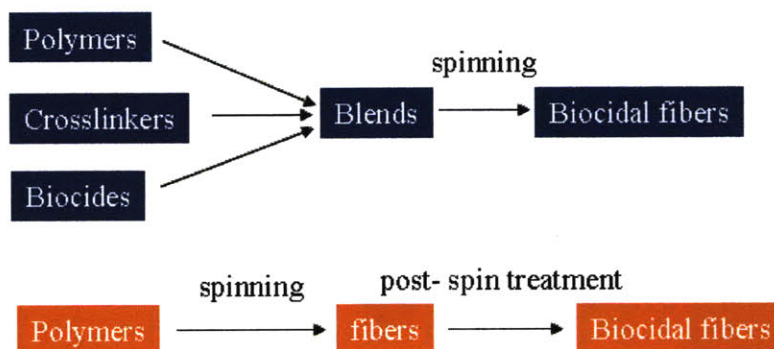
Figure 4.2. Strategies to produce bactericidal fibers containing CHX

In this chapter, we report on electrospun fiber meshes containing the biocide chlorhexidine, incorporated within and/or bound onto the surfaces of the fibers to obtain bactericidal membranes, intended for use in protective fabrics or antibacterial filtration media. Chlorhexidine (CHX) (Figure 4.1) has been widely used as an effective antibacterial agent in applications that range from common disinfectants to bactericidal agents in dentistry; this is largely due to its broad range of antimicrobial activities against bacteria and fungi, high killing rate and nontoxicity towards the mammalian cells.[5,6] The commonly cited mechanism of action of CHX is that two symmetrically positioned chlorophenyl guanide groups can penetrate through the cellular wall of bacteria and irreversibly disrupt the bacterial membrane, thus killing the microorganism. In most materials that include CHX as the biocide, CHX is simply enmeshed within the material and gradually leaches out to kill the bacteria.[7,8] The disadvantage of such a loose association is that the antibacterial agent is eventually exhausted and the material has a limited functional life. In this work, two strategies (Figure 4.2) were employed to obtain bactericidal fiber mats containing CHX. In the first strategy, dually functional antibacterial fibers were generated by electrospinning a series of blends of cellulose acetate (CA) and CHX with (a) a part of CHX bound to the CA polymer matrix by the organic titanate linker, Tyzor® TE (TTE), and (b) a significant fraction of CHX unbound but embedded within the fibers. In

91

the second strategy, antibacterial CHX fibers were also produced by a post-spin treatment process to immobilize CHX on already prepared CA fibers. The resulting bactericidal electrospun CA-CHX fibers possessed significant antibacterial activity against both the gram-negative strain of *Escherichia coli* (*E. coli*) and the gram-positive strain of *Staphylococcus epidermidis* (*S. epidermidis*).

4.2. Experimental method

4.2.1. Materials

Cellulose acetate (CA) (M_n 50kDa), chlorhexidine (CHX) (98%), poly (ethylene oxide) (PEO) (viscosity-average molecular weight, M_v, 2 MDa and 5 MDa), and N,N-dimethylformamide (DMF) were purchased from Sigma-Aldrich Chemical Co. (St. Louis, MO) and used as received. Tyzor[®] TE (TTE) (80 wt% titanium triethanolamine in isopropanol) was kindly supplied by Du Pont de Nemours & Co. (Wilmington, DE) and used as received. Chlorhexidine digluconate aqueous solution (20% w/v) was purchased from Alfa Aesar Co. (Ward Hill, MA) and used as received. Bacteria *E. coli* and *S. epidermidis* were purchased from ATCC (Manassas, VA) and stored at -80 °C prior to use.

4.2.2. Polymer solution characterization and electrospinning

DMF is a good solvent for chlorhexidine powders as well as CA and thus was employed as the electrospinning medium in this work. The lack of elasticity of the CA solutions in DMF did not permit the formation of uniform fibers, however, and droplets were formed instead. A recent study by Yu *et al.*[9] demonstrated that the addition of a small amount of high molecular weight PEO into the spin solution can significantly increase the elasticity (extensional viscosity) of the solution and thus facilitate the electrospinning process. Following this approach, we incorporated relatively small amounts of PEO (M_v 2 or 5 MDa) into the spin solutions in order to generate uniform fibers. A series of polymer solutions of 3 wt% CA with various concentrations of PEO in DMF were prepared. A capillary breakup extensional rheometer (CaBER 1) (Thermo Electron Co.) was used to examine the extensional properties of the polymer solutions and relate these to the properties of the resulting fibers, to determine the concentration of PEO in polymer solutions required for the

formation of uniform fibers.

CaBER is a filament stretching apparatus that measures the mid-point diameter, $D_{mid}(t)$, of the thinning filament over time when a fluid filament constrained axially between two coaxial disks is stretched rapidly over a short distance.[10,11] In these measurements, the Hencky strain, ε, and the apparent extensional viscosity, η_{app}, are related as follows:[10]

$$\varepsilon = 2\ln\left(\frac{D_0}{D_{mid}(t)}\right) \qquad (1)$$

$$\eta_{app} = -\frac{\sigma}{dD_{mid}(t)/dt} \qquad (2)$$

where D_0 is the initial diameter of the filament before stretching and σ is the surface tension of the fluid. The time evolution of $D_{mid}(t)$ for viscoelastic fluid is governed by a balance between surface tension and elasticity and can be described by the following model:[11]

$$D_{mid}(t) = D_1\left(\frac{D_1 G}{4\sigma}\right)^{1/3} e^{-t/3\lambda_p} \qquad (3)$$

where D_1 is the initial midpoint diameter just after stretching, G the elastic modulus, and λ_p the fluid relaxation time, which is the characteristic time scale of viscoelastic stress growth.

A series of polymer solutions of 3 wt% CA, 0.2 wt% PEO (M_v 5 MDa), 1 wt% TTE and various concentrations of CHX (0.3, 0.6, 0.9 and 1.2 wt%) were prepared by adding PEO, CA, chlorhexidine powders and TTE sequentially into DMF. The solutions were heated to 50 °C upon addition of PEO to facilitate the dissolution of the high molecular weight polymer. Then the polymer blends were stirred at room temperature until clear homogeneous solutions were obtained. The CHX-containing fibers produced from these solutions are denoted CA-CHX fibers. Polymer solutions of 3 wt% CA, 0.2 wt% PEO (M_v 5 MDa) and 1 wt% TTE without CHX were also

prepared to produce nonfunctional crosslinked CA fibers, which are denoted CA-TTE fibers. In addition, solutions of 3 wt% CA and 0.2 wt% PEO (M_v 5 MDa) were prepared for post-spin treatment to attach CHX on the fiber surface. These fibers are denoted CA-PEO fibers.

An electrospinning apparatus as described previously in chapter 1 was used, except that the spun fibers were collected on a rotating drum ground electrode (3.5cm in diameter, 20cm in length and rotation rate of 250 rpm) instead of a plate collector, where the collected fibers discharged less efficiently and impeded accumulation of the fiber mesh. A syringe pump (Harvard Apparatus PHD 2000) was used to deliver polymer solution via a Teflon feedline to a capillary nozzle. Voltages up to 30 kV, generated by a power supply (Gamma High Voltage Research ES-30P), were applied between the upper plate and the ground drum to provide the driving force for electrospinning. The electrical potential, solution flow rate, and distance between the capillary nozzle and the collector were adjusted to 16-19 kV, 0.04 ml/min, and 45 cm, respectively, to obtain a stable jet.

4.2.3. CHX binding to the fibers

TTE is an organic titanate that has been applied as a cross-linking agent in adhesives, coatings, oil and gas products, and textiles.[12,13] It cross-links or binds compounds with hydroxyl, amino, amido, carboxyl and thio groups.[12-15] The cross-linking and titanate polymerization to form titania is activated at high temperature (100-250 °C) and/or in the presence of water.[12] We conducted control experiments to test the binding capability of TTE to CHX. The CHX powder and TTE solution were mixed at a weight ratio of 1:8 to form a yellowish homogeneous suspension. The suspension gradually became clear upon addition of a small amount of water due to the reaction of TTE with CHX, which facilitates the dissolution of CHX. Heating the solution to 70 °C accelerated the reaction process. The viscosity

increased dramatically and the solution gradually became pink and pasty or gel-like in appearance, which is indicative of binding of TTE to CHX. (Figure 4.3)
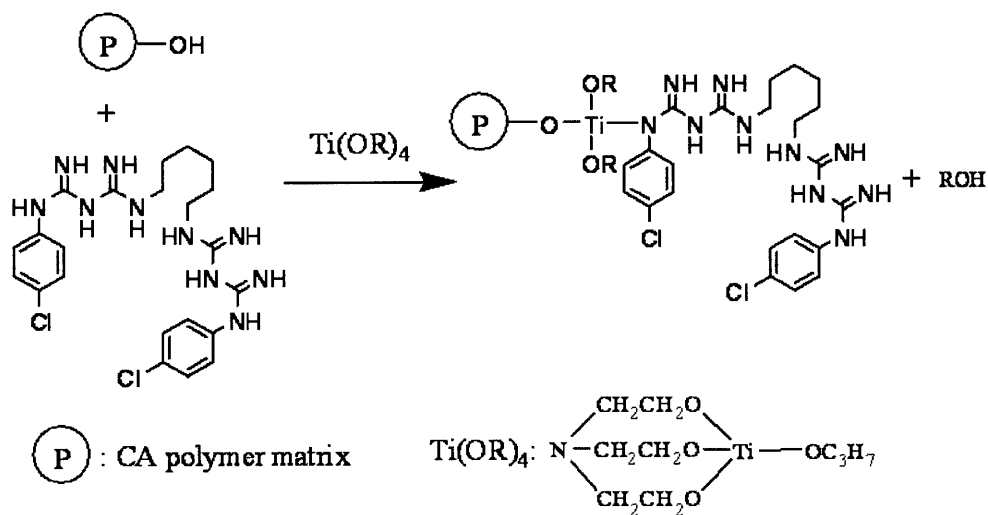
Figure 4.3. Binding of amino groups of CHX to hydroxyl groups of the CA polymer matrix via titanate links using Tyzor® TE (TTE).

In analogous experiments where binding between CHX and the CA polymer matrix via TTE linkers in the fiber meshes was desired, the fibers were placed in an environment of saturated water vapor at 70 °C for 4 days. The fibers turned slightly pink during the curing process, indicating the occurrence of a chemical reaction. A schematic of the binding chemistry (Figure 4.3) depicts the reaction of the organic titanate TTE with the hydroxyl groups of CA and amino groups of CHX, respectively, via transesterification reactions, to covalently bind CHX to the CA polymer matrix.

4.2.4. Quantification of CHX content in the fibers

Not all of the CHX molecules were covalently bound to the polymer matrix

during the curing experiments. To determine the fraction of CHX that was not bound to the fibers, weighed fibers (10 mg) were placed in a sufficient quantity of water (100-200 ml) to ensure essentially complete release of free CHX. The unbound CHX that was gradually released upon immersion of the mesh in water was measured using a Hewlett Packard 8453 UV-Vis spectrophotometer by monitoring a characteristic peak at 254 nm and using calibration (absorbance vs. CHX concentration) curves.

4.2.5. Fiber characterization

The fibers were examined by scanning electron microscopy (SEM) using a JEOL-6060 microscope (JEOL Ltd) to visualize their morphology. A thin layer of gold (*ca.* 10nm) was sputter-coated onto the fiber samples.

Prior to FTIR, Raman and XPS measurements, the crosslinked CA-CHX fiber meshes were placed in excess water for 12 hours to remove completely the unbound CHX and dried under vacuum at room temperature to constant weight. The complete removal of the CHX not covalently linked to the fiber was ensured by monitoring the CHX concentration in the wash-outs. When no further removal of the CHX from the fibers into water was detected, the fibers were considered to be fully depleted of the unbound CHX.

FTIR spectra were measured in absorbance mode using a Nexus 870 spectrophotometer (Thermo Nicolet Co.) equipped with an ATR accessory. Two hundred and fifty-six scans were accumulated with a resolution of 4 cm^{-1}.

Raman spectra were measured with a Kaiser Hololab 5000R Raman spectrometer (Kaiser Optical Systems Inc.) with an excitation wavelength of 785 nm.

XPS measurements were carried out with a Krato Axis Ultra Imaging X-ray photoelectron spectrometer (Kratos Analytical Co.) equipped with a monochromatized Al Kα X-ray source.

4.2.6. Post-spin treatment of fibers

Bactericidal, CHX-containing CA-CHX fibers were also produced by post-spin treatment of CA-PEO fiber meshes. CA-PEO Fibers were first electrospun from 3 wt% CA and 0.2 wt% PEO (M_v 5 MDa) solutions in DMF. The CA-PEO fiber meshes thus formed were immersed for 1 hour in 10 wt% titanium triethanolamine solution in isopropanol, which was obtained by dilution of the TTE solutions supplied by the manufacturer. The fiber meshes were cured at 110 °C for 10 minutes to bind TTE to CA. The fibers were then rinsed with water several times and dried. The resulting fibers were placed in 5% (w/v) chlorhexidine digluconate aqueous solution for 1 hour and cured in the oven at 90 °C for 30 minutes to immobilize the CHX via the titanate linkers. The treated fibers were rinsed with water several times and dried under vacuum to constant weight. The applied temperatures were used as in Reference [14], where organic titanates were successfully used to bind antibiotics onto cotton fabrics.

4.2.7. Antibacterial tests

4.2.7.1. Disk diffusion test

The release-killing capacity of unbound CHX in the CA-CHX fibers was determined by the disk diffusion test method. *E. coli* and *S. epidermidis* were cultured by adding 10 μL of the bacteria to 5 mL Luria-Bertani (LB) broth and incubating it under shaking at 37 °C overnight, followed by dilution with a phosphate buffer solution (PBS, pH 7.0) to approximately 5×10^6 cell/ml. The bacteria were spread onto LB agar plates with cotton swabs. The round slide disks (diameter =

22mm), to which the CA-CHX fibers were attached, were placed on top of the agar plates. The agar plates were inverted and incubated at 37 °C for 16-20 hours. Duplicate experiments were conducted and the zone of inhibition (ZoI) was measured.

4.2.7.2. ASTM E2149-01 method

The CA-CHX fiber meshes were placed in excess water for 12 hours to remove unbound CHX molecules, and dried under vacuum to constant weight. The contact-killing capacity of CA-CHX fibers was assayed according to a modified ASTM E2149-01 method (dynamic shake flask test).[16] Briefly, *E. coli* and *S. epidermidis* were cultured overnight and diluted in PBS to approximately 10^6 cell/ml. The fiber meshes (100 mg) were placed in a 50 ml bacterial suspension in a sterile flask and the suspension was shaken at 200 rpm at room temperature for 1 hour using an orbital shaker. A certain amount of the suspension (100 µL) was retrieved from the flask before and after exposure to the mesh and plated with serial dilutions. After incubation of agar plates at 37 °C for 16-20 hours, the number of viable colonies was counted visually and the reduction in the number of viable bacteria colonies was calculated after averaging the duplicate counts.

4.3. Results and discussion

4.3.1. Optimization of CA-PEO electrospinning process

(a)

(b)
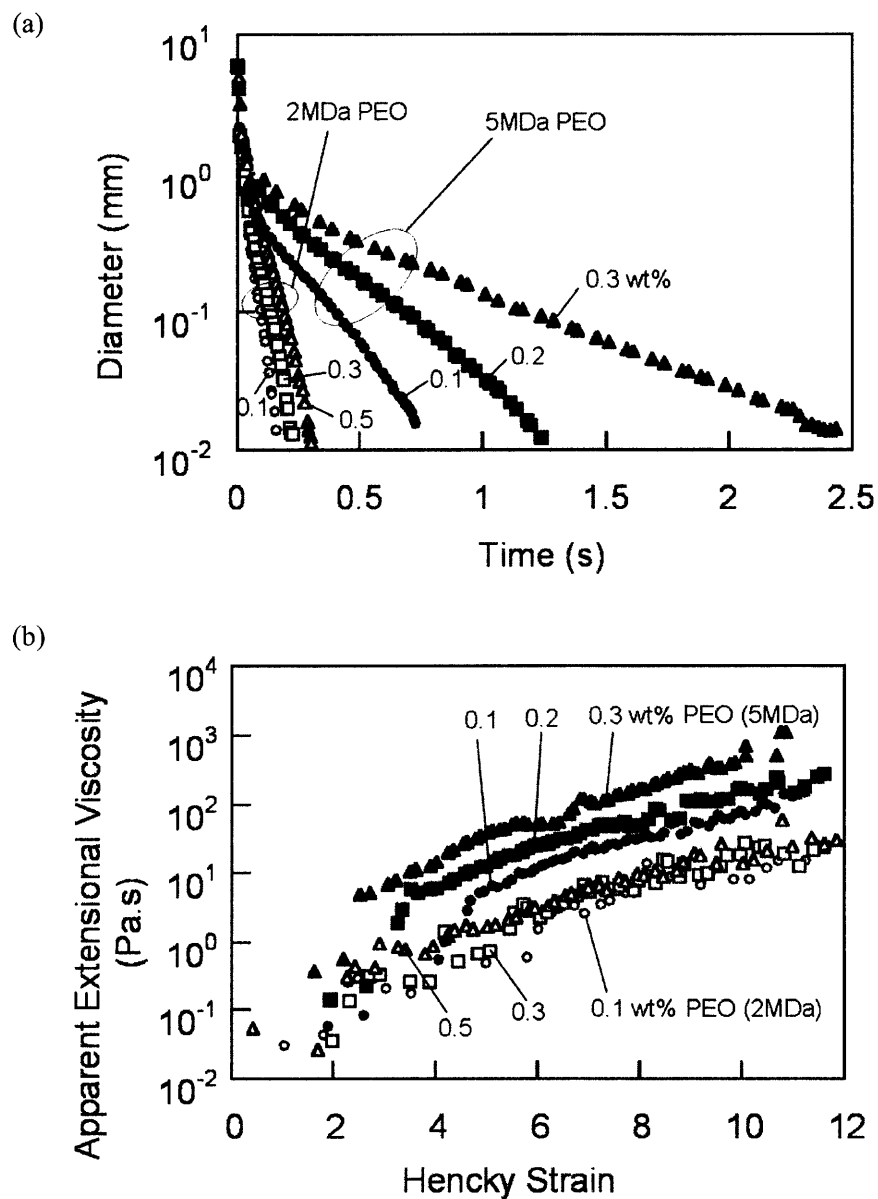
Figure 4.4. Extensional properties of CA-PEO solutions: (a) filament diameter evolution curves; (b) Extensional viscosity vs. Hencky strain.

Figure 4.4(a) shows the time evolution of the midpoint diameter during the CaBER measurements for six CA-PEO polymer solutions consisting of 3wt% CA with various concentrations of PEO (M_v 2 and 5MDa) ranging from 0.1 to 0.5 wt%. The filament breakup time increased with increasing PEO concentration, and was significantly higher for the higher (5 MDa) than for the lower molecular weight (2 MDa) PEO. The curves of apparent extensional viscosity vs. Hencky strain for these six solutions were derived from the time evolution data of midpoint diameter using eqns (1) and (2) and are shown in Figure 4.4(b). A clear tendency toward extensional strain hardening was observed for these polymer solutions. The apparent extensional viscosity increased with the PEO concentration and molecular weight. A more elastic solution possesses a slower thinning rate and a longer breakup time due to the resistance to the capillary breakup during extensional deformation afforded by the elastic force. This accounts for the observed increase in the filament breakup time as PEO concentration and molecular weight were increased.

Figure 4.5 shows the typical morphologies of the CA-PEO fibers electrospun from the above solutions. The lack of elasticity of the solutions with lower molecular weight and/or lower concentration of PEO leads to the formation of droplets (Figure 4.5(a)). A transition in fiber morphology from a beads-on-string structure to a uniform fiber is observed with increasing PEO concentration and molecular weight (Figures 4.5 (b) and (c)). Uniform fibers are generated when the concentration of PEO (M_v 5 MDa) is at least 0.2 wt% at 3 wt% CA in DMF (Table 4.1). The relaxation times, λ_p, were obtained by fitting the elastic model described in eqn (3) to the time evolution data of midpoint diameter in the range of exponential thinning. A dimensionless Deborah number, De, was introduced to examine the spinnability of the CA-PEO solutions. De is defined as the ratio of the fluid relaxation time, λ_p, to the Rayleigh instability growth time, t_R, as follows:[11,17]

$$De = \frac{\lambda_p}{t_R} \qquad (4)$$

where

$$t_R = \frac{1}{\omega_{max}} = \sqrt{\frac{\rho R_0^3}{\sigma} \cdot \frac{I_0(x_R)}{I_1(x_R)(1-x_R^2)x_R}} \qquad (5)$$

in which ω_{max} is the largest instability growth rate, σ the surface tension, ρ the density, R_0 the initial radius of the polymer jet (0.8 mm in this work), x_R the reduced wave number, and $I(x_R)$ the modified Bessel function. Prior studies[18,19] have shown that viscoelasticity does not significantly affect the classical Rayleigh wavelength and only slightly increases the growth rate. Therefore, the classical Rayleigh instability growth rate for Newtonian fluids was used to estimate the instability growth time as shown in eqn (5). The most unstable mode, corresponding to ω_{max}, occurs at $x_R = 0.697$. If the fluid relaxation time is much greater than the instability growth time ($De \gg 1$), the instability is fully suppressed or arrested by the viscoelastic response to produce uniform fibers. Table 4.1 shows the relaxation times, De numbers and fiber morphology for all six tested CA-PEO solutions. Only for $De > 7$ were uniform electrospun fibers produced, which is in accordance with the results on electrospun PEO/PEG fibers reported by Yu et al.[9] Therefore, De is a good indicator of the spinnability of CA-PEO solutions. The addition of a small amount of high molecular weight PEO can increase the elasticity of polymer solutions and substantially facilitate the electrospinning of CA fibers.

(a)

(b)

(c)
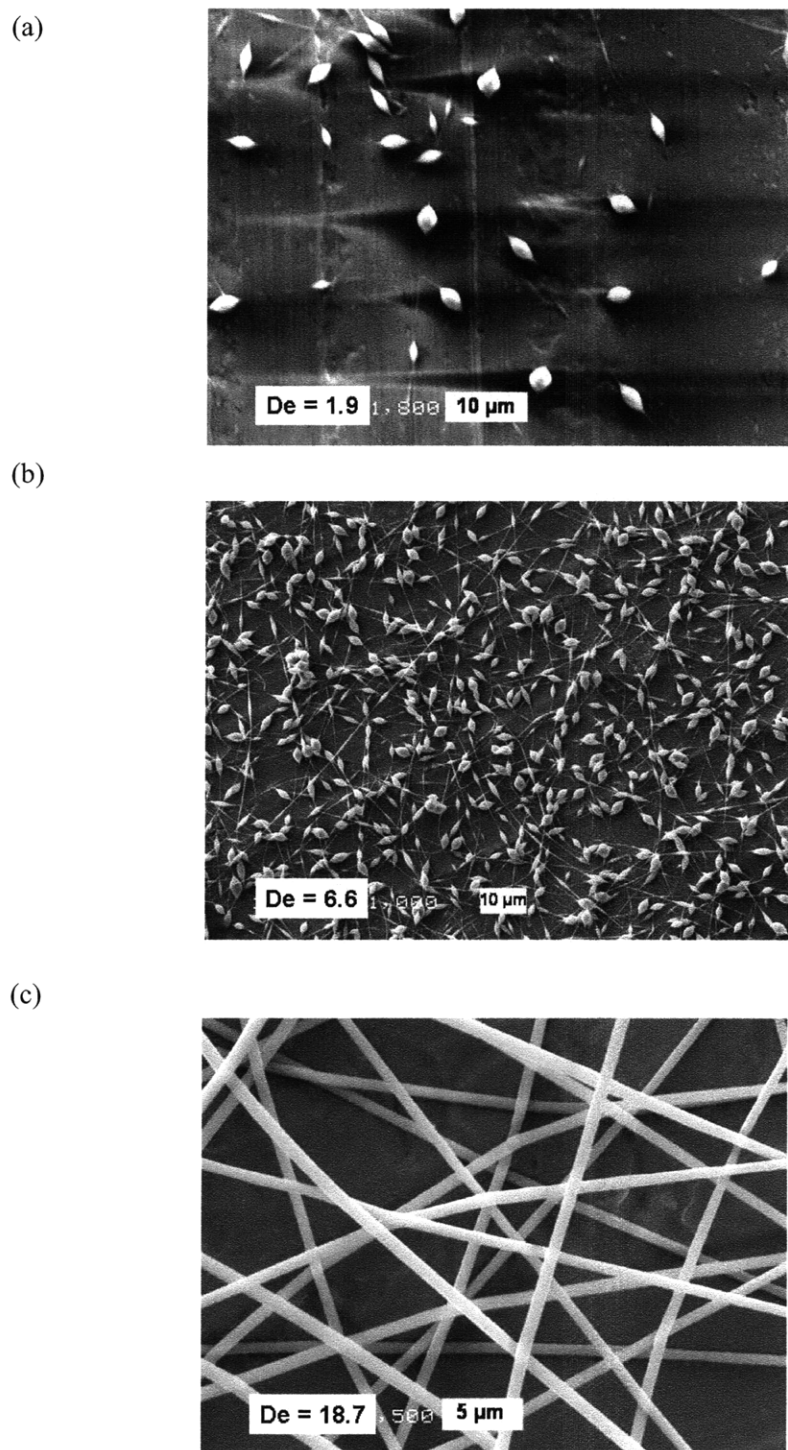
Figure 4.5. Typical electrospun fiber morphologies for CA-PEO solutions. (a) 3 wt% CA, 0.3 wt% PEO (2M), De=1.9, droplets; (b) 3 wt% CA, 0.1 wt% PEO (5M), De=6.6, beads-on-string; (c) 3 wt% CA, 0.3 wt% PEO (5M), De=18.7, uniform fibers.

Samples[a]	Relaxation time λ_p (s)	surface tension σ (mN/m)	De	Fiber morphology
0.1 wt% PEO (2M)	0.013	35.6	1.2	no fibers
0.3 wt% PEO (2M)	0.020	35.3	1.9	no fibers
0.5 wt% PEO (2M)	0.021	35.0	2.0	beads-on-string
0.1 wt% PEO (5M)	0.072	34.1	6.6	beads-on-string
0.2 wt% PEO (5M)	0.105	34.4	9.6	uniform fibers
0.3 wt% PEO (5M)	0.201	35.6	18.7	uniform fibers

[a] 3 wt% CA in DMF

Table 4.1. Relaxation times, Deborah numbers and fiber morphology of CA-PEO solutions

4.3.2. Bactericidal CA-CHX fibers electrospun from polymer blends

4.3.2.1. Electrospinning

Solutions[a]	Conductivity (μS/cm)	Relaxation time λ_p (s)	surface tension σ (mN/m)
0 wt% TTE, 0 wt% CHX	0.23	0.105	35.6
1.0 wt% TTE, 0 wt% CHX	0.36	0.104	34.6
1.0 wt% TTE, 0.3 wt% CHX	0.92	**0.101**	34.3
1.0 wt% TTE, 0.6 wt% CHX	1.50	0.096	34.5
1.0 wt% TTE, 0.9 wt% CHX	1.23	0.092	33.9
1.0 wt% TTE, 1.2 wt% CHX	1.45	0.081	34.5

[a] 3 wt% CA and 0.2 wt% PEO (5M) in all solutions

Table 4.2. Solution properties of polymer blends for electrospinning

A series of solutions with 3 wt% CA, 0.2 wt% PEO, 1.0 wt% TTE and various concentrations of CHX (0.3, 0.6, 0.9 and 1.2 wt%) in DMF were electrospun successfully into fibers. The addition of CHX and coupling agent TTE did not

impair the electrospinning process, and even facilitated it.   The time evolution curves by CaBER measurements for these CHX-containing polymer solutions showed very similar or slightly smaller relaxation times compared to those of the CA-PEO solution without CHX and TTE (Table 4.2).   However, the conductivity of polymer solutions was observed to increase upon the addition of TTE and CHX (Table 4.2), which is known to stabilize the electrospinning process.[20,21]   Figure 4.6(a) illustrates the typical morphology of electrospun CA-CHX fibers.   There was no obvious change in fiber size as the concentration of CHX in the solutions was varied.   The average size of these fibers was about 950 nm in diameter with the fiber sizes ranging from 700 to 1200 nm.   A typical SEM image of fibers after curing is shown in Figure 4.6(b). While the fiber size was not affected by the treatment, some fibers appeared to be coupled together at the junctions, and titanium clusters were observed to form on the surfaces of some fibers.   The resultant CA-CHX fibers did not dissolve in THF, which indicated cross-linking of the fiber meshes by the organic titanate, while CA-PEO fibers produced without titanate dissolved in THF readily.

(a)
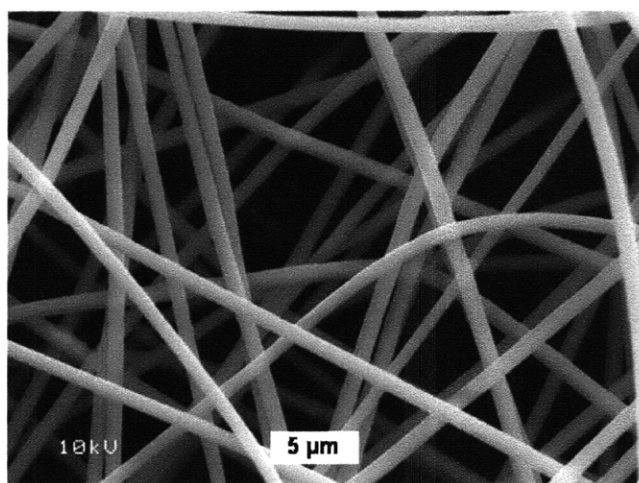
(b)
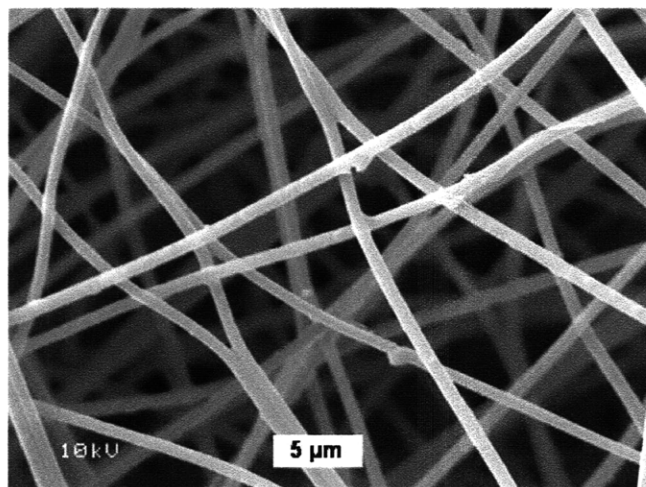
Figure 4.6. SEM images of CA-CHX fibers: (a) as-spun fibers (fiber diameter: 950±100nm); (b) fibers after curing under saturated water vapor at 70 °C for four days.

4.3.2.2. Quantification of CHX content in the fibers

Total concentration of CHX in fibers (wt%)[a]	7.0	13.0	18.4	23.1
bound CHX (wt%)	6.8 ± 0.1	5.5 ± 0.4	7.3 ± 0.7	8.1 ± 1.6
unbound CHX (wt%)	0.2 ± 0.1	7.5 ± 0.4	11.1 ± 0.7	15.0 ± 1.6

[a] derived from the solution compositions for electrospinning: 3.0 wt% CA, 0.2 wt% PEO, 1.0 wt% TTE and 0.3, 0.6, 0.9 or 1.2 wt% CHX

Table 4.3. Extent of binding of CHX to the fibers

Table 4.3 shows the extent of CHX binding in the fibers determined by the UV-Vis measurements.   As is seen, not all of the CHX was bound to the CA polymer

106

matrix during the curing experiments. In the case of 7.0 wt% total CHX content in the fibers, almost all CHX was coupled to the polymer matrix via TTE linkers. With increasing concentration of CHX in the fibers for a constant TTE concentration (1 wt% in spin solutions), the amount of unbound CHX increased dramatically, while the concentration of bound CHX varied in a narrow range between 5 to 9 wt%. When the TTE concentration was increased from 1 to 2 wt% for fixed CHX concentrations in spin solutions, the resulting fibers possessed a similar concentration of bound CHX to that of the fibers electrospun from 1 wt% TTE solutions, suggesting that both CHX and TTE concentrations have a weak effect on the extent of CHX binding in these fibers. Thus, the concentration of bound CHX varies in a narrow range in these fibers while concentration of unbound CHX can be manipulated by controlling the concentration of CHX in the spun solutions.

4.3.2.3. Fiber characterization
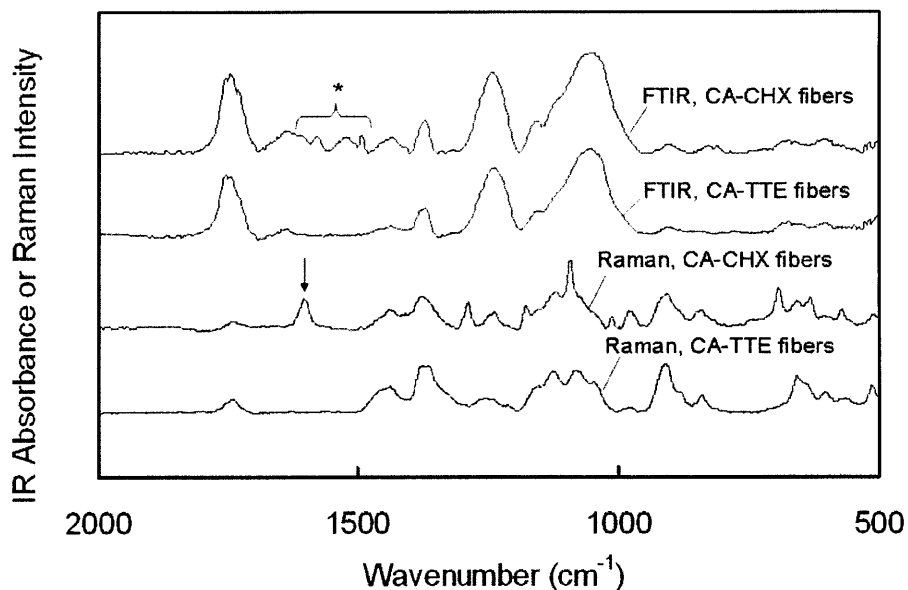
Figure 4.7. FTIR and Raman spectra of fully washed CA-CHX fibers and nonfunctional CA-TTE fibers.

107

The CA-CHX fibers were characterized by FTIR and Raman spectroscopy. FTIR and Raman spectra of fully washed CA-CHX fibers and crosslinked nonfunctional CA-TTE fibers are shown in Figure 4.7.

The characteristic IR peaks of CHX observed between 1500 and 1650 cm^{-1} (C=N stretching and aromatic C=C bending vibrations, respectively) marked by a star (*) indicate the presence of CHX bound to the CA of the fibers. The same characteristic peaks were observed in the ATR-FTIR spectrum of CA-CHX fibers as well, indicating the presence of CHX on the fiber surface. Note the absence of these peaks when the CA-TTE fibers contained no CHX. In the Raman spectrum of the CA-CHX fibers, the characteristic CHX peak at 1610 cm^{-1}, as indicated by an arrow in Figure 4.7, was observed. The peak is shifted 40 cm^{-1} to higher wavenumbers compared to that of pure CHX powders (1570 cm^{-1}), which could be attributed to the interaction of CHX with the polymer matrix in the fibers.[22] XPS was used to determine the surface composition of CA-CHX fibers; a typical XPS spectrum of fully washed CA-CHX fibers is shown in Figure 4.8.

The presence of titanium coupling agents on the surface layer was verified by the characteristic binding energy of Ti at 455 eV. The appearance of characteristic binding energies of N and Cl in the spectrum confirmed the presence of CHX bound within 10 nm of the surface of the fibers. The atomic ratio of Cl to C on the surface obtained from XPS measurements increased from 0.02 to 0.05, while the atomic ratio of Cl to O increased from 0.07 to 0.30, as the concentration of CHX in the spin solutions was increased from 0.3 to 1.2 wt%. Both atomic ratios on the surface layer of these fibers were much greater than their bulk values (Cl/C: 0.01-0.02, Cl/O: 0.01-0.03) obtained by elemental analysis; this is indicative of enrichment of CHX on the surface of the fibers rather than in the core. CHX has been reported to be a surface-active compound and to form small aggregates in aqueous solution.[23] Such surface-active properties may promote the accumulation of CHX close to or on the surface of the jet during the electrospinning process.
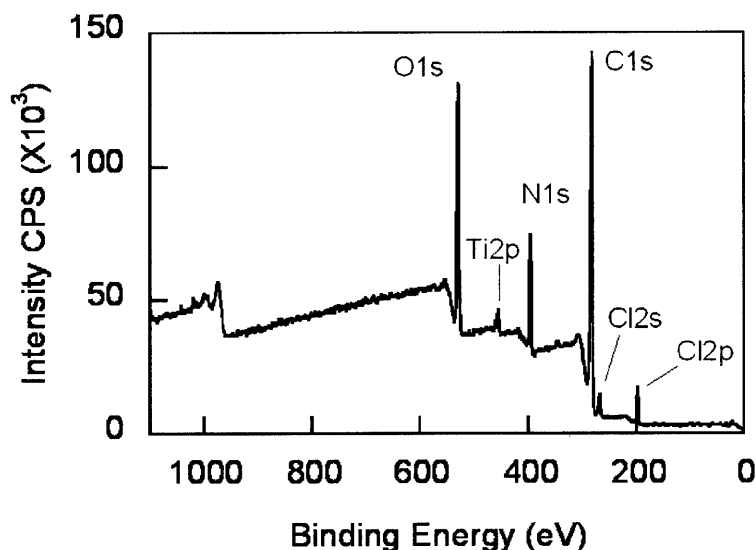
Figure 4.8. XPS spectrum of fully washed CA-CHX fibers with 7.3 wt% of bound CHX

4.3.2.4. Antibacterial activity

The release-killing capacity of unbound CHX in the fibers was evaluated by disk diffusion tests. The zone of inhibition (ZoI) was observed in all of the tested fiber samples, as indicated by the arrow shown in Figure 4.9(a). In this test, unbound CHX in the fibers diffused out of the fibers, killing the bacteria nearby until the minimum inhibitory concentration of CHX (2-8 μg/ml for *E. coli* and 0.5-2 μg/ml for *S. epidermidis* [24]) was reached, below which bacteria can survive and proliferate. This resulted in the formation of a circular zone area where no bacterial colonies were observed. The size of the ZoI was measured from the edge of the circular fiber sample (22 mm in diameter) to the edge of the inhibition zone. Figure 4.10(a) shows the ZoI determined by the disk diffusion tests against *E. coli* and *S. epidermidis* for four different fibers electrospun from four different CHX concentrations. Each datum point represents one type of fiber sample. The amount of CHX released per

109

unit area was calculated from the weight of the circular fiber sample with a diameter of 22 mm (3-5 mg) and the concentration of unbound CHX in the fibers listed in Table 4.3.   The curve shapes of ZoI *vs* amount of CHX released per unit area (*M*) are very similar for *E. coli* and *S. epidermidis*.   The ZoI increased significantly between zero and 0.05 mg/cm^2 of CHX released, and then increased more gradually for amounts of the released CHX in excess of 0.05 mg/cm^2.   Since this test method is based on the diffusion of unbound CHX, a simple one-dimensional diffusion model can describe the dependence of ZoI on the amount of released CHX from the fibers. That is, assuming radial diffusion of CHX the following relationship between *M* and ZoI can be derived:[25,26]

$$(\text{ZoI})^2 = 4Dt\left(\ln\left(\frac{M}{M'} \right) + \ln C \right) \qquad (6)$$

where M' is the critical inhibition amount of CHX released per unit area, below which bacteria can survive, *D* is the diffusion coefficient of CHX under the test conditions, *t is* the critical time for the formation of inhibition zone (less than the incubation time), and *C* is a constant.   Critical time, *t*, is a constant for a specific bacterium, which is determined by both growth rate of bacterium and the diffusion of the bactericide.   Critical time can be obtained by measuring ZoI when the period of preincubation (*h*) is varied.   According to equation (7), plotting (ZoI)^2 vs. *h* gives a straight line graph intercepting the axis when ZoI = 0 at *h* = *t*.   In such a way, constant *t* can be determined.   Therefore, given *t* is a constant, based on equation (6), ln(*M*) should be linearly proportional to (ZoI)^2.   The (ZoI)^2 versus ln(*M*) dependencies were linear (R^2>0.99) for both *E. coli* and *S. epidermidis*, as shown in Figure 4.10(b).

$$t - h = \frac{(\text{ZoI})^2}{4D} \ln(\frac{M}{M'}) \qquad (7)$$

110

(a)
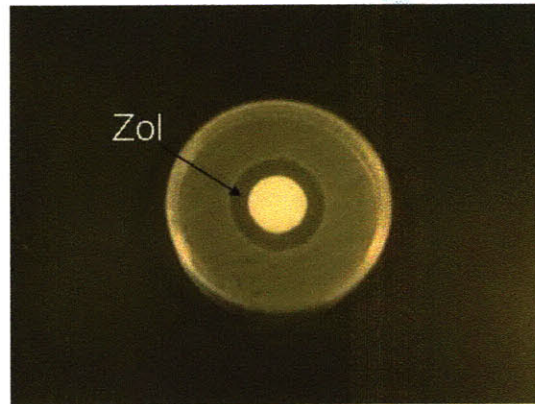
(b)
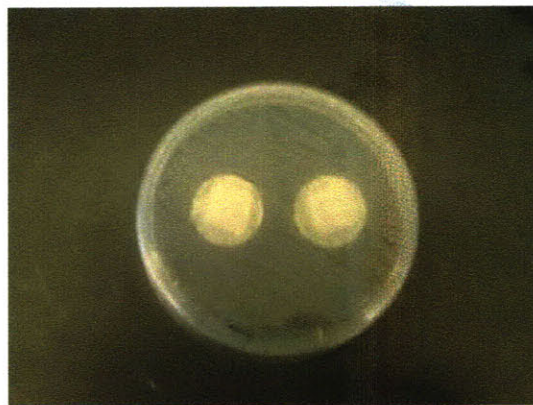
Figure 4.9. Photo images of agar plates after disk diffusion tests (*E. coli*). (a) CA-CHX fibers without water treatment; (b) CA-CHX fibers completely washed out prior to test. (The two samples shown in (b) are identical.)
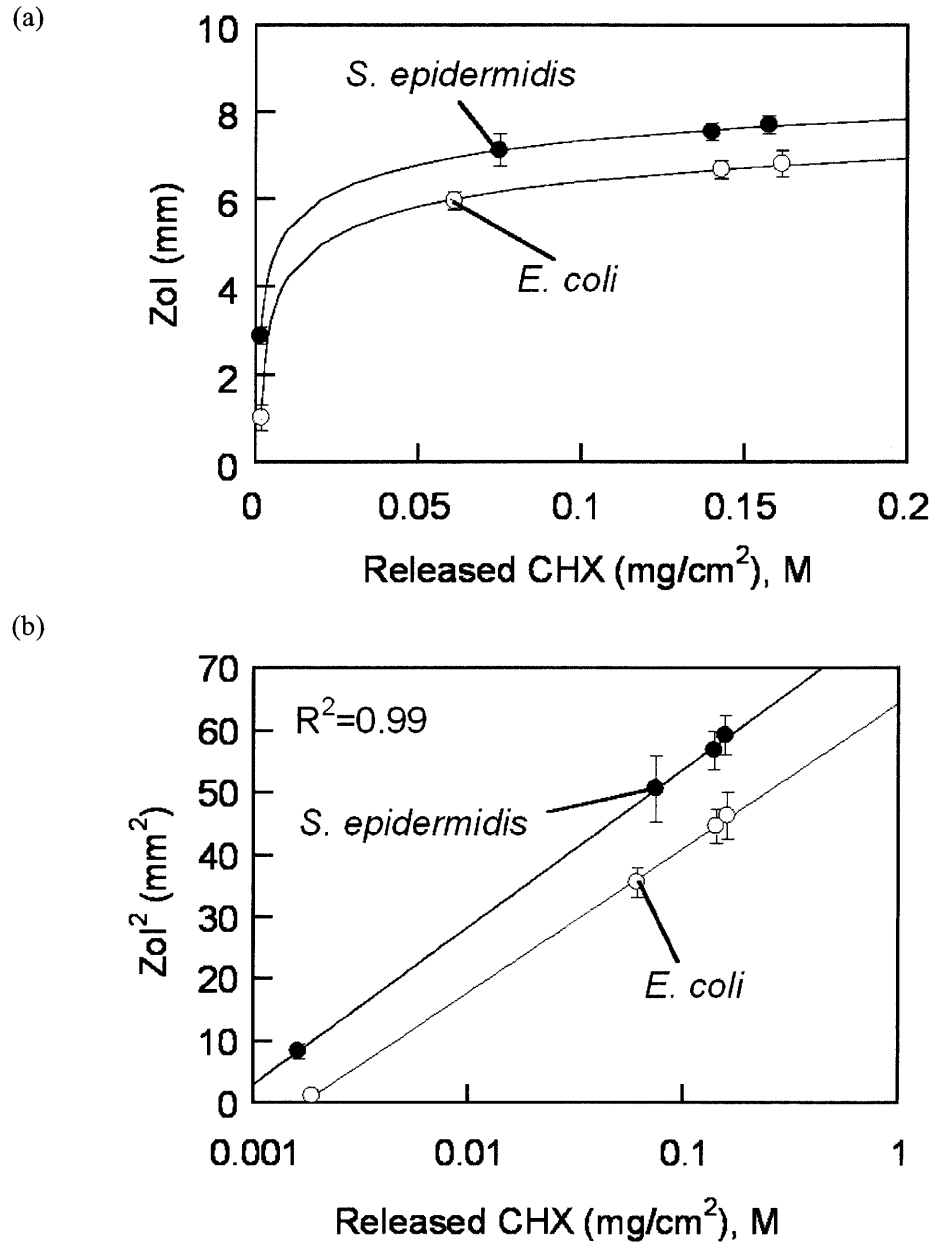
Figure 4.10. Disk diffusion test results for CA-CHX fibers. (a) Zone of inhibition (ZoI) vs. the amount of CHX released per unit area (M) of the fibers for *E. coli* and *S. epidermidis*. The solid curves were obtained by translating the corresponding linear regression lines of (ZoI)^2 vs. ln(M) in (b) into the ZoI vs. M plots. (b) (ZoI)^2 vs. ln(M) for *E. coli* and *S. epidermidis*. The solid lines are linear regression lines of (ZoI)^2 vs. ln(M).

CHX concentration in spin solutions (wt%)	Bound CHX[a] (wt%)	Bactericidal efficiency (%)	
		E. coli	S. epidermidis
0.3	6.8	94.2	96.4
0.6	5.5	96.0	99.0
0.9	7.3	98.1	96.0
1.2	8.1	99.1	99.9

[a] bulk value determined in Table 3

Table 4.4. Results of the contact-killing test by a modified ASTM E2149-01 procedure against E. coli and S. epidermidis.

The contact-killing capacity of CHX bound to the fibers was tested via a modified ASTM E2149-01 procedure. Figure 4.9(b) shows a typical photo image of the disk diffusion test results for these fully washed fibers. The absence of the ZoI confirmed the complete removal of free CHX. In the control experiment, the CA-TTE fibers without CHX were tested and did not show any killing of E. coli or S. epidermidis. Table 4.4 shows contact-killing bactericidal activity of the CHX fibers.

Since all four series of the tested fibers possessed a similar content of bound CHX, the fibers demonstrated similar contact-killing efficiencies, ranging from 94.2% to 99.9%. The XPS measurements indicate a trend towards increasing surface concentration of bound CHX with increasing CHX concentration in the spin solution, which could explain the slight increase in bactericidal efficiency (Table 4.4). Although the immobilization of CHX on/in the fibers may affect the CHX structure and the surrounding environment, our results indicate that the CHX bound on the CA fibers is still capable of killing the bacteria with as high as 3 log reduction or 99.9% bactericidal efficiency of the viable bacteria in 1 hour. For comparison, identical fibers with the unbound CHX not washed out were tested using the modified ASTM

E2149-01 procedure. The fibers with a total CHX content of 7.0 wt% exhibited a bactericidal efficiency similar to that of washed fibers with the same overall CHX content, because almost all of the CHX in the unwashed fibers was bound. However, the other three series of fibers with almost equal contents of the bound CHX ranging from 5 to 9 wt% and yet significant contents of unbound CHX (Table 4.3) showed more than 6 log reduction of viable bacteria due to the release of unbound CHX. Hence, the release of the unbound CHX in the fiber proximity seemed to lead to higher fiber efficiency.

4.3.3. Post-spin treatment of CA-PEO fibers

In addition to producing CHX-containing CA-CHX fibers via electrospinning of the blends of CA and CHX, we investigated a post-spin treatment process to prepare bactericidal fiber meshes. The post-spin treatment allowed us to attach the CHX onto the CA-PEO fibers via titanate linkers. The nonfunctional CA-PEO fiber meshes were immersed in diluted TTE solution and chlorhexidine digluconate solution, respectively, with each step followed by a curing process in the oven to covalently bind CHX onto the fibers. Figure 4.11 shows SEM images of as-spun CA-PEO as well as post-spin treated fibers. The size of CA-PEO fibers is 920±120nm, which is similar to that of CA-CHX fibers electrospun from the blends (Fig. 4.6(a)). The fiber size was not affected by the post-spin treatment process (Fig. 4.11(b)), but formation of the titania clusters (*ca.* 150 nm in diameter) on the post-spin treated fibers was clearly discernible. The fiber meshes remained intact after the post-treatment while the porosity of the fiber mats may have changed during the treatment, as evidenced by a slight but visually observable shrinkage of the fiber meshes. Appearance of the characteristic peaks of CHX located at 1500-1650 cm^{-1} in ATR-FTIR spectra of the post-spin treated fibers confirmed the presence of CHX bound on the fibers after washing. Elementary analysis indicated that the amount of CHX attached onto the post-spin treated fibers was approximately 1-2 wt% of the total fiber weight. The antibacterial tests by the modified ASTM E2149-01 method

showed that post-spin treated fibers (100mg) were effective against *E. coli* with 99.6% reduction and *S. epidermidis* with 95.0% reduction of viable bacteria in 1 hour. Compared with the results of the contact-killing tests of the CA-CHX fibers electrospun from polymer blends (Table 4.4), the post-spin treated fibers can achieve a similar antibacterial capacity with a much lower concentration of CHX attached to the fibers. We believe that repeated post-spin treatment of the fibers would increase the fiber loading for the bactericide, which would further enhance the bactericidal efficiency of the fibers.

(a)
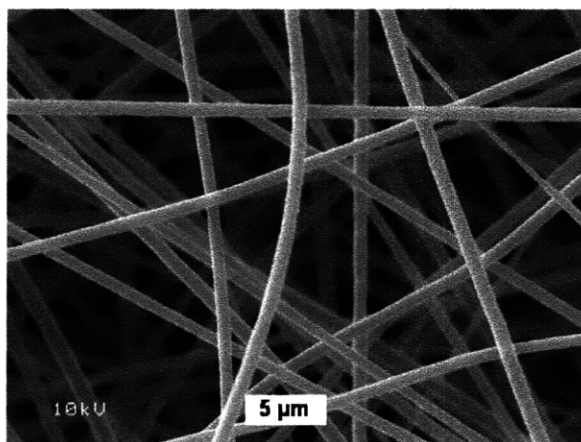
(b)
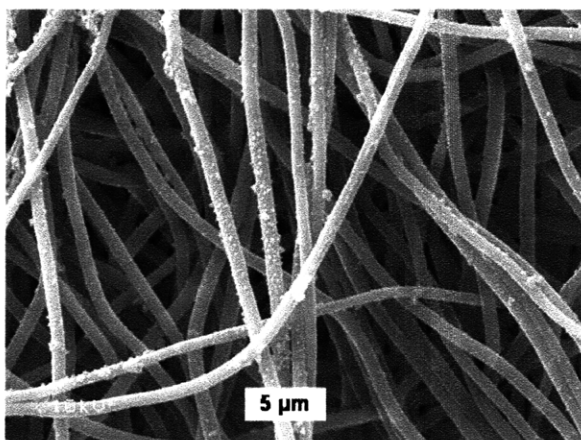
Figure 4.11. SEM images of (a) as-spun nonfunctional CA-PEO fibers and (b) post-spin treated CA-PEO fibers with the attachment of CHX onto the fibers.

4.4. Conclusions

Bactericidal fiber meshes were successfully produced by the electrospinning of polymer blends containing the biocide, chlorhexidine (CHX). We show that the addition of a high molecular weight PEO to CA solutions significantly improves the elasticity of the CA solutions and facilitates the formation of fibers. A dimensionless De number, defined as the ratio of fluid relaxation time to instability growth time, was used to characterize the spinnability of the blends. It was found that uniform fibers were produced in the region of De > 7. The CA-CHX fibers demonstrated bactericidal capability not only through a gradual release of unbound CHX from the fibers but also via contact with CHX bound on the fibers. Antibacterial fiber mats were also obtained by post-spin treatment of CA-PEO fibers to immobilize CHX on the fibers via titanate linkers. The post-spin treated fibers achieved similar bactericidal efficiency compared to that of the CA-CHX fibers electrospun from the blends, even with a much lower CHX content. We surmise that a repeated post-spin treatment of the fiber could result in even higher CHX loading on the fiber surface and may further enhance the bactericidal properties of the fibers. We believe that the strategies presented in this work are not limited to incorporation of CHX only, but will also enable incorporation of a wide range of antibacterial agents such as antibiotics in/on the fibers.

4.5. References

1. Melaiye, Y.; Sun, Z.; Hindi, K.; Milsted, A.; Ely, D.; Reneker, D. H.; Tessier, C. A.; Youngs, W. J. *J. Am. Chem. Soc.* 2005,127, 2285.

2. Son, W. K.; Youk, J. H.; Lee, T. S.; Park, W. H. *Macromol. Rapid. Commun.* 2004, 25, 1632.

3. Ignatova, M.; Starbova, K.; Markova, N.; Manolova, N.; Rashkov, I. *Carbohydr. Res.* 2006, 341, 2098.

4. Ignatova, M.; Manolova, N.; Rashkov, I. *Eur. Polym. J* 2007, 43, 1112.

5. Odore, R.; Valle, V. C.; Re, G. *Vet. Res. Commun.* 2000, 24, 229.

6. Gjermo, P. *J. Clin. Periodontol.* 1974, 1, 143.

7. Riggs, P. D.; Braden, M.; Patel, M. *Biomaterials* 2000, 21, 345.

8. Yue, I. C.; Poff, J.; Cortes, M. E.; Sinisterra, R. D.; Faris, C. B.; Hildgen, P.; Langer, R.; Shastri, V. P. *Biomaterials* 2004, 25, 3743.

9. Yu, J. H.; Fridrikh, S. V.; Rutledge, G. C. *Polymer* 2006, 47, 4789.

10. Anna, S. L.; McKinley, G. H. *J. Rheol.* 2001, 45, 115.

11. Rodd, L. E.; Scott, T. P.; Cooper-White, J. J.; McKinley, G. H. *Appl. Rheol.* 2005, 15, 12.

12. DuPont™ Tyzor® Organic Titanates General Brochure.

13. Kramer, J.; Prud'homme, R. K.; Wiltzius, P. *J. Colloid Interface Sci.* 1987, 118, 294.

14. Morris, C. E.; Welch, C. M. *Textile Res J* 1983, 53, 143.

15. Menon, N.; Blum, F. D.; Dharani, L. R. *J. Appl. Polym. Sci.* 1994, 54, 113.

16. ASTM E2149-01 standard test method for determining the antimicrobial activity of immobilized antimicrobial agents under dynamic contact conditions, American Society for Testing and Materials, West Conshohocken, PA.

17. Eggers, J. *Rev. Mod. Phys.* 1997, 69, 865.

18. Goldin, M.; Yerushalmi, J.; Pfeffer, R.; Shinnar, R. *J Fluid Mech.* 1969, 38, 689.

19. Chang, H. –C.; Demekhin, E. A.; Kalaidin, E. *Phys. Fluids* 1999, 11, 1717.

20. Hohman, M. M.; Shin, M.; Rutledge, G.; Brenner, M. P. *Phys. Fluids* 2001, 13, 2201.

21. Hohman, M. M.; Shin, M.; Rutledge, G.; Brenner, M. P. *Phys. Fluids* 2001, 13, 2221.

22. Jones, D. S.; Brown, A. F.; Woolfson, D.; Dennis, A. C.; Matchett, L. J.; Bell, S. E. J. *J. Pharm. Sci.* 2000, 89, 563.

23. Sarmiento, F.; del Rio, J. M.; Prieto, G.; Attwood, D.; Jones, M. N.; Mosquera, V. *J. Phys. Chem.* 1995, 99, 17628.

24. Buxbaum, A.; Kratzer, C.; Graninger, W.; Georgopoulos, A. *J. Antimicrob. Chemother.* 2006, 58, 193.

25. Cooper, K. E. Analytical Microbiology; Academic Press: New York, 1963; Vol. 1, Chapter 1.

26. Lee, D.; Cohen, R. E.; Rubner, M. F. *Langmuir* 2005, 21, 9651.

Chapter 5

Functionalized Electrospun Fabrics via Layer-by-layer Electrostatic Assembly for Chemical and Biological Protection

5.1. Introduction

In previous work, we have produced functionalized electrospun fiber mats containing α-nucleophilic oxime moieties or bactericide chlorhexidine for either chemical or biological protection. The new question coming into our mind is whether we can fabricate functionalized electrospun fiber mats with both properties, which are able to provide both chemical and biological protection.
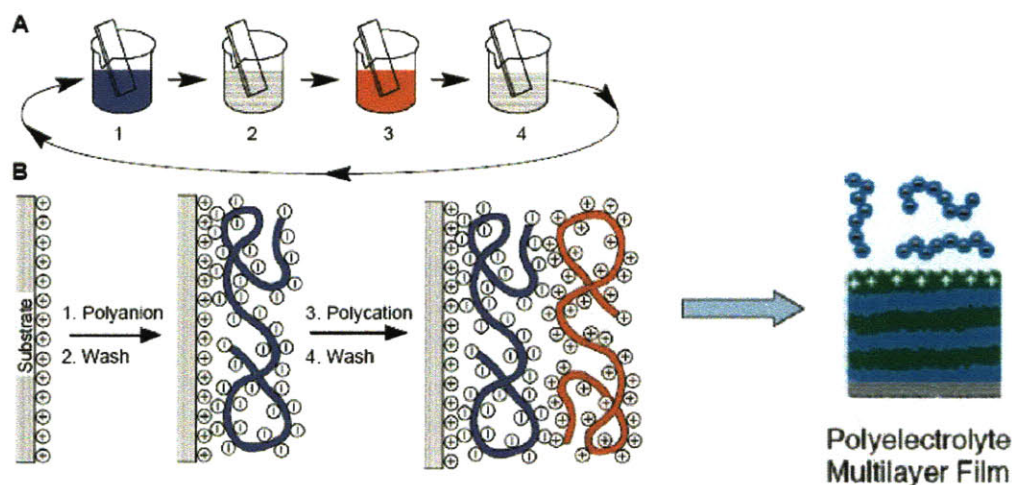
Figure 5.1. Layer-by-layer electrostatic assembly technique

In chapter 2 and 3, fiber mats functionalized with α-nucleophilic oxime moieties were prepared by either electrospinning blends of polyacrylamidoxime (PAAO) and polyacrylonitrile (PAN) or surface oximation of prefabricated PAN fiber mats, and demonstrated a pronounced capability to hydrolyze chemical nerve agent simulants in the presence of moisture.[1,2] We have proven that the fiber post-spin modification strategy has the advantages of higher surface density of oxime functional groups, enhanced reactivity and ease of implementation compared to the PAN/PAAO blending

strategy.[1] This indicates that we may only need to functionalize the surface layer of the electrospun fibers to produce functional mats. The layer-by-layer (LbL) assembly technique offers an effective strategy of functionalizing the surface of electrospun fibers. LbL electrostatic assembly is a simple, versatile and inexpensive approach to generate functional multilayer thin film coatings on surfaces.[3] The LbL assembly process involves the sequential adsorption of oppositely charged polyelectrolytes to construct multilayered functional coatings (Figure 5.1).[3,4] The utilization of electrospun fiber mats as substrates for LbL-based functional coatings significantly enhance the function of multi-layered coatings by increasing the specific surface area of substrates.[5-7,9] Samuelson et al. showed that a fluorescent probe LbL-assembled onto electrospun cellulose acetate membranes resulted in a significant increase in sensitivity of optical sensors.[5] Polyoxometalate functional coatings were electrostatically assembled onto electrospun poly (vinyl alcohol) fibers, which were collected on electrodes, for electrochemical application.[6] Specifically for the application in protective fabrics, Singh and coworkers generated organophosphorous hydrolase (OPH) coatings for protection over organophosphate nerve agents by using LbL assembly technique.[8] However, the low stability of enzyme OPH limits its practical application. Recently, Lee et al. demonstrated that LbL-assembled titanium dioxide nanoparticle coatings on various electrospun fibers can photo-catalytically decompose representative toxic industrial chemicals.[7] In addition, Krogman et al. employed a newly-developed spray LbL assembly technique to functionalize electrospun nylon fibers with titanium dioxide nanoparticles, in which they could obtain conformal coatings or bridge the surface voids by controlling the spraying conditions.[9] In that regard, they could achieve LbL-functionalized fiber mats possessing improved photocatalytic capability without sacrificing water vapor permeability.[9] In fact, by selecting appropriate polyelectrolytes of opposite charges and varying functionalities, one can generate multifunctional electrospun, fiber-based protection fabrics for both chemical and biological protection. In this study, a nucleophilic and chemically reactive polyanion, polyhydroxamic acid (PHA), and an antimicrobial polycation, poly (N-vinylguanidine) (PVG), were synthesized and

assembled onto prefabricated PAN fiber mats. The performance of the functionalized mats in OP decomposition was tested with diisopropyl fluorophosphate (DFP), a widely used simulant for G-type chemical warfare nerve agents.[10] The antibacterial properties of these functionalized mats were examined with a gram-negative strain of *Escherichia coli* (*E. coli*) and a gram-positive strain of *Staphylococcus epidermidis* (*S. epidermidis*).

5.2. Experimental method

5.2.1 Materials

Polyacrylonitrile (PAN) (M_w 150 kDa) was purchased from Scientific Polymer Products Inc. (Ontario, NY) and used as received. Poly(acrylamide-co-acrylic acid) (M_w 200 kDa, acrylamide 20 wt%), diisopropyl fluorophosphate (99%, DFP), hydroxylamine hydrochloride (99%), cyanamide (50 wt% in water) and N,N-dimethylformamide (DMF) were all obtained from Sigma-Aldrich Chemical Co. (St. Louis, MO) and used as received. Lupamin® 9095 (20-22% aqueous solution of polyvinylamine, average molecular weight 340 kDa) was kindly supplied by BTC (a specialty chemical distribution group of BASF, Germany). Bacteria *E. coli* (ATCC # 67876) and *S. epidermidis* (ATCC # 35984) were purchased from ATCC (Manassas, VA) and stored at -80 °C prior to use.

5.2.2. Electrospinning

PAN solutions in DMF (10 wt%) were prepared by dissolving the polymer at 50-70 °C followed by stirring at room temperature. The PAN solutions were electrospun into fiber mats using a home-built parallel plate apparatus, as described in previous chapters.[11] The applied voltage (28-30 kV), the flow rate (0.015 ml/min) and the distance between the upper electrode and grounded collector (~30 cm) were adjusted to stabilize the polymer jet to obtain fiber mats on the grounded collector.

5.2.3. Polymer Synthesis

5.2.3.1. Synthesis of poly(N-hydroxyacrylamide), or polyhydroxamic acid (PHA)

Figure 5.2 shows the modification of poly(acrylamide-*co*-acrylic acid) to

poly(N-hydroxyacrylamide) (PHA) by reacting with hydroxylamine. Poly(acrylamide-*co*-acrylic acid) was mixed with excess hydroxylamine hydrochloride in deionized water. The resulting solution was stirred for one day at 70 °C and then an aqueous solution of sodium hydroxide was added followed by stirring for three days at room temperature to convert completely into PHA solution. Conversion of poly(acrylic acid) and polyacrylamide into PHA by hydroxylamine is well-documented.[12-14] Release of ammonia by bubbling was observed. The solution was then frozen at -80 °C and lyophilized. The resultant PHA was dissolved in deionized water, dialyzed against excess deionized water and lyophilized. FTIR (KBr, cm^{-1}): 3600 (broad, -NHOH), 3430 (broad, OH stretching), 3210 (amide NH stretching), 1630 (CO-NH bending), 1450 (CH$_2$ scissor bending), 1425 (C-N stretching).

Figure 5.2. Synthesis of polyhydroxamic acid

5.2.3.2. Synthesis of poly(N-vinylguanidine) (PVG)

Polyvinylamine (90% hydrolyzed) received as Lupamin 9095 was completely hydrolyzed by 37% hydrochloric acid at 80 °C followed by polymer purification by precipitation into 2M NaOH and dialysis (molecular weight cutoff, 12-14 kDa) and drying. Then polyvinylamine was completely guanidinylated by cyanamide following the previously described procedure.[15] Figure 5.3 shows the guanidinylation process of polyvinylamine to poly(N-vinylguanidine). FTIR (KBr): 957 cm^{-1} (C-N stretching), 1510 cm^{-1} (C-N stretching), 1610 cm^{-1} (NH, NH$_2$

deformation), 1670 cm^{-1} (C=N stretching), 2940 cm^{-1} (aliphatic CH$_2$ stretching). ^{13}C NMR (D$_2$O, ppm): 151.6 (C in the guanidinium group), 45.0 (methylene C in backbone), 35.5 (methane C in backbone).
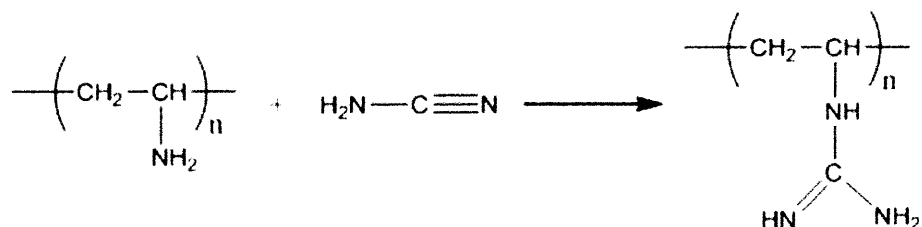
Figure 5.3. Synthesis of poly(N-vinylguanidine)

5.2.4. LbL Assembly Coating

Aqueous solutions of PHA and PVG (10 mM, pH 9) were prepared and used for LbL assembly. Electrospun PAN fiber mats were plasma treated for 1 min (Harrick PDC-32G, Harrick Plasma Inc.) prior to LbL deposition. A Carl Zeiss DS50 programmable slide stainer was used for LbL deposition. Multilayer polyelectrolyte coatings on PAN fibers were produced by alternately dipping the fiber mat in 10 mM PVG and PHA aqueous solutions at room temperature. The dipping time in each polyelectrolyte solution was 60 min, followed by rinse in deionized water for 3 min.

5.2.5. Characterization

The fiber morphology was visualized by scanning electron microscopy (SEM, JEOL-6060). FTIR spectra were measured using a Nicolet 8700 spectrometer (Thermo Scientific Corp.) in the absorbance mode by accumulation of 256 scans with a resolution of 4 cm^{-1}. A Krato Axis Ultra Imaging XPS spectrometer (Kratos Analytical Co.) equipped with a monochromatized Al Kα X-ray source was used to

125

analyze the surface chemistry of LbL-coated fibers. The take-off angle relative to the sample substrate was set at 20°. ^{13}C NMR spectra were carried out using a Bruker Avance 400 spectrometer operating at 100.61 MHz for ^{13}C at room temperature. Proton decoupling was applied and 15000 to 20000 scans were collected.

5.2.6. Breathability test[39]

Water vapor diffusion and gas convection properties of electrospun fiber mats were measured using an automated dynamic moisture permeation cell (DMPC) system (Figure 5.4).[16-18] Figure 5.5 shows the test configuration. The fiber sample was placed between two chambers. The sample area is about 10 cm^2. Air at two different relative humidities flows over the two sides of the test sample, and humidity detectors measure how much water vapor is transported through the sample. By measuring the temperature, water vapor concentration, and flow rates of the gas leaving the cell, one can determine the fluxes of gas and water vapor transported through the test sample. Results may be shown in terms of flux (g/m^2-day) or water vapor diffusion resistance, which has the units of s/m. The resistance units are preferred because results obtained at different environmental conditions can be easily compared. The lower the diffusion resistance, the more water vapor permeates through the material. Testing is done at a constant humidity gradient, but the mean relative humidity is increased at each setpoint. Mean relative humidity is the average of the incoming humidity on the two sides of the sample.

Dynamic Moisture Permeation Cell (DMPC)
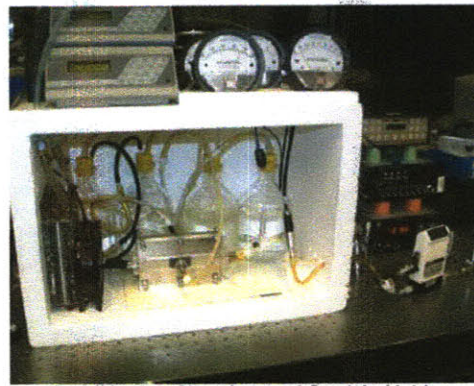
Conditioning Chamber and Sample Holder.

Figure 5.4. Dynamic moisture permeation cell (DMPC) system and conditioning chamber.

Mean Relative Humidity is Average of ϕ_1 and ϕ_2

Humidity Gradient is Difference of ϕ_1 and ϕ_2

ΔP

Pressure Difference Across Sample (not relevant for nonporous materials)

Humidified Air (ϕ_1) → → To Humidity Meter

Humidified Air (ϕ_2) → Sample → To Humidity Meter
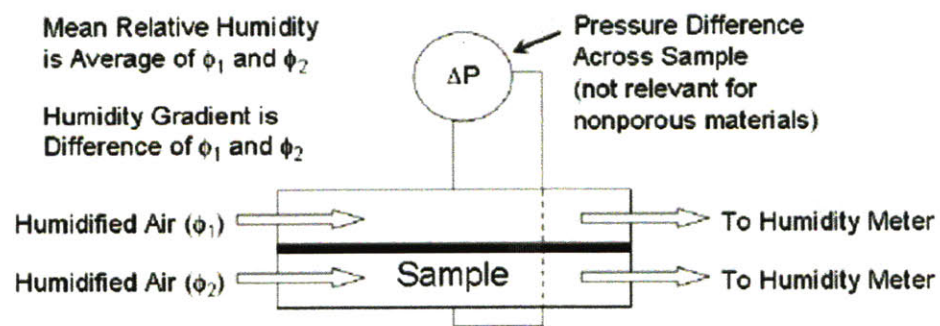
Figure 5.5. Schematic picture of test cell configuration

5.2.7. Kinetics of DFP degradation

Kinetics of DFP degradation hydrolyzed by PHA in aqueous solutions were assessed by liquid state ^{31}P NMR spectrometry using a Varian 500 spectrometer operating at 202.46 MHz. The reaction milieu consisted of 50 mM of TES buffer to keep solution pH constant at 7 and 20% (by volume) of deuterium oxide for signal locking. The spectra were recorded at ambient temperature (25 °C) by accumulation of 64 scans. The reaction time was taken to be the midpoint of the acquisition period.

Degradation of DFP mists on PVG/PHA functionalized fiber mats was monitored by solid state high-resolution magic angle spinning (HRMAS) ^{31}P NMR using a Bruker Avance 400 spectrometer (161.98 MHz for ^{31}P) as described previously.[1] The water content of the fiber mats, C_w, defined as the weight ratio of absorbed water to dry fiber mat, was maintained at 1.30 wt/wt in this work. The spectra were recorded at ambient temperature (21 °C) by accumulation of 64 scans. Triphenyl phosphate (TPP) in deuterated chloroform was used as an external reference for both liquid and solid state ^{31}P NMR measurements.

5.2.8. Antibacterial Tests

The antibacterial properties of the functionalized fiber mats were tested using the procedure of Tiller and coworkers,[19] with modifications. Briefly, *E. coli* (ATCC # 67876) and *S. epidermidis* (ATCC # 35984) were cultured overnight in LB broth and diluted in phosphate buffer solution (PBS, pH 7) to approximately $10^4 \sim 10^5$ cells/mL. The bacterial suspension was then sprayed onto a functionalized fiber mat (6 cm × 4 cm) and a control fiber mat (6 cm × 4 cm) in a fume hood using a commercial chromatography sprayer. After drying for several minutes, the fiber mats were placed on top of the growth agar plates. The plates were inverted and incubated at

37 °C for 16-20 hours.   The number of viable colonies was counted visually and the reduction in the number of viable bacteria colonies was calculated after averaging three experiments.

5.3. Results and discussion

5.3.1. DFP degradation mediated by PHA
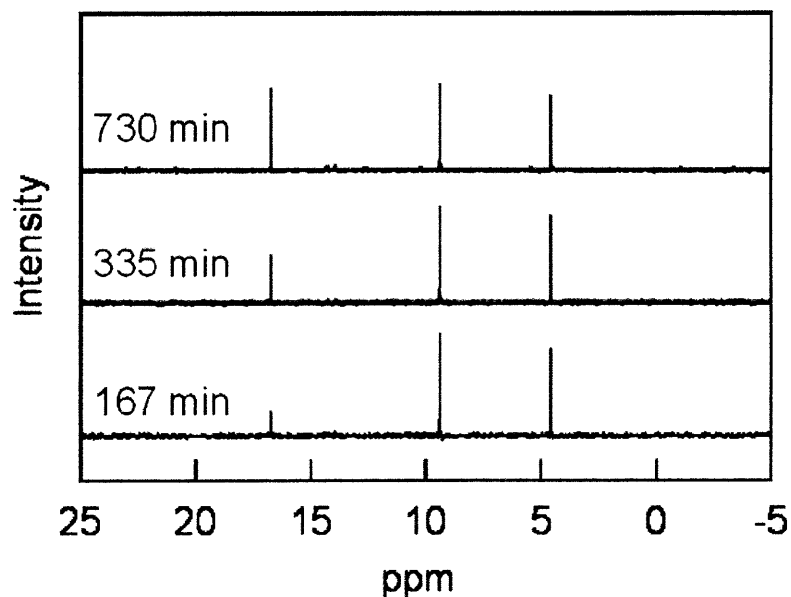
Figure 5.6. Typical 202.46 MHz ^{31}P NMR spectra of DFP degradation in aqueous solution. $[DFP]_o$=5 mM; $[HA]_o$=10 mM; 50 mM TES buffer, pH=7.0; T=25 °C.

Hydroxamic acid is a reactive α-nucleophile, capable of degrading organophosphate (OP) compounds or nerve agents.[12,20-21] Hydrolytic destruction of OPs by low molecular weight hydroxamic acid compounds has been established.[22,23] However, until recently[12] little work has been done to study the action of polymers with hydroxamic acid groups, such as polyhydroxamic acid (PHA), in the degradation of OPs. In this work, the capability of PHA to decompose DFP, a common simulant for G-type nerve agent, in aqueous solution was evaluated.
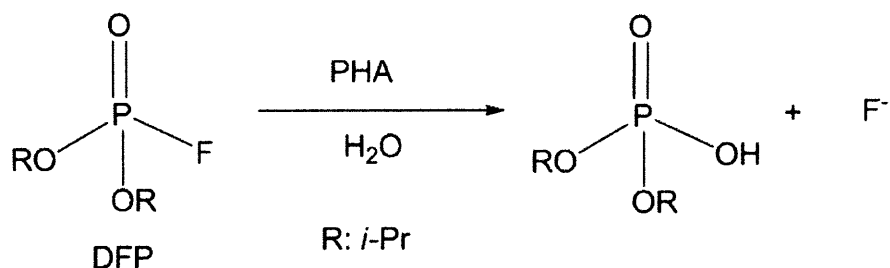
Figure 5.7. DFP degradation mediated by PHA in aqueous solution

Hydrolytic decomposition of DFP in aqueous solution in the presence of PHA was monitored by ^{31}P NMR spectra. All the experiments were conducted under conditions of excess hydroxamic acid relative to the substrate ($[HA]_o > [DFP]_o$) with pH maintained constant at 7.0 using 50 mM TES buffer. Figure 5.6 shows a typical series of NMR spectra of DFP degradation mediated by PHA in aqueous solution as a function of time. Doublet signals at 4.6 and 9.4 ppm are attributed to the reactant, DFP, due to the splitting of the ^{31}P signal from the coupling of the P-F bond ($J_{P-F} \approx$ 970Hz).[24] The singlet at 16.8 ppm is assigned to the product, diisopropyl phosphate (DIP). Degradation of DFP (Figure 5.7) is mediated by PHA through the nucleophilic attack of the >N-O-H oxygen in hydroxamic acid on the pentavalent phosphorus of DFP, resulting in P-F bond cleavage and fluorine ion release.

The ratio of the relative signal integrations is proportional to the ratio of the relative concentrations of the corresponding compounds, which allows us to estimate the kinetic parameters of DFP degradation in our experiments. The time-dependent relative degree of conversion, F_t, was defined as:

$$F_t = \Sigma I_r / (\Sigma I_r + \Sigma I_p)$$

where ΣI_r and ΣI_p are the sums of the integrations of the signals corresponding

131

to the reactant, DFP, and the product, DIP, respectively.

Figure 5.8 shows the plot of $\ln(F_t)$ vs. time for a series of experiments in which the hydroxamic acid concentration, $[HA]_o$, was varied while keeping DFP concentration constant; $[DFP]_o=5$ mM. All the experiments were observed to be pseudo-first order with respect to DFP, as evidenced by the linear fit of the curve $\ln(F_t)$ vs. time ($R^2>0.99$). The slope yields the observed reaction rate, k_{obs}, as described by the equation:

$$\ln(F_t) = -k_{obs}t$$

The observed rate constant without PHA (k_{sp}) was measured to be 1.9×10^{-6} s^{-1} at pH 7.0, which is in accord with previously reported values for the spontaneous hydrolysis of DFP.[15,22] The observed reaction rate increases as $[HA]_o$ increases. In the case of the PHA-aided hydrolysis, the observed reaction rate consists of the PHA-aided and spontaneous reaction rate contributions:

$$r_{obs} = r_{PHA} + r_{sp} \quad \text{or} \quad \frac{d[DFP]}{dt} = -k_{obs}[DFP] = -k_{PHA}[DFP] - k_{sp}[DFP]$$

$$k_{PHA} = k_2[HA]_o$$

Figure 5.9 shows the curve of k_{PHA} vs. hydroxamic acid concentration, $[HA]_o$, in which k_{PHA} is obtained by subtracting spontaneous term, k_{sp}, from the observed overall reaction rate, k_{obs}. The slope of the linear fit of this curve ($R^2>0.99$) yields the second order rate constant, k_2, which was determined to be 5.1×10^{-4} $M^{-1}s^{-1}$ for DFP hydrolysis mediated by PHA at pH 7.0. Given that the reaction rate is significantly affected by solution pH, the nature of the reaction medium, temperature and pK_a of hydroxamic acid compounds,[20-21, 25-26] it is difficult to compare directly the

reactivity of PHA with small molecular weight hydroxamic acid compounds. Based on the reported data, we estimated that the second order rate constant for the DFP degradation via hydrolysis by isonicotinhydroxamic acid methiodide (pK_a 7.8) in aqueous solution at pH 7.0 is in the order of 10^{-3} $M^{-1}s^{-1}$.[22] Therefore, the reactivity of PHA (pK_a 7.5) towards DFP degradation in this study is comparable to that of isonicotinhydroxamic acid methiodide, a small molecular weight hydroxamic acid compound.
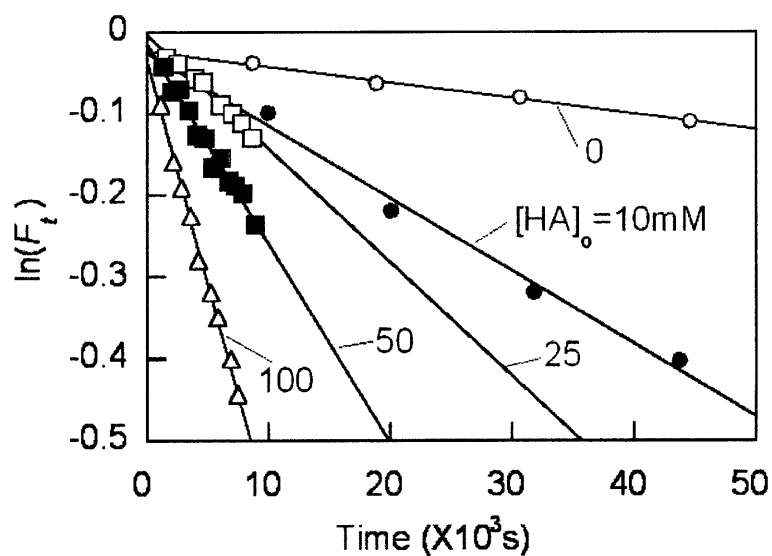
Figure 5.8. Kinetics of DFP hydrolysis with the presence of PHA in aqueous solution. $[DFP]_o$=5 mM; 50 mM TES buffer, pH 7.0.
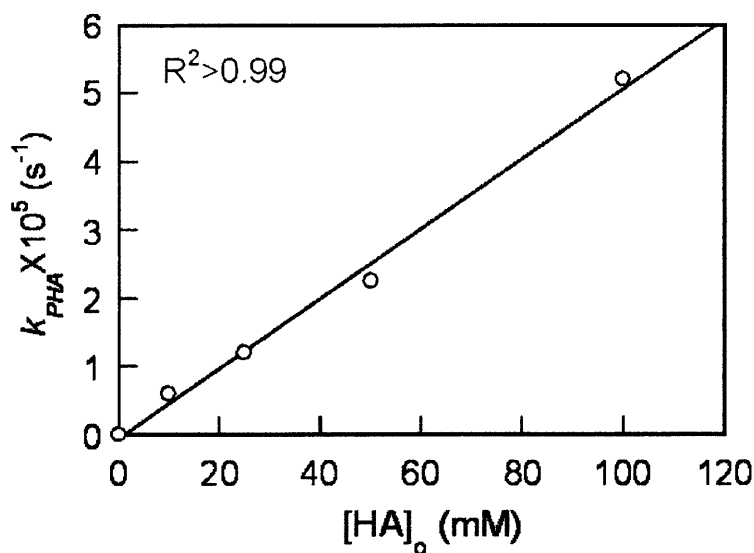
Figure 5.9. Observed reaction constant of DFP hydrolysis vs. $[HA]_o$ in aqueous solution. $[DFP]_o=5$ mM; 50 mM TES buffer, pH 7.0; spontaneous hydrolysis of DFP $=1.9\times10^{-6}$ s^{-1} at pH 7.0.

It is well known that amines and their derivatives can decompose OPs catalytically via a general base catalyzed hydrolysis.[27,28] Since antimicrobial poly(N-vinyl guanidine) (PVG) is a strong polybase bearing amine groups, it can degrade DFP catalytically as well.[15] To compare the reactivity of PVG with that of PHA, the reaction kinetics of PVG with DFP under identical conditions with the same concentration of functional groups (e.g. $[VG]_o=[HA]_o$) was conducted. Figure 5.10 shows the plot of $\ln(F_t)$ vs. time for PHA and PVG, the slop of which yield the observed first-order reaction rates, at pH 7.0 with $[DFP]_o=5$ mM and $[VG]_o=[HA]_o=100$ mM. The k_{PHA} and k_{PVG} values obtained after subtracting the spontaneous hydrolysis term were 5.5×10^{-5} s^{-1} and 7.7×10^{-6} s^{-1}, respectively. These values indicate that the reactivity of PHA towards DFP is seven-fold higher than that of PVG. Therefore, the reactivity of the PHA/PVG LbL coatings is primarily due to the presence of PHA rather than that of PVG.

134
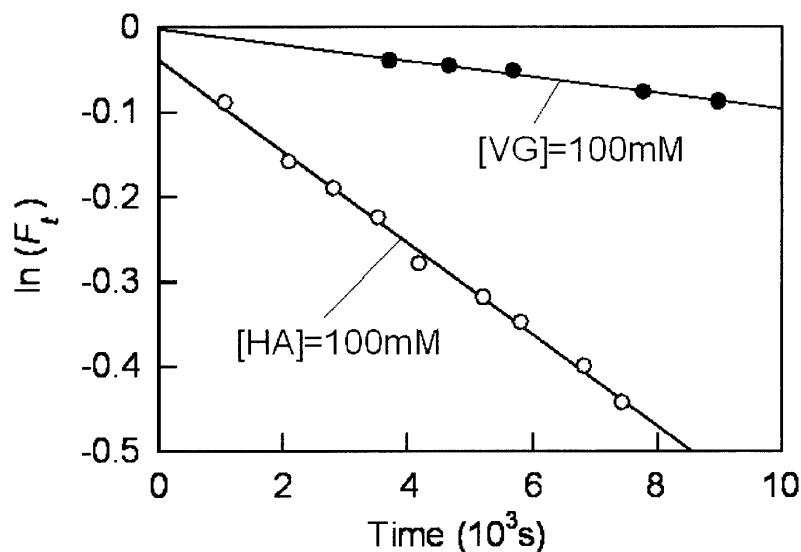
Figure 5.10. Kinetics of DFP hydrolysis with the presence of PHA or PVG in aqueous solution. $[DFP]_o = 5$ mM; 50 mM TES buffer, pH 7.0; $[HA]_o = [VG]_o = 100$ mM.

5.3.2. Multifunctional protective fabrics

LbL electrostatic assembly involves alternate adsorption of oppositely charged materials to construct the ultrathin coatings. PHA is a weak polyelectrolyte with pKa of 7.5,[12] indicative of a negatively charged species at pH 9.0. Antimicrobial PVG is a strong polyelectrolyte. The protonated PVG possesses a pK_a of 13.4 and is positively charged over a broad range of pH.[15] Electrospun fiber mats enable the generation of porous fabric scaffolds with tunable, high specific surface area and surface properties compared to conventional woven fabrics. Lee *et al.* showed that the surface area of electrospun poly(dimethylsiloxane-b-etherimide) (PSEI) is 1.5×10^4 times higher than that of the flat PSEI film, resulting in the enhanced reactivity of LbL-assembled titanium dioxide coating on the electrospun PSEI fibers.[7] A broad range of electrospun polymer fiber mats have been demonstrated to be effective

substrates for LbL-assembled titanium dioxide functional coatings for protection fabrics against toxic industrial chemicals or chemical warfare mustard agents.[7,9] The chemistry of substrate electrospun fiber mats has little effect on LbL electrostatic assembly process. Herein, we have selected the commercially available polymer PAN as a model for the fabrication of electrospun fiber mats. Figure 5.11(a) shows a typical SEM image of PAN fiber mats electrospun from 10 wt% solution of DMF. The average diameter of the PAN fibers is about 350 nm with the fiber size ranging from 250 to 500 nm. The measured BET surface area is about 15 m^2/g. The prefabricated PAN fiber mats were treated with low-pressure air plasma for 1 min to introduce negatively charged surface groups prior to LbL coating of functional polyelectrolytes PVG and PHA.[29,30] Figure 5.11(b) shows the typical fiber morphology of the functionalized PAN fiber mats with ten bilayers of PVG/PHA, denoted as (PVG/PHA)$_{10}$. Conformal coatings on individual fibers were observed over the fiber mat. The characteristic oxygen peak observed at 529 eV in the XPS spectra (Figure 5.12) shows the presence of oxygen on the surfaces of functionalized PAN fibers, which indicates that the presence of PHA on the surfaces of prefabricated PAN fibers. With twenty bilayers of PVG/PHA, rough surface of functional coatings is clearly observed and the functional coatings start to bridge the pore structures in the fiber mats (Figure 5.11(c)). As shown in Figure 5.11(d), with 30 coating bilayers, (PVG/PHA)$_{30}$, surface pores are partially filled, which accounts for about 20-30 % pores. Bridging of surface pores may affect the transport properties of electrospun fiber mats. Figure 5.13 and 5.14 shows the air flow resistances and water vapor diffusion resistances of functionalized PAN fiber mats compared to standard reference materials. As shown in Figure 5.13, air flow resistance of untreated electrospun PAN fiber mats is comparable to that of Nylon/Cotton woven fabrics, which is widely used as outer fabrics in the US army chemical/biological protective suit. The LbL coatings on the functionalized fiber mats, (PVG/PHA)$_{20}$ and (PVG/PHA)$_{30}$, may cause pore size reduction by occupying the pores to some extent, consequently increasing the convective air flow resistance for these functionalized fiber mats (Figure 5.13). As shown in Figure 5.14, both functionalized PAN fiber mats,

(PVG/PHA)$_{20}$ and (PVG/PHA)$_{30}$, have water vapor diffusion properties equivalent to the expanded polytetrafluorethylene (ePTFE) membrane, which is a standard porous breathable material. Materials that achieve the water vapor diffusion properties comparable to the ePTFE membrane are excellent candidates for "breathable" protective clothing materials. However, the untreated PAN control fiber mats were observed to have the lower water vapor transport than functionalized PAN fiber mats. The LbL electrostatic assembly involves dipping fiber mats into aqueous solution followed by drying process, which results in the significant reduction in thickness of fiber mats as observed in our previous work.[1] This actually improved the "breathability" of the functionalized fiber mats as compared to PAN control mats. In addition, functional polyelectrolytes coated on fibers are more hydrophilic than PAN, which may further enhance the water vapor transport. All the experiment results indicate that LbL-functionalized PAN fiber mats are still very breathable, suitably used for protective clothing materials, even after the surface pores are partially filled for (PVG/PHA)$_{30}$.
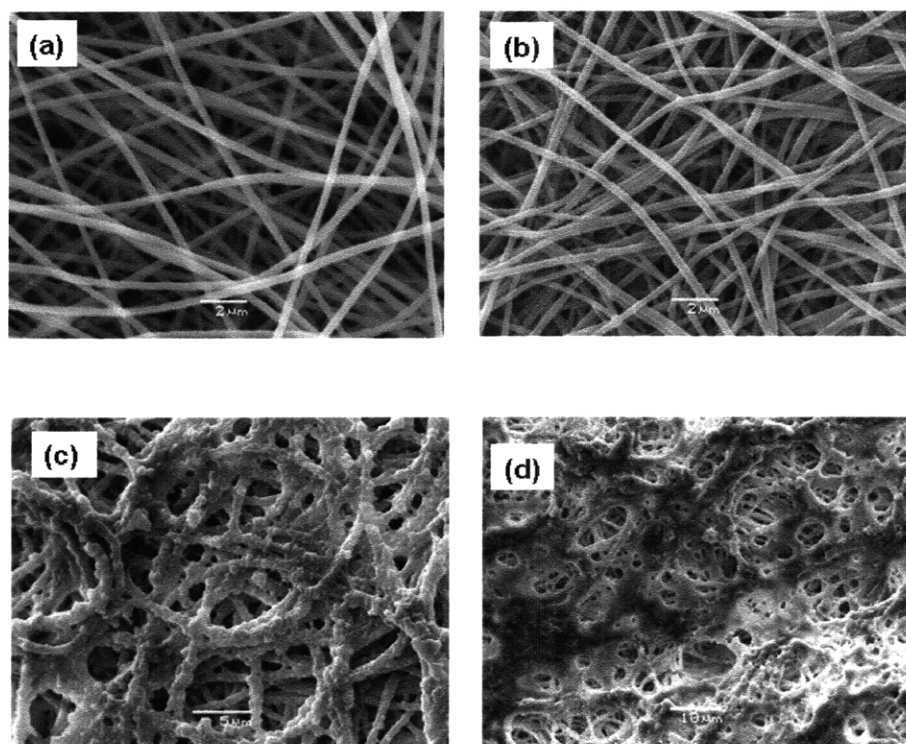
Figure 5.11. Typical SEM images of (a) prefabricated PAN fiber mat (scale bar: 2 μm); (b) functionalized PAN fiber mat $(PVG/PHA)_{10}$ (scale bar: 2 μm); (c) functionalized PAN fiber mat $(PVG/PHA)_{20}$ (scale bar: 5 μm); and (d) functionalized PAN fiber mat $(PVG/PHA)_{30}$ (scale bar: 10 μm).
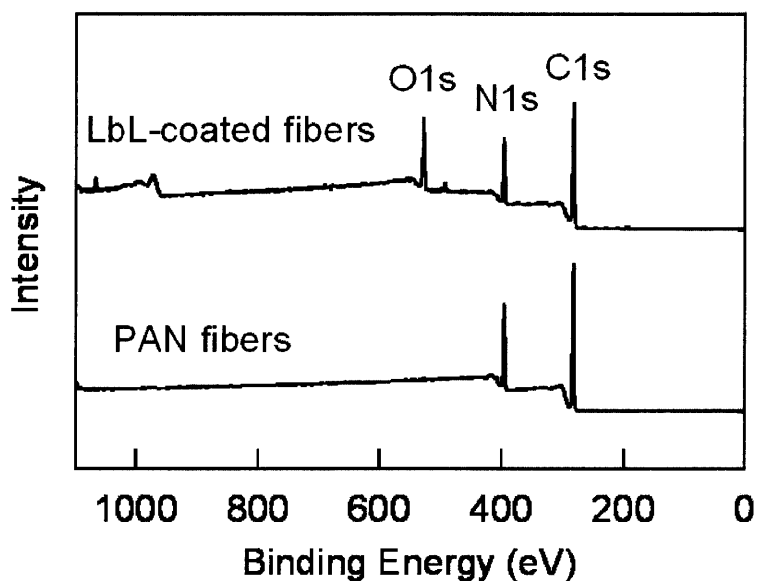
Figure 5.12. XPS spectra of untreated PAN and LbL-functionalized fiber mats
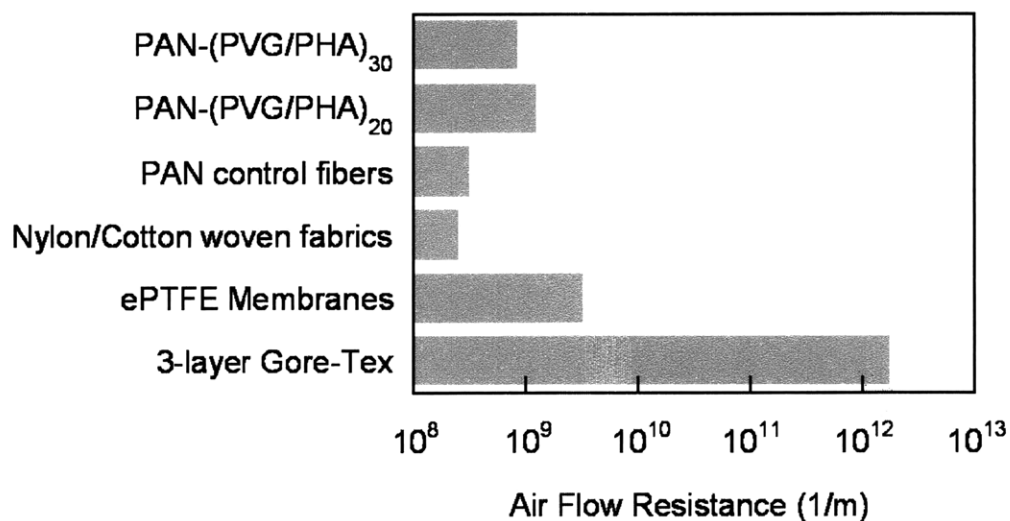
Figure 5.13. Air flow resistance of functionalized fiber mats. T=30 °C, constant humidity gradient of 0.90 (relative humidity of 0.95 and 0.05 on the two sides of the test sample). 3-layer Gore-Tex: a commercially available water proof, breathable fabrics for consumer market; ePTFE membrane: the expanded polytetrafluorethylene (ePTFE) membrane with pores in the range of 200 nm, a standard reference material for breathable protective clothing; Nylon/Cotton woven fabrics: outer fabrics used in the US army protective suit.
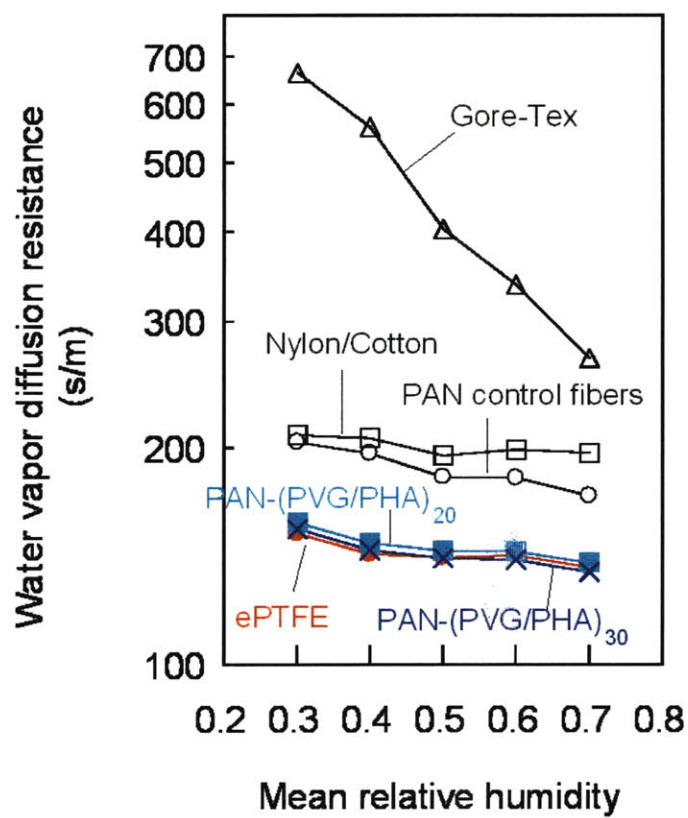
Figure 5.14. Water vapor diffusion resistance of functionalized PAN fiber mats compared to standard reference materials.

The performance of functionalized fiber mats serving as chemical detoxification fabrics was tested with DFP. A DFP mist (3 μL of DFP with 7 μL of air in a 10μL syringe) was sprayed onto the prepared fiber mat (the mass of dry fiber mat, W_{f0}=30 mg) to mimic an attack of G-type nerve agents. The DFP degradation mediated by PVG/PHA-functionalized fiber mats was monitored by HRMAS ^{31}P NMR. Figure 5.15 shows three representative NMR spectra of a DFP misted fiber mat functionalized with (PVG/PHA)$_{20}$, showing decomposition as a function of time. Doublets at 3.7 and 9.7 ppm (J_{P-F}≈970Hz) are assigned to DFP.[24] With time, the doublet peaks for DFP decreased and the singlet peak at 16.6 ppm, assigned to the product DIP, increased. The signals for the reactant and product correspond well with the NMR assessment we have reported previously.[1] The doublets at 12.5 and 6.9 ppm observed after 24 hr are attributed to the unreacted DFP that is absorbed onto the charged polyelectrolyte coating on the fiber surfaces, which shifts the signal positions.[27] Figure 5.16 shows the DFP degradation kinetics on PVG/PHA-functionalized fiber mat (PVG/PHA)$_{20}$ as well as an untreated PAN control fiber mat, under identical test conditions (W_{f0}=30 mg, W_{DFP}=3 mg, C_w=1.3 wt/wt, 21 °C). The DFP degradation mediated by the PVG/PHA-functionalized fiber mat in the presence of water was observed to be pseudo-first order with respect to DFP. The observed reaction rate is 2.1×10^{-5} s^{-1}, which is approximately 60-fold faster than the observed spontaneous decomposition rate of DFP in the presence of the control fiber mat with the same water content. The reactivity of the functionalized fiber mats modified via the LbL electrostatic assembly method is also comparable to that for oxime-functionalized fiber mats prepared via surface oximation reported previously.[1] The advantage of the LbL assembly method is the broader selection of available polymeric fiber substrate materials compared to the methodology of direct chemical modification of the fiber material, where the material choice is limited to fiber-forming polymers expressing certain functional groups that can be converted to the reactive groups. The PVG/PHA-functionalized fabrics also demonstrate better reactivity towards DFP as compared to XE-555, a commonly used decontaminating,

cleaning solution recommended for personal equipment.[24]
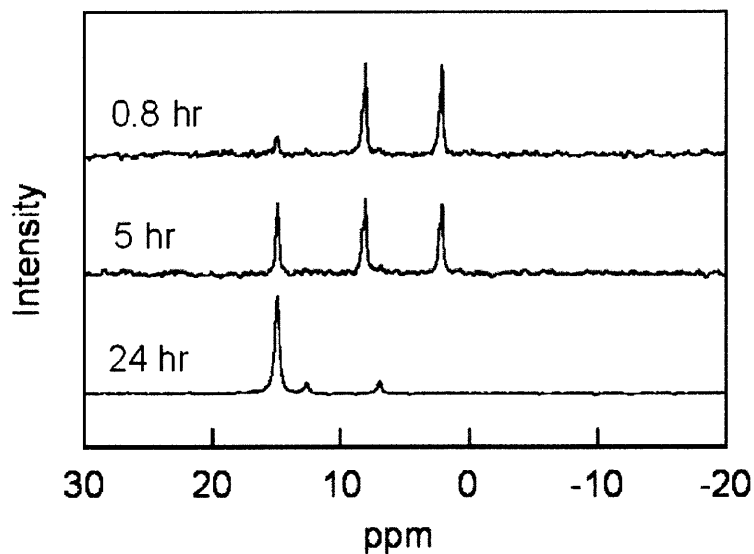
Figure 5.15. Representative 161.98 MHz ^{31}P HRMAS NMR spectra of DFP mist (3 µL) deposited onto functionalized fiber mat (PVG/PHA)$_{20}$ as a function of time. The mass of dry fiber mat, W_{f0}=30 mg; water content in the fiber mat, C_w=1.3 wt/wt; W_{DFP}=3 mg.
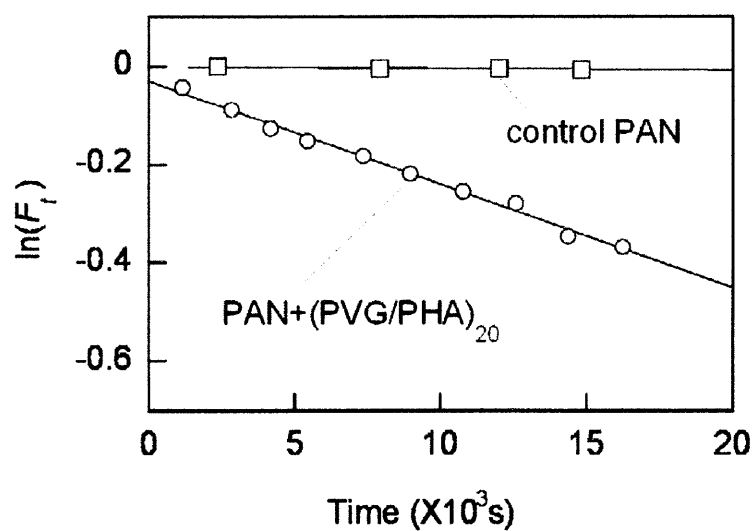
Figure 5.16. Kinetics of DFP degradation with the presence of functionalized or control fiber mat at 21 °C. The mass of dry fiber mat, W_{f0}=30 mg; water content in the fiber mat, C_w=1.3 wt/wt; W_{DFP}=3 mg.

The performance of the PVG/PHA functionalized fiber mats to protect against bacterial contaminants was tested with a representative gram-negative strain of $E.$ $coli$ and a gram-positive strain of $S.$ $epidermidis$. The functionalized fabrics were challenged with airborne bacteria in the form of sprayed mists, to mimic combat situations, as described in the Experimental section. Table 5.1 shows the bactericidal efficiency of the functionalized fiber mats with different levels of PVG/PHA coating. The bactericidal action of PVG with its large positive charge density, has been attributed to its excellent capability to bind onto negatively charged cell surfaces or cytoplasmic membranes and irreversibly disrupt cell membranes, thereby killing the microorganisms.[31-34] With one bilayer coating, the fiber mat demonstrates only 20% and 25% killing efficiency, respectively, against $E.$ $coli$ and $S.$ $epidermidis$. This low activity is due to the PVG concentration on the fiber surfaces being less than the minimum inhibitory concentration of PVG (34 µg/mL for $E.$ $coli$ and 68 µg/mL for $S.$ $epidermidis$[15]). As the number of bilayers increases, the killing efficiency increases significantly due to the increase of surface concentration of PVG. In the case of five bilayer coatings, the functionalized fiber mats are capable of killing 99.8 % of the viable bacteria. With ten or more bilayers functional coatings on the fiber mats, no bacterial colonies were observed on the functionalized fiber mats after the test. We also examined the effect of the last applied coating layer on the bactericidal property of PVG/PHA functionalized fiber mats. The same bactericidal efficiencies (>99.9%) were observed for functionalized fiber mats (PVG/PHA)$_{20}$ or (PVG/PHA)$_{20.5}$ and (PVG/PHA)$_{10}$ or (PVG/PHA)$_{10.5}$ with either PVG or PHA as a last applied coating layer in electrostatic assembly. This may be due to interpenetration between neighboring layers or interlayer diffusion of polyelectrolytes, resulting in the presence of PVG in the outer layer of functional coatings on fiber surfaces.[35-37] This also

explains the better bactericidal efficiency as bilayers of functional coatings increases. A disk diffusion (Kirby Bauer) test was conducted on functionalized fiber mat $(PVG/PHA)_{20}$ to test for possible release of PVG from the bilayers to the surrounding solutions. No zone of inhibition (Figure 5.17) was observed for the fiber mat after the test, indicating that functional PVG/PHA coatings on fiber surfaces do not release PVG out to the proximity under test conditions, and only kill bacteria on contact.

Number of bilayers	Bactericidal Efficiency (%)	
	E. coli	S. epidermidis
1	20.0	25.0
5	99.5	99.8
10	>99.9	>99.9
20	>99.9	>99.9

Table 5.1. Antibacterial capability of PVG/PHA functionalized fiber mats
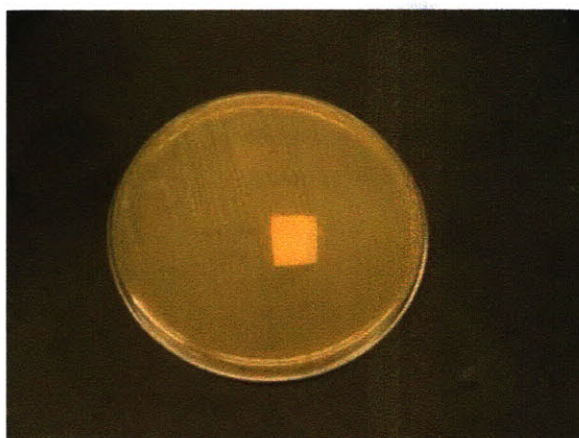
Figure 5.17. A photo image of the agar plate after disk diffusion test (*E. coli*) for functionalized fiber mat, $(PVG/PHA)_{20}$.

5.4. Simulation of reactive fiber systems

All the previous work demonstrated that lightweight breathable reactive and/or bactericidal electrospun fiber mats can be fabricated by various methods. These functionalized fiber mats could be incorporated into next generation of protective clothing system as key reactive layer(s). Although the good performance of these functionalized fiber mats to detoxify representative chemical and biological toxins have been illustrated, the functioning of self-detoxifying protective fabrics containing these functional mats as a reactive barrier against chemical warfare agents in combat situations remains unanswered. However, given the acute toxicity of organophosphate chemical warfare agents and limited facility, we are unable to conduct experiments to test the performance of these new self-detoxifying protective fabrics. Herein, we simulate the reactive protective fabric systems to provide insights on the performance of these reactive fiber systems, which could guide us for the further design of new protective clothing.

Figure 5.18 shows a schematic picture of 1-D reactive fiber system. One reactive electrospun fiber mat is placed between two identical commercial fabrics. Herein we only consider the worst case with toxic chemical agent in the environment in its vapor state since liquid toxin will diffuse through fabrics system much more slowly than vaporous toxin. We assume the concentration of vaporous toxin constant (C_o) in the environment. Then we monitor the concentration of toxin inside clothing system as a function of time. To simplify the problem, we only consider the diffusion of toxin through the reactive fiber system, neglecting the convective transport of toxins through the system. In commercial membrane region, I and III, only diffusion of toxins occurs. However, in reactive electrospun membrane region, II, both diffusion of toxins and reaction with toxins exist. The dimensionless governing equations for these regions are described as follows:

$$\text{II:} \qquad \frac{\partial \theta}{\partial \tau} = \frac{\partial^2 \theta}{\partial \eta^2} - Da\theta$$

$$\text{I and III:} \qquad \frac{\partial \theta}{\partial \tau} = \frac{D_t}{D_e} \frac{\partial^2 \theta}{\partial \eta^2}$$

$$\theta = \frac{C}{C_0} \qquad \eta = \frac{x}{L} \qquad \tau = \frac{t}{t_D} \qquad t_D = \frac{L^2}{D_e} \qquad Da = \frac{kL^2}{D_e}$$

where C is concentration; x is length along x axis; t is time; D_e is diffusivity of toxin in electrospun membrane; D_t is diffusivity in commercial membrane; k is first-order reaction constant; L is characteristic length scale; t_D is characteristic time scale; Da is a dimensionless number to characterize the ratio of reaction rate vs. diffusion rate; θ, η, τ is dimensionless concentration, length and time, respectively.
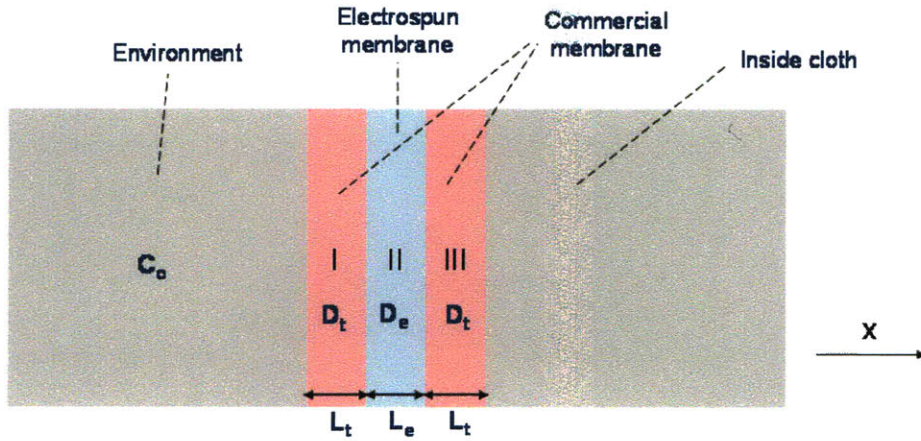
Figure 5.18. A schematic diagram of the reactive fiber system.

146

The diffusion through the porous membranes is significantly affected by the structure of porous materials (i.e. porosity and tortuosity). The porous membrane provides a partial barrier to diffusion, so the membrane porosity must be taken into account. In addition, the distance a gaseous molecule must travel to cross the barrier is a winding path through interconnecting voids rather than the membrane thickness; it requires the tortuosity correction factor. Therefore, the effective diffusivity is described as follows:[40]

$$D_{eff} = \frac{\varepsilon}{\tau} D$$

where ε is porosity, and τ is tortuosity. Since ε is smaller than 1 and τ is larger than 1, D_{eff} is smaller than D. The form of the diffusivity depends on the diffusion mechanism (i.e. Fickian, Knudsen, or transition). The mean free path of gaseous molecule can be described as follows:[41]

$$\lambda = kT / (\pi d_{gas}^2 P \sqrt{2})$$

where d_{gas} is the diameter of the molecule, P is the pressure and T is the temperature. At room temperature and atmosphere pressure, the mean free path for OP is about 5-10 nm. However, the pore size diameter (d) for electrospun fiber mats is about 5-10 μm, which is much larger than the mean free path. Knudsen diffusion is only dominant when $\lambda/d > 10$; in our case, with $\lambda/d < 1/100$, the diffusion mechanism will primarily determined by Fickian diffusion.[40] Based on previous water vapor diffusion resistance measurements, the diffusivity of water vapor through our functionalized fiber mats is estimated to be 10^{-7}-10^{-8} m^2/s. Considering organophosphates are larger than water molecule in size, diffusivity D_e for organophosphates is estimated to be in the order of 10^{-8} m^2/s. A reasonable length scale for protective fabric layers is in the order of millimeter. Herein, we selected L = 1mm, and the reaction constant k is estimated to be in the order of 10^{-3} s^{-1} according to our previously reported reactivity results. In this regard, Da is in the order of 0.1. Characteristic time scale, t_D, through L (1 mm) is 100 s. According to reference [38], D_i/D_e is in the order of 0.01.
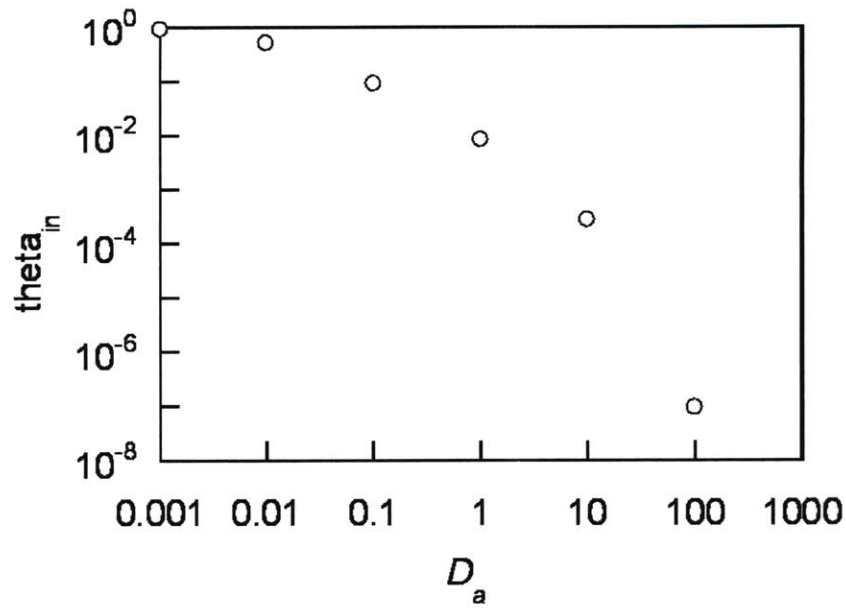
Figure 5.19. θ_{in} vs. D_a at steady state. $D_t/D_e = 0.01$; $L_e = L_t = L = 1$mm. θ_{in}: dimensionless concentration θ inside cloth.

Figure 5.20. Normalized θ_{in} vs. time for various Da. Normalized θ_{in}: dimensionless concentration θ inside cloth, normalized by steady state value.

Figure 5.21. Normalized θ_{in} vs. time for various L_t/L. $L_e/L = 1$; $D_a = 1$; Normalized θ_{in}: dimensionless concentration θ inside cloth, normalized by steady state value.

Figure 5.22. Normalized θ_{in} vs. time for various L_e/L. $L_t/L = 1$; $D_a = 1$; Normalized θ_{in}: dimensionless concentration θ inside cloth, normalized by steady state value.

Figure 5.23. θ_{in} vs. L_t/L at $L_e/L = 1$. θ_{in} vs. L_e/L at $L_t/L = 1$. $D_t/D_e = 0.01$; $D_a = 1$.

All numerical simulation work was performed using commercial Comsol Multiphysics® software. Figure 5.19 shows dimensionless concentration of toxins inside cloth as a function of D_a at steady state. When dimensionless concentration is normalized by its steady state value (Figure 5.20), we observe that the time scales to steady state for all cases of D_a are very similar (5000 t_D), which is attributed to the constant thicknesses (L_e, L_t) of membranes in the system. Therefore, the reaction (or contact) time with reactive electrospun membrane is constant in these situations. As D_a increases, the reactivity (k) of functionalized electrospun fiber mats increases, leading to the consumption of more toxins at the same reaction time. It results in the significant decrease in toxin concentration (θ_{in}) inside cloth (Figure 5.19). At $D_a = 0.1$, which is a typical value representing our previously reported reactive fiber mats, the steady state toxin concentration inside cloth is 8.9% of the toxin concentration (C_0) in the environment. The time scale to steady state is 5×10^5 s, corresponding to 140 hour. Depending on the absolute value of toxin concentration, C_0, in the environment along with the known lethal dosage of toxins, we may estimate the valid protection time for our reactive protective fabric system.

We also conduct several simulations to evaluate the effect of the thickness of reactive fiber system on the performance. Figure 5.21 shows curves of the normalized θ_{in} vs. time as a function of L_t, the thickness of commercial fabric, when L_e, the thickness of reactive electrospun membrane, is fixed. The increase in L_t leads to the corresponding increase in time scale to the steady state. Figure 5.22 shows the curves of normalized θ_{in} vs. time as a function of L_e when L_t is kept constant. The time scale remains approximately constant when L_e is varied and L_t is kept constant. These results indicated the diffusion through the commercial membrane is the rate-determine step in reaching the steady state. This can be explained by two orders of magnitude smaller of diffusivity in commercial membrane, D_t, compared to diffusivity in reactive electrospun membrane, D_e. We further compare steady state θ_{in} in these two series of experiments. Interestingly, L_e has a larger effect on steady state θ_{in} than L_t. An increase in L_e results in more reduction in steady state θ_{in} compared to that for L_t (Figure 5.23). In fact increasing L_e leads to longer reaction or contact time of toxins with reactive electrospun membrane, which allows for detoxification of more toxins and results in the reduction in steady state θ_{in}. On the other hand, in term of increasing L_t while maintaining L_e constant, the reaction or contact time with reactive electrospun membrane remains constant; the diffusion resistance in commercial membrane significantly increases as L_t increases, causing an increase in toxin concentration in reactive electrospun membrane. Consequently, more toxins are decomposed since reaction rate is essentially determined by $k\theta$. In this regard, by manipulating the thicknesses of these composite membranes, we could tune the transport properties and reactivity of these self-detoxifying protective clothing.

In summary, our simulation results show that chemical detoxifying protective fabrics containing a functionalized electrospun membrane as a reactive layer/barrier in combat situations could provide effective protection to some extent. The experimental validation of these simulation results need to be further addressed in future work.

5.5. Conclusions

The layer-by-layer electrostatic assembly technique has been applied to electrospun nanofibers and used to fabricate novel, breathable electrospun fiber-based protection fabrics and filters for chemical and biological protection. The combination of LbL assembly and electrospinning techniques allows us to take advantage of high specific surface area and high breathability of electrospun fiber mats while simultaneously providing the versatility to incorporate different functional polyelectrolytes to achieve bifunctional coatings for both chemical and biological protection together. The reactive polyanion, polyhydroxamic acid, and antimicrobial polycation, poly(N-vinyl guanidine), were synthesized. The ability of PHA to degrade the OP nerve agent simulant, DFP, hydrolytically was demonstrated. The PVG/PHA-functionalized fiber mats are proven to be highly breathable. DFP degradation mediated by PVG/PHA functionalized fiber mat was found to be 60-fold faster than that with a control fiber mat under identical conditions. Furthermore, PVG/PHA functionalized fiber mats demonstrate potent bactericidal capability over representative strains of E. coli and S. epidermidis when used as biological protective fabrics. The simplicity of preparation and meaningful performance of the functionalized fiber mats in decomposing nerve agents and bacterial contaminants, suggest they can be readily incorporated into a new generation of breathable self-detoxifying chemical and biological protective fabrics or filters. In addition, LbL electrostatic coating of porous non-woven materials provides the versatility to generate multifunctional polymer-based membrane materials for other applications.

5.6. References

1. Chen, L.; Bromberg, L.; Schreuder-Gibson, H.; Walker, J.; Hatton, T. A; Rutledge, G. C. *J. Mater. Chem.* 2009, 19, 2432.

2. Chen, L.; Bromberg, L.; Hatton, T. A.; Rutledge, G. C. *Polymer* 2007, 48, 4675.

3. Hammond, P. T. *Adv. Mater.* 2004, 16, 1271.

4. Decher, G. *Science* 1997, 277, 1232.

5. Wang, X.; Kim, Y-G.; Drew, C.; Ku, B-C.; Kumar, J.; Samuelson, L. A. *Nano Lett.* 2004, 4, 331.

6. Yang, G.; Gong, J.; Yang, R.; Guo, H.; Wang, Y.; Liu, B.; Dong, S. *Electrochem. Commun.* 2006, 8, 790.

7. Lee, J. A.; Krogman, K. C.; Ma, M.; Hill, R. M.; Hammond, P. T.; Rutledge, G. C. *Adv. Mater.* 2009, 21, 1252.

8. Singh, A.; Lee, Y.; Dressick, W. J. *Adv. Mater.* 2004, 16, 2112.

9. Krogman, K. C.; Lowery, J. L.; Zacharia, N. S.; Rutledge, G. C.; Hammond, P. T. *Nat. Mat.* 2009, 8, 512.

10. Yang, Y.-C.; Baker, J. A.; Ward, J. R. *Chem. Rev.* 1992, 92, 1729.

11. Shin, Y. M.; Hohman, M. M.; Brenner, M. P.; Rutledge, G. C. *Polymer* 2001, 42, 9955.

12. Bromberg, L.; Schreuder-Gibson, H.; Creasy, W. R.; McGarvey, D. J.; Fry, R. A.; Hatton, T. A. *Ind. Eng. Chem. Res.* 2009, 48, 1650.

13. Zhang, J.-F.; Hu, Y.-H.; Wang, D.-Z. *J. Cent. South Univ. Technol.* 2002, 9, 177.

14. Domb, A. J.; Cravalho, E. G.; Langer, R. J. *Polym. Sci., Pt A: Polym. Chem.* 1988, 26, 2623.

15. Bromberg, L.; Hatton, T. A. *Polymer* 2007, 48, 7490.

16. Gibson, P. W. *Journal of Coated Fabrics* 1999, 28, 300.

17. Gibson, P. *Journal of Polymer Testing* 2000, 19, 673.

18. Gibson, P. W.; Rivin, D.; Kendrick, C. *International Journal of Clothing Science and Technology* 2000, 12, 96.

19. Tiller, J. C.; Liao, C.-J.; Lewis, K.; Klibanov, M. *PNAS* 2001, 98, 5981.

20. Aubort, J. D.; Hudson, R. F. *J. Chem. Soc. D: Chem. Commun.* 1970, 938.

21. Bunton, C. A.; Ihara, Y. *J. Org. Chem.* 1977, 42, 2865.

22. Hackley, B. E.; Plainger, R.; Stolberg, M. A.; Wagner-Jauregg, T. *J. Am. Chem. Soc.* 1955, 77, 3651.

23. Endres, G. F.; Epstein, J. *J. Org. Chem.* 1959, 24, 1497.

24. Wagner, G. W.; Bartram, P. W. *J. Mol. Catal. A: Chem.* 1999, 144, 419.

25. Stolberg, M. A.; Mosher, W. A. *J. Am. Chem. Soc.* 1957, 79, 2618.

26. Ghosh, K. K.; Satnami, M. L.; Sinha, D.; Vaidya, Jyoti. *J. Mol. Liq.* 2005, 116, 55.

27. Wagner-Jauregg, T.; O'Neill J. J.; Summerson, W. J. *J. Am. Chem. Soc.* 1951, 73, 5202.

28. Epstein, J.; Cannon, P. L.; Sowa, J. R. *J. Am. Chem. Soc.* 1970, 92, 7390.

29. Gerenser, L. J. *J. Adhes. Sci. Technol.* 1993, 7, 1019.

30. Dupont-Gillain, C. C.; Adriaensen, Y.; Derclaye, S.; Rouxhet, P. G. *Langmuir* 2000, 16, 8194.

31. Browton, P.; Woodcock, P. M.; Heatley, F.; Gilbert, P. *J. Appl. Bacteriol.* 1984, 57, 115.

32. Gilbert, P.; Pemberton, D.; Wilkinson, D. E. *J. Appl. Bacteriol.* 1990, 69, 585.

33. Pemberton, D.; Wilkinson, D. E. *J. Appl. Bacteriol.* 1990, 69, 593.

34. Khunkitti, W.; Hann, A. C.; Lloyd, D.; Furr, J. R.; Russell, A. D. *J. Appl. Microbiol.* 1998, 84, 53.

35. Picart, C.; Mutterer, J.; Richert, L.; Luo, Y.; Prestwich, G. D.; Schaaf, P.; Voegel, J. –C.; Lavalle, P. *Proc. Natl. Acad. Sci. USA* 2002, 99, 12531.

36. Wood, K. C.; Chuang, H. F.; Batten, R. D.; Lynn, D. M.; Hammond, P. T. *P. Proc. Natl. Acad. Sci. USA* 2006, 103, 10207.

37. Decher, G.; Lvov, Y.; Schmitt, J. *Thin Solid Films* 1994, 244, 772.

38. Gibson, P.; Schreuder-Gibson, H.; Rivin, D. *Colloids Surf. A* 2001, 187-188, 469.

39. Breathability test of functionalized fiber mats was performed by Dr. Phillip Gibson and Dr. Heidi Schreuder-Gibson of US Army Natick Soldier Research, Development & Engineering Center, Natick, Massachusetts.

40. Hale, W. R.; Dohrer, K. K.; Tant, M. R.; Sand, I. D. *Colloids Surf. A* 2001, 187-188, 483.

41. Mulder, M. Basic principles of membrane technology; Kluwer: Dordrecht, The Netherlands, 1996.

Chapter 6

Conclusions and Future Work

6.1. Research summary

Protective clothing is used widely to provide protection for military personnel and emergency responders when they are at risk of exposure to chemical or biological threats. Function of the protective clothing is primarily based on full barrier protection by absorbing or blocking toxic agents. Current multilayer fabric systems are bulky and possess low moisture vapor permeability. Extensive contamination may occur as the absorbed toxins leave the surfaces of protective fabrics. These challenges motivate the development of a new generation of protective clothing system that is lightweight, breathable, and capable of selectively decomposing toxic agents on the fabric surfaces. In this regard, an electrospun fiber-based protective clothing system wields a lot of promise. Electrospun fabrics are remarkable for their breathability, light weight and high specific surface area. Moreover, high surface area of electrospun fibers allows the attachment of functional compounds to fabricate chemical and biological detoxifying protective clothing system. Such fabrics emerge as candidates for the next generation of chemical and biological protective fabrics.

In this study, we aimed at developing electrospun fiber-based chemical and/or biological detoxifying protective fabrics containing α-nucleophilic oxime moieties, which are capable of hydrolytically decomposing toxic organophosphate chemical nerve agents and pesticide, and/or biocides, which can act against biological bacterial contaminants.

Modification of polyacrylonitrile (PAN) by hydroxylamine results in polyacrylamidoxime (PAAO), the amidoxime groups of which are nucleophilic and capable of hydrolyzing esters. Functionalized nanofiber mats were produced via electrospinning of a suspension of PAAO blended with PAN. The functioning of the reactive fiber mats was tested by the esterolysis of p-nitrophenyl acetate (PNPA).

157

The presence of the PAAO/PAN nanofiber mats significantly accelerated the hydrolysis of PNPA compared to its spontaneous hydrolysis at pH ranging from 7.0 to 9.0. The effect of the fiber size on the reaction rates indicated that intra-fiber diffusional resistances might limit the accessibility of the oxime catalytic sites inside the fibers, and that the catalytic hydrolysis probably occurs primarily on the surface of the oximated nanofibers. In addition, the capability of polyacrylamidoxime powders to decompose combat organophosphate chemical warfare agents, such as soman (GD) and VX, in the presence of moisture was demonstrated. We believe that PAAO groups are capable of decomposing chemical warfare agents when they are present on the PAAO/PAN nanofibers. This work demonstrates the concept of incorporation of the α-nucleophilies into the electrospun nanofibers capable of catalytically decomposing toxic chemicals.

In light of possible diffusional limitations observed in PAAO/PAN blend fibers, we adopt a somewhat analogous concept of having the majority of the reactive groups on the fiber surface by modification of prefabricated electrospun fibers. Allocating all of the active reactive sites on the fiber surface rather than distributing the reactive sites in the whole volume of the fibers should improve the reactivity. Prefabricated PAN submicron fiber mats were modified by an efficient, one-step oximation reaction, resulting in conversion of the surfaces of the fibers into PAAO. Surface modification strategy results in a higher density of functional amidoxime groups and enhanced reactivity compared to the previous blending strategy, as indicated by XPS spectra. The nucleophilic amidoxime groups on the surfaces of fibers enable the functionalized fiber mats to hydrolytically degrade chemical warfare agent (CWA) simulant, diisopropyl fluorophosphates (DFP), in the presence of moisture. At a water content (C_w) of 130 wt/wt%, the DFP hydrolysis, monitored by ^{31}P MAS NMR, is 80-fold faster in the presence of surface-modified fiber mats than with the unmodified PAN fibers. The reaction rate constant was observed to increase with the amount of water in the fiber mats. The water serves as a medium to promote the nucleophilic action of the amidoxime groups in the fibers by facilitating the proton

158

transfer and stabilizing the substrate's transition state. The simplicity of preparation and efficiency of the functionalized, electrospun fiber mats in degrading toxic organophosphates make them good candidates for incorporation into a new generation of chemical detoxifying, lightweight fabrics and textiles.

To provide protection against bacterial contaminants, submicron fibers with bactericidal properties were successfully produced by electrospinning of blends containing cellulose acetate (CA) as a polymer base, chlorhexidine (CHX) as a bactericidal agent, and organic titanate Tyzor® TE (TTE) as a cross-linker. A small amount of high molecular weight poly(ethylene oxide) (PEO) was incorporated into the blends to facilitate the electrospinning by improving the elasticity of the solution. A dimensionless De number, defined as the ratio of fluid relaxation time to instability growth time, was used to characterize the spinnability of the blends. It was found that uniform fibers were produced in the region of $De > 7$. The De number can generally be utilized for prediction of spinnability of other polymer solutions. The CHX-containing fiber meshes (CA-CHX) were cured by TTE in the presence of water vapor, which creates covalent links between the CA and CHX. The immobilization of CHX on or within the fibers was confirmed by FTIR, Raman and XPS measurements. The CA-CHX fibers demonstrated bactericidal activity against representative gram-negative *E. coli* and gram-positive *S. epidermidis* not only through a gradual release of unbound CHX from the fibers but also via contact with CHX bound on the fibers. In addition, antibacterial fiber mats were obtained by post-spin treatment of the CA-PEO fibers to immobilize CHX on the fibers via titanate linkers. The post-spin treated fibers achieved similar bactericidal efficiency compared to that of the CA-CHX fibers electrospun from the blends, even with a much lower CHX content. We believe that the strategies presented herein are not limited to incorporation of CHX only, but will also enable incorporation of a wide range of antibacterial agents such as antibiotics in/on the fibers.

The fiber post-spin modification strategy has the advantages of higher surface density of functional groups, enhanced reactivity and ease of implementation compared to the blending strategy. The layer-by-layer (LbL) electrostatic assembly technique offers another strategy by which to functionalize the surfaces of electrospun fibers. Another advantage of LbL technique is that, by selecting appropriate functional polyelectrolytes, one could generate multifunctional coatings on the electrospun fiber mats. In this regard, breathable, chemical and biological detoxifying protective fabrics are obtained via functionalization of the electrospun fiber mats using LbL electrostatic assembly technique. The reactive polyanion, polyhydroxamic acid, which can decompose CWA, and the antimicrobial polycation, poly(N-vinyl guanidine), were synthesized and electrostatically assembled to generate multifunctional coatings on prefabricated PAN fiber mats. The ability of PHA to hydrolytically degrade the OP nerve agent simulant, DFP, was demonstrated. The degradation rate with PHA is comparable to that of low molecular weight hydroxamic acid compounds such as isonicotinhydroxamic acid methiodide, an efficient catalyst in the hydrolytic degradation of OP. DFP degradation mediated by PVG/PHA functionalized fiber mat was found to be 60-fold faster than that with a control fiber mat under identical conditions. Furthermore, PVG/PHA functionalized fiber mats demonstrate potent bactericidal activity against representative strains of *E. coli* and *S. epidermidis* when used as biological protective fabrics. The water vapor diffusion and airflow resistance results indicate that the PVG/PHA-functionalized fiber mats are highly breathable. The simplicity of preparation and meaningful performance of the functionalized fiber mats in decomposing nerve agents and bacterial contaminants make them good candidates for chemical and biological protective clothing. In addition, LbL electrostatic coating of porous non-woven materials provides the versatility to generate multifunctional polymer-based membrane materials for other applications.

In summary, we have successfully fabricated several reactive and/or bactericidal electrospun fiber mats by various methods; all of the resulting fibers have been

demonstrated to be capable of selectively decontaminating organophosphate nerve agents/pesticides and/or bacterial contaminants. We envision utilization of such chemical and biological detoxifying, lightweight and breathable fiber mats as key functional components in a new generation of chemical and biological protective fabrics, filters and masks.

6.2. Suggestions for future work

In this work, we primarily focus on the development of functionalized electrospun fiber mats for chemical and biological detoxifying protective fabrics. The research work emphasizes the methodology to incorporate functional compounds or groups on/in the electrospun fiber mats and the evaluation of these functionalized fiber mats. We have successfully achieved these goals in this dissertation and developed several functionalized fiber mats with good performance for chemical and biological protection. However, little work has been done to incorporate these functionalized fiber mats into a new generation of chemical and biological detoxifying protective clothing system. This system will need to be evaluated in a practical way, which involves a test of the transport properties of the reactive fiber system besides the reactivity. We have concluded some simulation work demonstrating that our reactive fiber system will be effective to some extent still. The experimental evaluation of the new protective system containing functionalized electrospun fiber mats in the field needs to be addressed to validate our simulation results.

Functioning of the reactive electrospun fiber mats containing α-nucleophilic amidoxime moieties was demonstrated to be dependent on the amount of water absorbed in the fiber mats. This significantly limits practical application of our reactive fiber fabrics in an extremely dry environment, such as desert. One solution is the incorporation of another hygroscopic compound or polymer into our reactive fiber mats. A hygroscopic polymer in the fibers may help to absorb water from the surrounding environment, which could enhance the reactivity of reactive amidoxime groups in the fibers.

Post-spin modification strategy has been proven to be more effective to functionalize the surfaces of the fibers in order to obtain reactive and/or bactericidal

162

fiber mats. Surface chemical modification and layer-by-layer electrostatic assembly methods have been adopted to functionalize the fiber surfaces. Some other techniques, such as chemical vapor deposition (CVD) and core-shell coaxial spinning, could be used to obtain functionalized fiber surfaces as well. By using CVD technique, one can directly polymerize reactive monomers to generate conformal reactive polymer coatings on the surfaces of prefabricated fiber mats. We expect that the functional coatings obtained in such a way will be more stable in wet conditions compared to those made by the LbL electrostatic assembly technique. Core-shell coaxial spinning provides another strategy to functionalize the fiber surfaces. The functional compounds or polymers will be placed in a solution of shell material. By selecting appropriate core materials, one could facilitate the electrospinning and produce uniform fibers with functional groups in the shell, which can enhance the function of fiber mats.

In this work, we only incorporated the biocides with biguanide functional groups into our fiber mats to produce bactericidal fibers. There is a great variety of other antibacterial agents, such as quaternary amine compounds, phosphonium compounds, and sulfonium compounds, which could also be incorporated into the fibers for antibacterial properties.